REGULATION OF PLATELET INTEGRIN MECHANOBIOLOGY BY TALIN

A Dissertation
Presented to
The Academic Faculty

by

Jiexi Liao

In Partial Fulfillment
of the Requirements for the Degree
Doctor of Philosophy in the
School of Biomedical Engineering

Georgia Institute of Technology
Emory University
August 2020

REGULATION OF PLATELET INTEGRIN MECHANOBIOLOGY BY TALIN

Approved by:

Dr. Cheng Zhu, Advisor
Department of Biomedical Engineering
Georgia Institute of Technology

Dr. Manu Platt
Department of Biomedical Engineering
Georgia Institute of Technology

Dr. Shaun Jackson
Heart Research Institute
University of Sydney

Dr. Shuichi Takayama
Department of Biomedical Engineering
Georgia Institute of Technology

Dr. Brian Petrich
Department of Pediatrics
Emory University

Date Approved: 07/16/2020

To my husband David, mom, dad, and papa Fritz

ACKNOWLEDGEMENTS

I want to express my deepest gratitude to so many people I met during my PhD who have given me support and guidance for the work described in this dissertation. I would like to thank my advisor Dr. Cheng Zhu, for creating a lab environment that grants us freedom to explore research topics and techniques and cultivates warm and supportive relationships amongst colleagues (labmates). Thank you for your guidance and support all these years; your technical reasoning and passion and dedication to science has never ceased to amaze me. Sincere appreciation also goes to my committee members: Drs. Brian Petrich, Shaun Jackson, Shuichi Takayama, and Manu Platt for their support and helpful suggestions to my thesis work. Especially, Dr. Brian Petrich provided almost all the animal resources for my thesis work: I owe so many thanks to your time and input. Dr. Shaun Jackson hosted me in his lab in Sydney twice: thank you for all the resources you generously provided and the bleeding-edge discussions on platelet mechanobiology.

Special thanks to Dr. Arnold Ju in Sydney, Australia, who had been an invaluable mentor for me since my third year. You opened new avenue and dedicated countless hours to train me and chat with me about science and life lessons and thank your graduate student Yunduo (Charles) Zhao for offering to run the CFD simulations. I thank Dr. Yunfeng Chen for being my mentor when I first joined the lab and taught me the notoriously difficult BFP technique and offered publication opportunities. I thank the researchers in the Heart Research Institute in Sydney: Dr. Yuping Yuan for your rigorous guidance on my experiments, Dr. Simone for your kind support, Dr. Roxanne for your consistent help in getting the human blood samples, Dr. Angela Chen for your dedication in getting the diabetic patient samples, and Dr. Tara Wu (Olympus) for your dedication in helping me

get beautiful confocal images and videos. Thank Dr. Freda Passam for the stimulating discussions and kind words and Alex Dupuy for offering to run the Western blots. Thank Dr. Wolfgang and his postdocs Drs. Rob Lee and Dave Paul for providing the transgenic mice and helping us with sample collection. Thank Drs. Yongzhi Qiu, David Myers, and Yumiko Sakurai in Dr. Lam's lab for always helping us collect human blood samples. And I am always grateful for my undergraduate advisor Dr. Jeremy Gulley for encouraging me on the path of pursuing PhD and being the one to tell me that grad school was like "you are dropped into a forest to make your way out."

Of course, I appreciate my labmates in the Zhu lab – my everyday friends: Larissa, Prithi, Muaz, Billy, and Kristine my political pal, and those who helped with this thesis or made the experiments easier: Fangyuan, Sam, Jeffrey, Kaitao, Qinghua, Steve, and Aaron. I thank Sara and Tracie who for made my research trips easier. To my friends: Ariel, Jennie, Shuang, Ning, Lingyi, for your emotional support and lasting friendship. And to my friend that hosted me in Sydney, Xiaoxue and her fiance Peng: so glad we could connect again.

Last but not least, I wish to acknowledge my husband David, whom I met during my second year of graduate school. Thank you for enduring my many difficult days and nights with my research and giving your unwavering support and encouragement. To the rest of my family: dad – thank you for patiently listening to my long monologues of exploring and defining my career path; mom and papa Fritz – I cannot express enough appreciation for all the support you generously provided throughout my PhD journey.

TABLE OF CONTENTS

LIST OF TABLES

LIST OF FIGURES

LIST OF SYMBOLS AND ABBREVIATIONS

$<n>$	Average number of bonds per contact
2D	Two dimensional
3D	Three dimensional
A_c	Contact area
A_cK_a	2D effective affinity
ADP	Adenosine diphosphate
Bc	Botrocetin
BFP	Biomembrane force probe
CalDAG-GEFI	Ca^{2+} DAG-regulated guanine nucleotide exchange factor 1
CFD	Computational fluid dynamics
ctrl	Control
DAG	diacylglycerol
DM	Diabetic
Fg	Fibrinogen
GPCR	G protein-coupled receptor
GPIIbIIIa	$\alpha_{IIb}\beta_3$
HT	Hepes Tyrode's buffer
IL4	Interleukin 4
KO	Knock-out
k_{off}	Off-rate
LA	β_3 L746A mutant
LBD	Ligand binding domain
LIBS	Ligand-induced binding sites

LR	Talin L325R mutant
MDR	Membrane distal region
m_l	Ligand density
MPR	Membrane proximal region
m_r	Receptor expression level
mut	Mutant
P_a	Probability of adhesion (adhesion frequency)
PI3K	Phosphoinositide 3-kinase
PIP2	Phosphatidylinositol 4,5-bisphosphate
PKC	Protein kinase C
PTB	Phosphotyrosine-binding
PWB	Platelet washing buffer
RBC	Red blood cell
RGD	Arginine-Glycine-Aspartic Acid
RIAM	Rap1-interacting adapter molecule
SA	Streptavidin
STIM1	Stromal interaction molecule 1
STZ	Streptozotocin
T1DM	Type 1 diabetes
T2DM	Type 2 diabetes
TMD	Transmembrane domains
vWF	von Willebrand factor
WA	Talin W359A mutant
WT	Wild type
WT/fl	WT/flox

SUMMARY

Platelets are exquisitely reactive to mechanical forces in disturbed blood flow caused by vessel branching, stenosis, and interventional medical devices, leading to life-threatening clots comprised of platelet aggregates. How forces drive platelet aggregation on the molecular level is incompletely understood. Integrins, particularly the platelet-specific $\alpha_{IIb}\beta_3$ (GPIIbIIIa), mediate the gradient shear-induced platelet aggregation not in their well-known fully activated form but an intermediate state. This intermediate state can be induced by merely mechano-signaling of GPIbα, the receptor that initiates platelet rolling on endothelium. Since integrins require the cytoplasmic adaptor molecule, talin, for activation and cytoskeletal linkage, elucidating talin's role is critical to understand this process.

Using stenosis-modeling microfluidics and mouse models that perturb specific interactions in the Rap-1-talin-integrin axis, we first demonstrated that talin indeed regulates platelet aggregation in disturbed flow and proposed the mechanism that aggregate buildup is achieved by membrane-recruited talin providing cytoskeletal linkage to the integrins. Our results also suggested that GPIbα-induced GPIIbIIIa maturation to the intermediate state requires normal talin-integrin binding.

To gain mechanistic insights on the molecular level, we used single-cell force spectroscopy to characterize the two-dimensional (2D) kinetics of integrin-ligand binding with talin perturbations in the presence and absence of force. We found that talin, a mechanosensor itself, is particularly important for force-mediated integrin binding without prior inside-out activation. The formation of catch bond (force prolonged bond lifetime)

between the fibrinogen ligand and β_3 integrin may be crucial for the "biomechanical" platelet aggregation in disturbed flow.

Lastly, we extended the platelet mechanobiology study to investigate a disease known to dysregulate platelets: diabetes. We focused on type I diabetes to reduce metabolic confounding factors. Using the stenosis microfluidics to screen patients' blood, we preliminarily concluded that diabetes could amplify platelet aggregation by promoting more integrins to the intermediate state, but many other factors including racial heritage could cause large variance in patient samples' responses.

Overall, we identified talin's critical role in gradient shear-induced platelet aggregation. The biophysics studies offered a clearer understanding of how integrins finely tune their kinetics in response to mechanical cues. Our results showed the anti-thrombotic potential of specific talin and Rap1 blockade and could inform rational design of novel therapeutics that address the mechanosensitivity of integrins.

CHAPTER 1. MOTIVATION

Cardiovascular diseases (CVDs) are the leading cause of death globally. Heart attack and stroke alone leads to >15 million global deaths annually (World Health Organization, 2017, May 17). Despite the aggressive aspirin and clopidogrel dual platelet therapy that can lead to bleeding side effects, patients still die from blood clots which are mostly comprised of platelet aggregates. Among other reasons, the combinatory treatment showed limited efficacy in treating clots that were induced by disturbed flow in vessel branching, stenosis, and interventional medical devices (Ajzenberg et al., 2005; Nesbitt et al., 2009; Rana, Westein, Niego, & Hagemeyer, 2019; Yong et al., 2011). Multiple studies revealed that shear-induced platelet aggregates are hierarchical with a bulky outer shell consisted of discoid platelets in low activation state (Jackson, Nesbitt, & Westein, 2009; Stalker et al., 2013). Platelet integrin GPIIbIIIa is the primary mediator of platelet aggregation. In the context of biomechanical aggregation, GPIbα signaling to induce GPIIbIIIa affinity maturation is required to form substantial aggregates (Y. Chen et al., 2019; Nesbitt et al., 2009); since integrin needs its adaptor molecule, talin, to properly function, understanding how talin regulates integrin mechanobiology will inform the design of novel therapeutics that can target platelet biomechanical pathways.

Talin is a nexus of both outside-in and inside-out signaling of integrins. As part of an ancient scaffolding and signaling machinery, talin was suggested to have emerged before integrins (Sebe-Pedros, Roger, Lang, King, & Ruiz-Trillo, 2010), reinforcing its "master orchestrator" role of integrin adhesion functionality. Previous studies have shown different mutations in talin rendered distinct phenotypical behavior of platelets and the anti-thrombotic potential of specific blockade of talin (Petrich, Fogelstrand, et al., 2007;

Stefanini et al., 2014). These studies elucidated talin's role in soluble agonist-induced integrin activation and paved the way to investigate 1) whether talin participates in biomechanical discoid platelet (without prior activation by agonists) aggregation and 2) how talin regulates integrin's response to mechanical cues. It has long been difficult to elucidate the significance of talin-mediated integrin affinity changes for integrin-ECM interactions (Klapholz & Brown, 2017) due to possible concurrent outside-in activation and lack of tools to study affinity (single bond) rather than avidity (multiple bonds and clustering). We are equipped with appropriate and effective biophysics tools to interrogate how talin fine-tunes integrin 2D kinetics (affinity and off-rate). The crosstalk between GPIbα and GPIIbIIIa has long been studied as their functions are tightly connected (Savage, Saldivar, & Ruggeri, 1996), but limited to assays that did not separate GPIbα's contribution. We propose to characterize tools that could expand the study mechanistically.

Diabetes is known to dysregulate platelets, specifically GPIIbIIIa function, and the dual antiplatelet therapy was demonstrated even less effective for diabetic patients that developed CVDs (Ju et al., 2018). We herein compare platelet aggregation and GPIIbIIIa's response to GPIbα mechano-signaling and force loading of diabetic patients vs non-diabetic controls in hopes of providing new insights on how diabetes causes platelet hyperreactivity.

CHAPTER 2. BACKGROUND

2.1 Platelet integrin GPIIbIIIa

2.1.1 Structure of GPIIbIIIa

Integrins are a family of adhesion and signalling molecules that can transmit signals in both outside-in (from extracellular matrix to cytoplasmic domain) and inside-out (from intracellular activity to ectodomain) directions. Like all surface receptors, the integrin consists of an ectodomain, transmembrane domains (TMD), and short cytoplasmic domains (except for β_4 integrins). Interestingly, their ligand binding domain are away from where large conformational changes occur on the α and β legs, making them allosteric machines (Hynes, 2002). The α and β subunits in combinations form 24 distinct types of known integrins, which can be further classified into αI and αI-less integrins (Hynes, 2002). The platelet-unique $\alpha_{IIb}\beta_3$ integrin, also known as GPIIbIIIa, is an αI-less integrin of ~ 250 kD. Its ligand-binding domain (LBD) is at the cusp of the α and β subunits, although ligand peptides predominantly crosslink to the βI domain (Bennett, 1996; D'Souza, Ginsberg, Burke, & Plow, 1990), and it mainly recognizes RGD sequence on ligands such as fibrinogen (Fg), fibronectin (Fn), and von Willebrand factor (vWF).

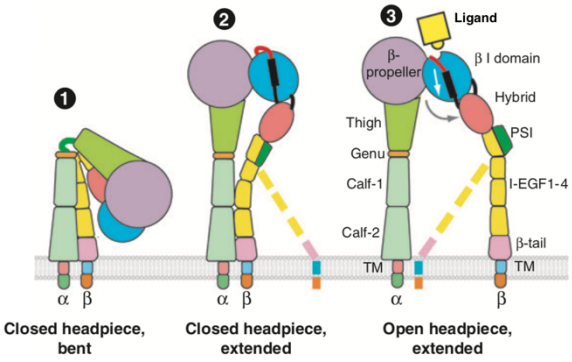

Figure 2.1. Schematic of integrin structure and conformations. 1, 2, and 3 show αI-less integrin (such as GPIIbIIIa) in bent closed (BC), extended closed (EC), and extended open (EO) conformations, respectively. 3 depicts structural components of the integrin in its active, high affinity form – fully extended with hybrid domain swung out. Adapted from (Luo, Carman, & Springer, 2007).

Integrins extend from the genu domain upwards when activated (Figure 2.1). There are at least five divalent cation binding sites on GPIIbIIIa, some dedicated to Ca^{2+} (K. Zhang & Chen, 2012). Cations such as Mg^{2+} and Ca^{2+} keep the integrin's structural integrity and facilitate in its activation or the need to stay quiescent – the mechanisms of the dual-role remain elusive.

2.1.2 Function of GPIIbIIIa

The GPIIbIIIa integrin in platelets is an adhesion and signalling molecule that is crucial in hemostasis and thrombosis. It is by far the most abundant integrin on the platelet (~80,000 copies). It can be activated via inside-out signalling with soluble agonists such as ADP, thromboxane A_2 (TxA_2), C-reactive protein (CRP), and thrombin, in generally weak to strong order. Another platelet-specific surface receptor, GPIbα, can also activate GPIIbIIIa when it binds its ligand – A1 domain of vWF – under tension (Y. Chen et al., 2019; Yap et al., 2002). Integrin activation is a direct consequence of its structural change.

Two models have been proposed: Springer's "switchblade" model describes that integrins would extend from the genu up to bind ligand, and Arnaout's "deadbolt" model suggests that integrin extension occurs only after ligand binding (Fan et al., 2016; Moser, Legate, Zent, & Fassler, 2009), with the switchblade model being more favourable for the GPIIbIIIa integrins. Despite the differences of the proposed models, consensus is that conformational changes facilitate ligand binding. The integrin can also initiate outside-in signaling when it can bind ligands, although this process is often in parallel with inside-out signaling (Shen, Delaney, & Du, 2012). Outside-in signaling, as signified by strong and sustained intracellular calcium flux (Nesbitt et al., 2002), often leads to more robust platelet adhesion and spreading past the early events of platelet rolling and tumbling at reactive endothelial surface.

2.2 Talin in platelet

2.2.1 Structure and general function of talin

Talin is a 270 kD large scaffolding/adaptor protein that interacts primarily with integrins and other cytoplasmic molecules such as vinculin and actin. Only talin 1 isoform is expressed in hematopoietic cells. Talin 1 consists of a 47 kD N-terminal head domain containing four subunits: F0, F1, F2, and F3 (altogether called FERM domain) and a linear ~220 kD C-terminal rod (Garcia-Alvarez et al., 2003; Moser et al., 2009) (Figure 2.2). The F3 subdomain resembles a non-canonical phosphotyrosine-binding (PTB) domain that can bind to β-integrin tails to activate integrins. Talin is regarded essential in agonist-driven inside-out activation of integrin (Shattil, Kim, & Ginsberg, 2010), but is not the only gateway in outside-in activation of integrin that induces platelet spreading, due to the feasibility of exogenous activation of integrin by Mn^{2+} or LIBS antibodies (Shen et al.,

2013; Tadokoro et al., 2003). However, talin still regulates the outside-in signalling (Haling, Monkley, Critchley, & Petrich, 2011), though it and Gα13 seem to bind integrin on and off throughout the course of cell ligation (Hynes, 2002; Shen et al., 2013).

Talin notably has been identified as a tension sensor and mechano-buffer as it exhibits the ability to unfold and refold in the rod domain, sense stiffness of the ECM, and activate – release from its autoinhibited form – upon applied forces to reveal its cryptic vinculin binding sites (Austen et al., 2015; Gingras et al., 2006; Kumar et al., 2016; Yao et al., 2016). Talin contains at least three actin binding sites which are all next to vinculin binding sites (Hemmings et al., 1996), making it a multi-functional mechanosensing adaptor for integrins.

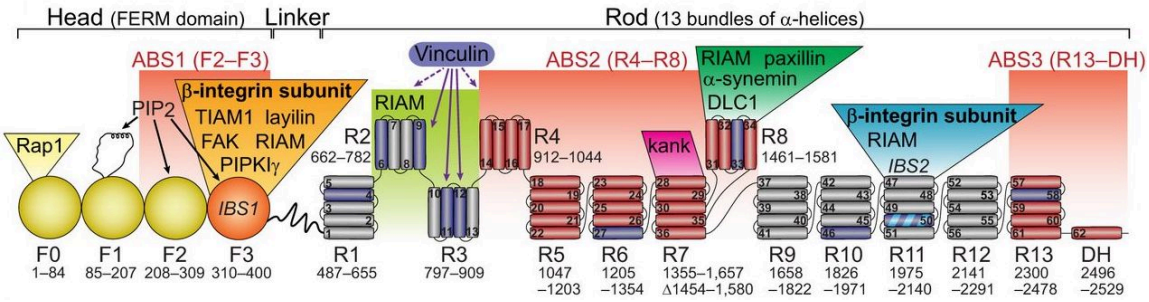

Figure 2.2. Schematic of the structure of talin. Adapted from (Klapholz & Brown, 2017).

2.2.2 Interaction between β_3 integrins and talin

Without intracellular or stimulatory cues, talin is mostly in a globular, autoinhibited form where head (mostly F3) and rod (mostly R9) domains constitutively interact (Khan & Goult, 2019). Structural and fluorescent imaging evidence show that talin F3 domain first binds to β_3 integrins NPxY motif at the membrane distal region (MDR) and subsequently the membrane proximal helix region (MPR), breaking the salt bridge between

the α and β legs (R995 and D723 in the case of GPIIbIIIa) that locks the integrin in a low affinity state (Roberts & Critchley, 2009; Watanabe et al., 2008; Wegener et al., 2007). Both biochemical experiments and molecular dynamics simulations show that the plasma membrane phospholipid phosphatidylinositol 4,5-bisphosphate (PIP2) will need to bind talin to activate integrins (Orlowski et al., 2015; Saltel et al., 2009). Electrostatic interactions and steric clash drive this process: PIP2 lipids attract positively charged talin FERM domains while repelling the negatively charged talin rod domains to relieve talin's autoinhibitory form (Saltel et al., 2009; Song et al., 2012).

The W359A (WA) and L325R (LR) mutations disrupt talin binding to two distinct sites on the integrin cytoplasmic tail: the MDR NPxY motif and the MPR, respectively (Stefanini et al., 2014; Tadokoro et al., 2003). Our current understanding is that talin binds to integrin β tail via the MDR (W359 on talin) first, which is the highest-affinity interaction between integrin and talin; then talin activates the integrin via the second, weaker interaction at the MPR (Moser et al., 2009). The weaker interaction at the MPR (L325 on talin) is what made talin "special and unique" in its ability to activate integrins, differentiating from other PTB-containing adaptor molecules (such as Dok1 and Numb) that do not activate integrins (Wegener et al., 2007). Both the LR and WA mutants have been shown to abrogate talin-dependent integrin activation in CHO cells (Garcia-Alvarez et al., 2003), but the WA mutant impedes GPIIbIIIa function in human megakaryoblastic cell line and murine platelets to a significantly lesser degree (Nakazawa et al., 2013; Stefanini et al., 2014).

2.2.3 Interaction between talin and Rap1

In leukocytes, talin membrane recruitment is triggered by the Rap1 effector Rap1 interacting adaptor molecule (RIAM) that binds the talin rod domain. However, RIAM pathway is dispensable for integrin activation in platelets (Stritt et al., 2015). Rap1 has direct binding sites on talin F0 (K15, R35) and F1 (K98, R118) domains, where F1 R118 was found to be more crucial for platelet GPIIbIIIa activation with the lipid binding loop on F1 (Bromberger, Zhu, Klapproth, Qin, & Moser, 2019; Lagarrigue et al., 2020). Rap1 needs to be in its activated GTP- instead of GDP-bound form to bind talin. A schematic is provided below (Figure 2.3) for a clearer flow of the process: from left to right are Rap1-talin and Rap1-talin-integrin tail.

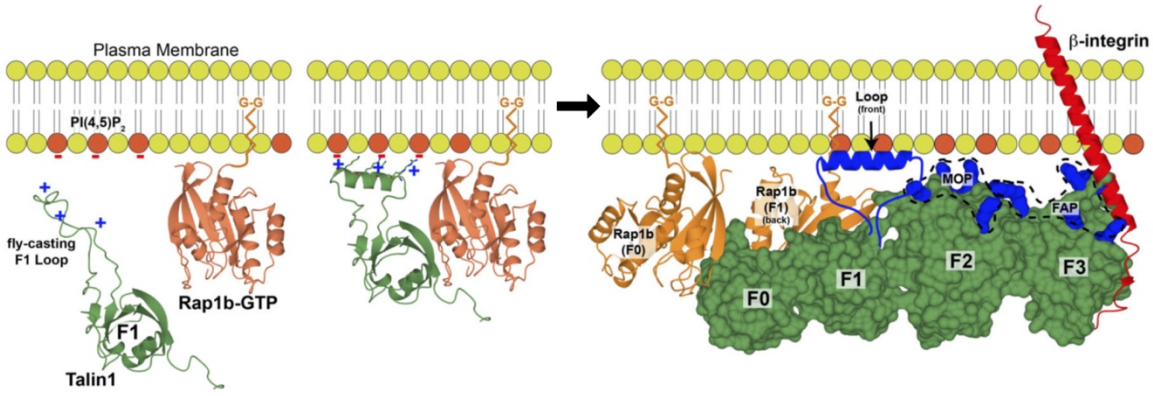

Figure 2.3. Schematic of the Rap1-talin-integrin axis for GPIIbIIIa activation. Adapted from (Gingras et al., 2019).

2.3 Platelet GPIbα

2.3.1 Structure of GPIbα

GPIbα is a ~145 kD platelet-specific receptor that is a part of the GPIb-IX-V complex, which consists of three other glycoprotein units: GPIbβ, GPIX, and GPV with 2:4:2:1 ratio (McEwan et al., 2011). GPIbα is covalently linked to two GPIbβs with a disulfide bond at the membrane-proximal end of the ectodomain (Calverley, Kavanagh, &

Roth, 1998). Its ectodomain comprises a leucine rich repeat domain (LRRD) which contains the binding site for the ligand vWF-A1 and a long stalk that connects the TMD (W. Zhang et al., 2015). GPIbα is abundantly expressed on the platelet with ~25,000 copies (Varga-Szabo, Pleines, & Nieswandt, 2008).

2.3.2 Binding of GPIbα and vWF-A1

Through hemodynamic forces, vWF can reveal its cryptic A1 domain to rapidly associate and dissociate with GPIbα on platelets with fast kinetics (high on-rate and off-rate) to initiate slow rolling of platelets on the injured endothelial surface (Schneider et al., 2007; Yago et al., 2008). Crystal structure of GPIbα in complex with vWF-A1 showed both ends of the LRRD on GPIbα, termed β-finger and β-switch, bind to the top and bottom of A1, respectively (Dumas et al., 2004). This receptor-ligand pair does not support firm adhesion due to the relatively low affinity, but their interaction leads to signalling that can upregulate integrin (mostly GPIIbIIIa) affinity to realize platelet arrest and subsequent outside-in signalling to feedforward the hemostasis cascade (Y. Chen et al., 2019; Shen et al., 2012). In the context of thrombosis, the mechanism is similar, which imposed the challenging of developing safe and effective therapeutics that can separate the hemostasis from thrombosis pathways. Figure 2.4 shows the mechano-signaling of GPIbα-vWF binding under pulling force to activate integrins, in which the cytoplasmic molecules involved are mostly unknown. Botrocetin (Bc, or botro) is a snake venom that was found to enhance affinity of vWF-A1 to GPIbα, resulting in agglutination (aggregation through GPIbα instead of integrins). Kinetic and crystallographic studies showed that Bc reduced GPIbα-A1 off-rate by two-fold in both human and mouse complexes without affecting the

on-rate by two-step a slide-binding mechanism (Fukuda, Doggett, Laurenzi, Liddington, & Diacovo, 2005). Bc binds both GPIbα and vWF-A1.

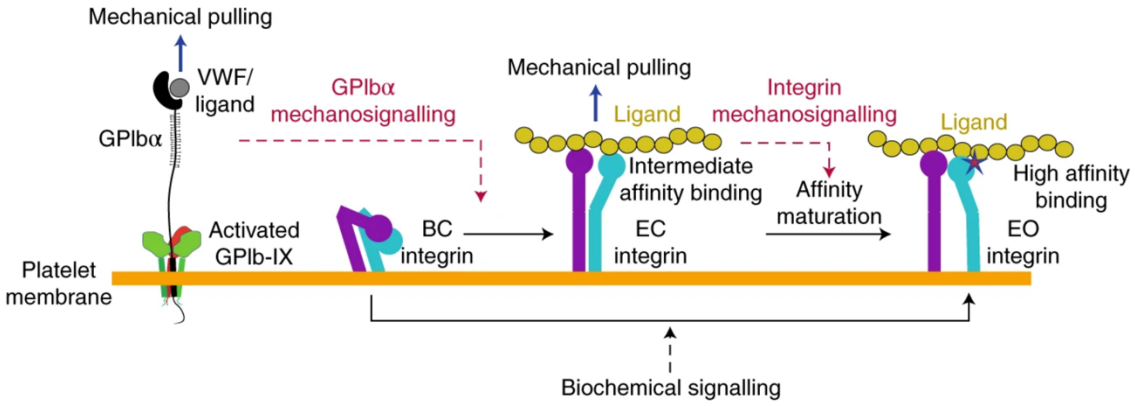

Figure 2.4. Schematic of mechano-signaling of GPIbα to activate GPIIbIIIa. Adapted from (X. F. Zhang & Cheng, 2019).

2.4 Platelet, adhesion, aggregation, and activation

In the early stage of hemostasis or some pathological condition where subendothelial proteins are exposed, platelets are recruited to the active site. In veins and venules where blood flow is relatively slow (< 400 s^{-1}), the initiation of platelet recruitment is mostly mediated by GPVI-collagen interaction; in arterioles and arteries where blood flow is faster (> 800 s^{-1}), interaction between GPIbα and collagen- and endothelium-bound vWF is the first to mediate platelet rolling and adhesion (Nuyttens, Thijs, Deckmyn, & Broos, 2011). GPVI and GPIbα can both initiate signalling cascade (with GPVI considered a more potent signalling molecule) to activate β_1 and β_3 integrins to enable platelet arrest and aggregation. In pathological conditions where disturbed flow and gradient shear are present, platelets can aggregate, which is initiated by GPIbα-vWF binding as well.

Platelets can be activated via multiple pathways, which can be generally classified into two categories: a "biomechanical" (mechano-) pathway that is initiated by mechanosensitive surface glycoproteins (such as GPIbα and GPVI) and a "biochemical" pathway that includes soluble agonist-bound G protein-coupled receptor (GPCR) signalling (such as thrombin receptors PAR1, PAR4, thromboxane A_2 receptor TP, and ADP receptors $P2Y_1$, $P2Y_{12}$). The end results (other than integrin upregulation) of the biomechanical pathway are still elusive, while the biochemical pathway leads to much more potent response of the platelet, especially with strong agonists such as thrombin: integrin activation, cytoskeletal remodelling and degranulation (Kaplan & Jackson, 2011). When platelets are fully activated, the α- and dense granules release more agonists, inflammatory and clotting factors, P-selectin are expressed on the membrane surface, and phosphatidylserine (PS) are exposed (inner leaflet flipped inside-out) by lipid scrambling, which will allow more platelets to get activated, leukocytes to interact, and blood coagulation factors to be recruited to the platelet surface as part of the coagulation cascade (Bevers, Comfurius, & Zwaal, 1983; Rosing et al., 1985). Calcium as a secondary messenger plays a central role in both types of pathways. The calcium signals differ in intensity and duration depending on the stimuli, and the source is from both cytosolic store release and extracellular influx (Varga-Szabo, Braun, & Nieswandt, 2009).

2.5 Transgenic mouse models used in the force spectroscopy study

The phenotypical information of the major mouse models used are listed below:

Table 2.1. Phenotypical and mutation efficiency information of mutant mice that were used for stenosis aggregation and single-cell studies.

PHENOTYPE	WT CTRL	TALIN KO	TALIN W359A MUT	TALIN L325R MUT	B_3 L746A MUT	TALIN F1/F0 MUT	TALIN F1 MUT
Function disrupted		All talin's function	Talin-integrin binding	Integrin activation by talin	Talin-integrin binding	Talin-Rap1 binding	Talin-Rap1 binding
Thrombosis, $FeCl_3$ induced	Thrombosis	Negligible	Negligible	Negligible	Negligible	Unknown	Unknown
Hemostasis, tail clipped	Normal	Uncontrol-lable bleeding	Slight bleeding	Uncontrol-lable bleeding	Uncontrol-lable bleeding	Increased bleeding	Almost normal
Agonists activation	Normal	Minimal	Reduced	Minimal	Minimal	Minimal	Reduced

CHAPTER 3. MATERIALS AND METHODS

3.1 Mice

3.1.1 Mouse strains

Conditional talin1-deficient mice ($Tln1^{fl/fl}$Pf4-Cre+, i.e. talin KO), conditional talin1 (L325R) mutant ($Tln1^{L325R/fl}$Pf4-Cre+) and talin 1 (W359A) mutant mice ($Tln1^{W359A/fl}$Pf4-Cre+), and β_3(L746A/L746A) integrin mutant mice along with their controls $Tln1^{fl/fl}$Pf4-Cre–, $Tln1^{fl/wt}$Pf4-Cre+ (WT/fl) and WT/wt (WT) were generously provided by Dr. Brian Petrich's lab housed at Emory University and described previously (Haling et al., 2011; Petrich, Fogelstrand, et al., 2007; Petrich, Marchese, et al., 2007; Stefanini et al., 2014). CalDAG-GEFI (CalDAG-GEFI$^{-/-}$), conditional STIM1 KO ($STIM1^{fl/fl}$Pf4-Cre+), conditional Rap1 KO ($Rap1a^{fl/fl}Rap1b^{fl/fl}$Pf4-Cre+), conditional talin1 KO ($Tln1^{fl/fl}$Pf4-Cre+) and the control Pf4-Cre+ (Cre+) mice were generously provided by Dr. Wolfgang Bergmeier's lab housed in University of North Carolina, Chapel Hill and described previously (Ahmad et al., 2011; Crittenden et al., 2004; Stefanini et al., 2018). IL4Rα/GPIbα-tg (IL4) mice and streptozotocin (STZ)-induced diabetic mice were generously provided by Dr. Shaun Jackon's lab housed in University of Sydney. Talin1 F1 single mutant ($Tln1^{R118E/R118E}$) and conditional talin1 F1/F0 double mutant mice ($Tln1^{fl/R35E,R118E}$Pf4-Cre+) and their controls $Tln1^{fl/wt}$Pf4-Cre+ and WT/wt mice were generously provided by Dr. Mark Ginsberg's lab housed in animal facilities University of California, San Diego. B6 mice (from Jackson Laboratory) were housed at Georgia Tech.

3.1.2 Mouse handling

The breeding and colony maintenance of the mutant mice and their littermate controls cited above were handled in the respective institutions. The only procedure of handling performed at Georgia Tech was for the STZ-induced diabetic mice. Briefly, B6 mice received were acclimatized for at least 5 days. Male mice of at least 20 g and 6 weeks of age onwards that had been fasted for 6 hours would be converted diabetic by IP injection of STZ at a dose of 55mg/kg in 0.5 M sodium citrate buffer made fresh and used within one hour 5 times over 5 consecutive days. The goal was to create severely and chronically diabetic mice without lateral organ damage that could potentially give rise to platelet diabetic phenotype.

3.2 Reagents

Mouse monomeric and dimeric A1 were generously provided by Dr. Zaverio Ruggeri's lab (The Scripps Research Institute, La Jolla, CA). Human plasma vWF, botrocetin (Bc), antibodies MBC370.2 and SZ22, and clinical integrilin (Eptifibatide) and hirudin were generous gifts from Dr. Shaun Jackson's lab (The University of Sydney, Australia). The antibody AP5 was generously provided by Dr. Peter Newman's lab (Blood Center of Wisconsin). The canonical platelet agonist amplification loop blockade (ALB) cocktail was made from the following pharmacological inhibitors from Sigma: apyrase (0.16 U/ml) to scavenge ADP, MRS2179 (100 μM) to block P2Y1 signalling, 2MeSAMP (10 μM) to block P2Y12 activation, and Indomethacin (10 μM) to block TXA2 generation.

Key commercially available reagents are listed below:

Name	Reagent type	Usage	Company
JON/A-PE	Fluorescently labelled Antibody	Identify activated murine GPIIbIIIa	Emfret Analytics

Leo.F2-PE	Fluorescently labelled Antibody	Stain murine GPIIbIIIa of all conformations	Emfret Analytics
MWReg30-Alexa Fluor 488	Fluorescently labelled Antibody	Stain the expression of murine GPIIbIIIa	BioLegend
Fibrinogen (1D6)-Alexa Fluor 488	Fluorescently labelled Antibody	Stain the site density of human fibrinogen	NOVUS
Xia.B4-FITC	Fluorescently labelled Antibody	Stain the expression of murine GPIX	Emfret Analytics
Xia.G7-FITC	Fluorescently labelled Antibody	Stain the expression of murine GPIbα	Emfret Analytics
Xia.B2	Antibody	Block vWF binding site on GPIbα	Emfret Analytics
PAC-1 (FITC)	Fluorescently labelled Antibody	Identify activated human GPIIbIIIa	BD Biosciences
Zenon Alexa Fluor Mouse IgG Labeling Kit	Fluorescence labelling reagent	Label MBC370.2, SZ22, and AP5 antibodies	Invitrogen
Human fibrinogen	Protein	Interact with human and mouse integrins (predominantly GPIIbIIIa)	Enzyme Research Laboratories
Thrombin (α)	Enzyme	Agonist to platelet	Enzyme Research Laboratories
ADP	Small nucleotide molecule	Agonist to platelet	Sigma Aldrich
Clexane (Enoxaparin sodium)	Pharmaceutical	Anticoagulant	USP Reference Standards
Cytochalasin D	Pharmacological reagent (inhibitor)	Inhibit actin polymerization	Sigma Aldrich
Gouml 6983	Chemical (inhibitor)	Broad spectrum PKC inhibitor	abcam
GsMTx-4	Peptide toxin (inhibitor)	inhibit Na^+ voltage-gated channels and cation-selective mechanosensitive	alomone labs

		and stretch-activated channels	
Quantibrite PE Beads	Standard calibration beads	Calibrate fluorescence intensity	BD Biosciences
Quantum Alexa Fluor 488 MESF	Standard calibration beads	Calibrate fluorescence intensity	Bangs Laboratories
Quantum FITC-5 MESF	Standard calibration beads	Calibrate fluorescence intensity	Bangs Laboratories

3.3 Blood draw

3.3.1 Mouse

Blood draw was described in (Stefanini et al., 2014); briefly, mice were anesthetized with ketamine/xylazine mix (150 mg/kg, 15 mg/kg) at the volume ten times the body weight (diluted with saline); once completely anesthetized, blood was slowly drawn with 22-23 G needle into syringe that contained 40 U/ml clexane (low molecular weight heparin) to prevent platelet activation via inferior vena cava.

3.3.2 Human

For the stenosis microfluidics experiments in Chapter 6, blood was drawn from the vein with butterfly syringe to 800 U/ml hirudin in saline (Sydney) or 20 U/ml clexane with 0.005 U/ml apyrase in modified Hepes Tyrode's (HT) buffer (134 mM NaCl, 12 mM $NaHCO_3$, 2.9 mM KCl, 0.34 mM sodium phosphate monobasic, 5 mM HEPES and 5 mM D-glucose, 1% BSA, pH 7.4) (Atlanta, Emory).

3.4 Cell purification

3.4.1 Platelets

For single cell force spectroscopy experiments, mouse blood after the blood draw was supplemented with additional anticoagulants, 0.005 U/ml apyrase and ACD buffer (85 mM sodium citrate, 72.9 mM citric acid anhydrous, 110 mM D-glucose and 70 mM theophylline, pH 4.6), and transferred to a separation tube supplemented with platelet washing buffer (PWB) (4.3 mM K_2HPO_4, 4.3 mM Na_2HPO_4, 24.3 mM NaH_2PO_4, 113 mM NaCl, 5.5 mM D-glucose, 10 mM theophylline and 0.5% BSA, pH 6.5). The blood was centrifuged at 250 g for 2.5 min with soft brake to separate platelet rich plasma (PRP) from rest of the blood components. The PRP was extracted and centrifuged at 1950 g for 1 min. the platelet pellet was gently resuspended with PWB supplemented with 0.01 U/ml apyrase and 20 U/ml clexane and rested for 5 min before centrifuging again at 1950 g for 1 min. the platelet pellet was then resuspended in HT buffer with 1 mM Ca^{2+} supplemented with 0.02 U/ml apyrase and placed in a 37 °C water bath for 30 min before use. For activation by ADP in BFP, the platelet suspension was incubated with ADP 5 min before experiment; for activation by Mn^{2+} in BFP, the Ca^{2+} in HT buffer was replaced with 0.5 mM Mn^{2+}. For cytochalasin D inhibition, platelets were treated with 10 μM cytochalasin D (or e.q. volume DMSO for control which were both ~4,000 x dilution) at 37 °C for 45 min prior to experiment. For shearing PRP on cone/plate viscometer, mouse blood after the blood draw was supplemented with 0.005 U/ml apyrase and 1 U/ml hirudin and diluted with 1x ACD buffer without the theophylline and HT buffer before centrifuging at 250 g for 2.5 min with soft brake to separate the PRP. The PRP was diluted further with HT buffer (with 1 mM Ca^{2+} unless specified otherwise) a few folds to achieve ~ 50–200k/μL platelet count, and the count was not characterized each time because 20–200k/μL showed similar results as previously published (Deng et al., 2016).

3.4.2 Red blood cells (RBCs)

For single cell force spectroscopy experiments, blood collections followed the protocol approved by the IRB of Georgia Tech after written informed consent was obtained from subjects. ~10 µl of human blood were collected from finger prick and centrifuged to isolate the RBCs which were biotinylated by incubating with biotin-PEG3500-NHS (JenKem) solution and partially swollen by incubation with nystatin (Sigma-Aldrich). Detailed protocol described in (Yunfeng Chen et al., 2015).

3.5 Stenosis microfluidics

3.5.1 Fabrication and operation of the stenosis microfluidics devices

The stenosis device wafer was designed on AutoCad (Figure 3.1) and fabricated at the Georgia Tech nanofacility using photolithography with SU-8 photoresist. The devices were made from casting PDMS on the wafer, where the feature side were attached to air plasma-treated coverslip. The channels were 50 µm thick, 200 µm wide, with two symmetrical pillars. Two types of channels were used: 80% and 90% stenosis corresponding to the gap between the two pillars that create the stenosis; 20 µm gap means the channel is 90% stenosis, and 40 µm gap means 80% stenosis. For the diabetic human study in chapter 6, only one pillar with the same geometry as the 80% stenosis was present in a 130 µm thick, 100 µm wide channel and the flow rate was set to be 16 µL/min.

The channel was coated with 100 µg/mL human vWF mixed with 2.5 µg/mL botrocetin (Bc) from the outlet for 20+ min, then blocked with 2% BSA for 10+ min from the inlet, and then flushing the channel through with HT buffer before starting the experiment. Whole blood from mouse incubated with ALB (1:50 dilution from the cocktail

stock) and anti-GPIX-FITC (1:20 dilution) for 10+ min was perfused through the channel at 13 µL/min for the 90% stenosis and 18 µL/min for the 80% stenosis for 5 min and the flow rates were determined empirically to optimize stable aggregation for the blood from WT mice. Confocal was used (with pin hole at maximum opening) to image the DIC and fluorescence of the whole perfusion process. The imaging plane was set to be close to cover glass on the bottom and adjusted manually for maximum signal-to-noise ratio for the fluorescent channel for thresholding purpose in data analysis.

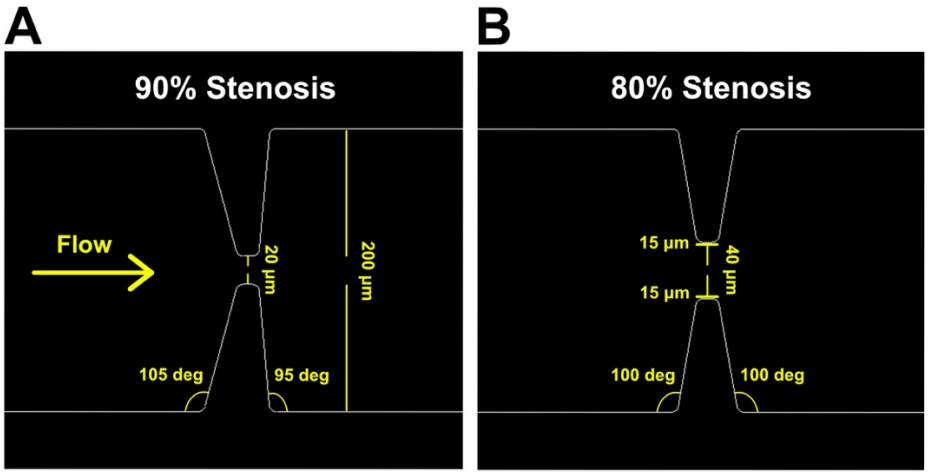

Figure 3.1. CAD drawing with dimensions of the 90% and 80% stenosis region. Channel thickness (z-direction, out of plane) is 50 µm.

For human study in chapter 6, single-pillar channel was used. Human whole blood incubated 10+ min with a combination of two specified antibodies (MBC370.2 or AP5, with SZ22/P2, 1 µg/ml, labeled with either Alexa fluor 488 or 647 by Zenon labeling reagent [Invitrogen]) was perfused through HT buffer-washed channel (no coating or blocking) at 16 µL/min to achieve bulk shear rate of 1800 s^{-1}. Confocal was used (with the same pin hole opening across samples) to image the DIC and fluorescence of the perfusion. The imaging plane was set to be close to cover glass and adjusted manually for maximum

signal-to-noise ratio for the fluorescent channel for thresholding purpose in data analysis. All whole blood perfusion was driven by a syringe pump (Harvard).

3.5.2 CFD simulation (done by Yunduo "Charles" Zhao)

CFD simulations were performed using 354,564 and 359,991 meshing elements for the 80% and 90% stenosis channels, respectively. The mass flow rate was defined as:

$$Q = \frac{2AD_h\gamma_0}{\lambda}, \qquad (1)$$

where γ_0(s^{-1}) was the bulk shear rate, A (m^2) was the cross-sectional area, D_h (m) was the hydraulic diameter, and λ was the shape factor of the device's cross-section. And the parameters were given by the following equations.

$$A = y_0 z_0 \qquad D_h = \frac{4A}{2(y_0+z_0)} \qquad \lambda = \frac{24}{[\left(1-\frac{0.351z_0}{y_0}\right)\left(1+\frac{z_0}{y_0}\right)]^2} \qquad (2)$$

3.5.3 Analysis and fitting of the platelet aggregation growth

All image analyses were performed ImageJ using the program's default image intensity thresholding with stack histogram. GPIX-labeled fluorescent platelet aggregates were auto-thresholded with manual checking such that the earliest micro-aggregates were included in the analysis with minimal background noise. For the set of experiments using talin WA, LR, F1 mutants, β_3 LA mutant, and their controls, since the aggregate growth seemed nonlinear/sigmoidal, the mean traces were all fitted on GraphPad Prism with Hill equation below:

$$Y = \frac{A}{1+(\frac{K}{t})^N}, \qquad (3)$$

where A reflects the amplitude, or saturation level of the curve, K reflects the rate to reach saturation, and N (the Hill coefficient) reflects cooperativity – for this case how much lag till the first platelet deposit. The independent variable is *t* (time). For the set of experiments using talin KO, Rap1 KO, CalDAG-GEFI KO, STIM1 KO, and the Cre+ control, the mean traces were fitted with linear equation.

3.6 Cone/plate viscometer-FACS (flow cytometry assay)

Freshly prepared 50 μL murine PRP was gently mixed with 2.5 μg/mL Bc and 1.25 μL undiluted JON/A-PE and incubated at 37 °C for 1 min and transferred to the stationary plate surface of a CAP2000+ cone/plate viscometer (Brookfield Engineering Laboratories, Middleboro, MA, USA). The sample was uniformly sheared at rates ranging from 0 (stationary control) to 10k s^{-1} for 2 min at 37 °C, after which the sample was collected and fixed with 2% paraformaldehyde (PFA) for 15+ min. The sample was then analysed by Accuri C6 flow cytometer (BD Biosciences) after it was diluted 10x with HT buffer.

3.7 2D Kinetic assays and analyses

3.7.1 Biomembrane force probe (BFP) force-clamp and rupture assays

The BFP is a single-cell force spectroscopy and the method in detail was described in (Yunfeng Chen et al., 2015). Briefly, the experiment setup of the BFP is shown in Figure 3.2: a bead coated with ligand of interest (in most cases of the thesis, fibrinogen) is attached to the apex of a spherical red blood cell (RBC) via SA-biotin interaction, which acts as an ultra-sensitive force transducer and is aspirated by a micropipette. A second pipette holds a live platelet (right side) is brought into contact with the bead, allowing binding between fibrinogen and GPIIbIIIa under a user-selected compression. The platelet holding pipette

will then retract to a predefined nano-scale distance, applying tensile force on the interacting molecules. This process is done in repeated cycles to increase the statistical power of the experiment.

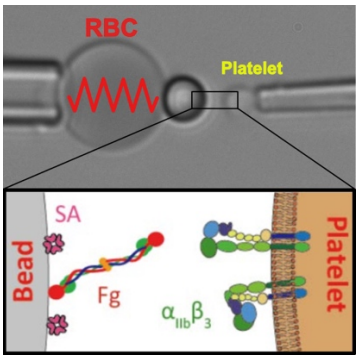

Figure 3.2. The setup of BFP and schematic of bead-coated ligand interacting with the integrin receptor on platelet. Adapted and modified from (Ju et al., 2018).

The deformation of the RBC tracked by the bead-RBC interface records 1) whether a binding event occurred and 2) the bond lifetime under a tensile (clamped) force, with a longer lifetime implying stronger binding. Figure 3.3 illustrates the types of events recorded – lifetime event shows a bond is formed and lasts certain amount of time, rupture event shows the bond dissociated before reaching the set clamp force, and no adhesion shows no bond was detected. We could also raise the retraction distance to correspond to > 1000 pN that would guarantee to rupture noncovalent bonds to measure rupture forces of receptor-ligand of interest. For the lifetime measurement (force clamp), the adhesion frequency between the receptor and ligand is kept ~20% to ensure most (~89%) interactions are single-bond (B. T. Marshall et al., 2003). The data recording and analysis were performed using customized LabView (National Instrument) programs.

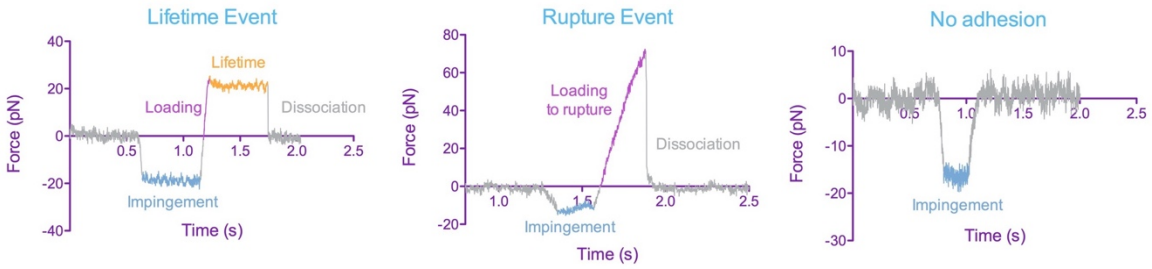

Figure 3.3. BFP raw data: individual events force over time traces.

3.7.2 Dual BFP setup

To probe the crosstalk between GPIbα and GPIIbIIIa, a dual BFP is used instead (Ju et al., 2017). A platelet would be subjected to interact with two different ligands: first a bead coated with vWF-A1 (GPIbα ligand); once a bond lifetime is formed, the platelet would be (within one minute) switched to a second bead coated with fibrinogen (GPIIbIIIa ligand), where adhesion frequency would be measured. Details in (Ju et al., 2017).

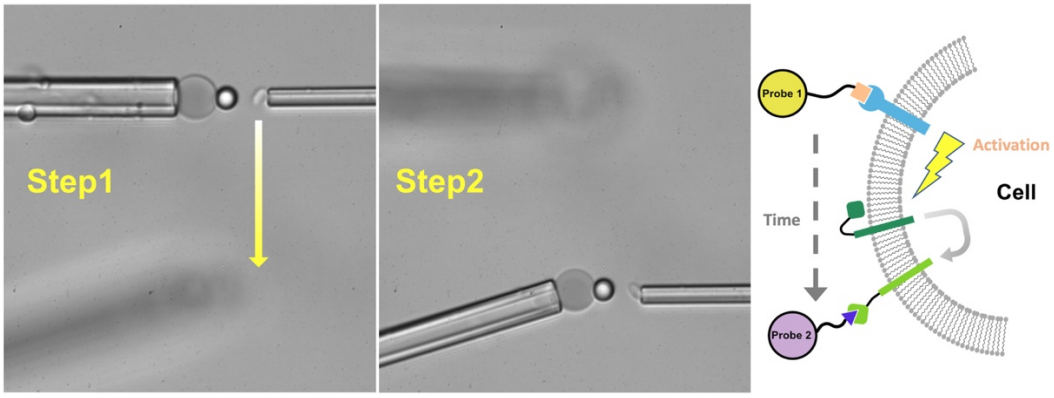

Figure 3.4. Illustration of the dual BFP process.

3.7.3 General BFP bead functionalization

Glass beads (~2µm diameter) were first functionalized with 3-Mercapto-propyltrimethoxysilane (MPTMS) to be thiolated. Maleimide-PEG3500-N-

hydroxysuccinimide (MAL-PEG3500-NHS, JenKem) linker was used to mix with the protein of interest (fibrinogen, vWF-A1), enabling the protein to attach to the thiolated glass bead surface. Then, streptavidin (SA)−MAL (Sigma) was added to so that the bead can be attached to biotinylated RBC.

3.7.4 Adhesion frequency assay

The BFP setup can also be used for the adhesion frequency assay, where the adhesion frequency of the cell and ligand-coated bead is measured by counting adhesion events over 50 contact cycles. Longer contact time would increase the probability of adhesion (Chesla, Selvaraj, & Zhu, 1998). The contact time vary from 0.1 s, 0.2 s, 0.5 s… all the way till adhesion saturation (for mouse GPIIbIIIa and fibrinogen interaction, saturation reached within 2 s of contact time, Figure 5.4). Thus, adhesion frequency over contact time can be fitted with the equation below assuming single step 1st order reaction (Chesla et al., 1998):

$$P_a = 1 - \exp(-< n >) \qquad (4)$$

$$\text{and} \quad < n > = m_r m_l A_c K_a \left[1 - \exp\left(-k_{off} t_c\right)\right], \qquad (5)$$

where $<n>$ is the average number of bonds per contact, m_r the expression level of the receptor (GPIIbIIIa) on the platelet, m_l the density of coated ligand (Fg) on the bead (both can be measured with flow cytometry), A_c the contact area, K_a the 2D affinity (in μm^2), k_{off} the off-rate (s^{-1}), and t_c the contact time. A_c and K_a are lumped together as the effective 2D affinity A_cK_a since they cannot be separated in curve fitting (Chesla et al., 1998).

3.7.5 Measurement of molecular site density and receptor expression

The m_l and m_r were determined via flow cytometry (FACS). Platelets or beads were incubated with fluorescently tagged monoclonal antibody against the molecule of interest at 10 μg/ml (or as suggested by product instruction) at room temperature for beads and 37 °C for platelets for 30 minutes and washed for 2 times – platelets were fixed with 2% PFA for 10+ min before washing. The washing buffer for the beads was phosphate buffer while for the platelets, the HT buffer. Isotype IgGs were added at equal amount to the respective samples. The fluorescence intensities were measured by Accuri C6 flow cytometer (BD Biosciences) and compared to standard calibration beads (for PE, FITC, or Alexa fluor 488) to determine the fluorescence intensity per cell or bead. The site densities were estimated by assuming both the platelet and the bead were spheres with 2 μm diameter.

3.7.6 Lifetime by force bin analyses

The lifetime distributions for each force bin can be presented by a survival curve: Ln of fraction of measurements with a bond lifetime > the lifetime shown on the x-axis (Figure 5.6). For each force bin, the survival frequency can either be fitted to a two-state or three-state models that are extension of Bell model (Bell, 1978), by differentiating bonds to be fast-, intermediate-, and slow-dissociation species (Wei Chen, Lou, & Zhu, 2011; Ju, Dong, Cruz, & Zhu, 2013). The theory is that there exist multiple species of bonds with off-rates that all follow the Bell model. The two-state fitting equation is shown below:

$$Survival\ frequency = \omega_1 \exp(-k_1 t_b) + \omega_2 \exp(-k_2 t_b), \qquad (6)$$

where $\omega_1 + \omega_2 = 1$, and for three-state fitting, equation (7) is used:

$$Survival\ frequency = \omega_1 \exp(-k_1 t_b) + \omega_2 \exp(-k_2 t_b) + \omega_3 \exp(-k_3 t_b), \qquad (7)$$

where $\omega_1 + \omega_2 + \omega_3 = 1$. $k_1, k_2, and\ k_3$ are the forced off-rates, and $\omega_1, \omega_2, and\ \omega_3$ are fractions of the short-, long-, and intermediate-lived bonds. For two-state fitting, only two species of bonds (or two states of the receptor) are considered.

3.7.7 Bond memory effect analysis

Memory index was used to quantify the memory effect of bonds, i.e. how likely is another bond to form again after a previous bond formation (Zarnitsyna et al., 2007). The memory index can be obtained by calculation or by modelling. The method used for this thesis was by calculation using the following equation (Zarnitsyna et al., 2007):

$$\Delta p = p_{11} - p_{01} = \frac{n_{11}}{n_{11}+n_{10}} - \frac{n_{01}}{n_{01}+n_{00}}, \qquad (8)$$

where Δp is the memory index, or the difference between the probability of having adhesion in the next contact if the previous contact also resulted in adhesion and the probability of having adhesion in the next contact if the previous contact was no adhesion. The probabilities were calculated by counting the events of transitioning from no adhesion to adhesion and vice versa, and consecutive adhesions or no adhesions; the details were explained in (Zarnitsyna et al., 2007). For the data included for this analysis, the inclusion criteria are: 1) adhesion frequency higher than 15%, 2) cannot have less than 50 events as well less than ten of the 0-1, 1-0 transitions.

3.8 Statistical analyses

Methods for statistical analyses were all indicated for each data graph in the caption. For significance, N.S. means not significant, * means $P < 0.05$, ** means $P < 0.01$, *** means $P < 0.001$, and **** means $P < 0.001$.

CHAPTER 4. TALIN REGULATES DISCOID PLATELET AGGREGATION IN DISTURBED FLOW

Disclaimer: this chapter was made possible with the help of graduate student Sam Ehrlich (mentee) to run and provide initial analysis of the stenosis microfluidics experiments, graduate student Yunduo (Charles) Zhao's contribution of the CFD simulation (University of Sydney), the transgenic mice and blood sample collection provided by Dr. Wolfgang Bergmeier's lab (University of North Carolina, Chapel Hill), and the transgenic mice provided by Dr. Brian Petrich (Emory University) and Dr. Mark Ginsberg (University of California, San Diego).

4.1 Introduction

"Biomechanical" platelet aggregation, which was coined to define platelet aggregation induced by disturbed flow (Y. Chen et al., 2019), had not been strategically studied using mouse models and suitable flow chambers. Most of the previous studies used collagen-coated flat channels for whole blood perfusion to examine platelet adhesion and aggregation, where the phenotypes of the mouse models were cataloged (Lagarrigue et al., 2020; Nieswandt et al., 2007; Petrich, Marchese, et al., 2007; Stefanini et al., 2014). Despite the importance and relevance to in vivo situations, collagen flow study is not mechanistic as a myriad of processes would happen simultaneously: collagen capturing plasma vWF, engagement and signaling of vWF receptors (GPIbα, GPIIbIIIa) and collagen receptors (GPVI, $\alpha_2\beta_1$), and agonist feed-forward loops amplifying platelet activation (Cosemans, Iserbyt, Deckmyn, & Heemskerk, 2008; Kaplan & Jackson, 2011). Thus, tools

that can isolate the biomechanical contribution for the aggregation are pressingly needed for understanding platelet mechanobiology.

A microfluidics-based stenosis device elegantly showed change of shear alone drove thrombus formation in a seminal paper (Nesbitt et al., 2009). In this study, the agonist amplification loop was blocked with a cocktail of inhibitors, and GPIbα and GPIIbIIIa emerged to be major initiator and mediator of the process. Similar studies demonstrated that gradient shear was more pro-thrombotic than constant, high shear (Goncalves, Nesbitt, Yuan, & Jackson, 2005; Nesbitt et al., 2009; Tovar-Lopez et al., 2010). Among other reasons, explanations include that the leading end of vWF experiences a different strain rate than the trailing end, thus lowering the forces needed to unfold the protein (Rana et al., 2019), and that low oscillatory flow is needed for maintaining stable and bulky platelet aggregates (Nesbitt et al., 2009). Another study identified GPIIbIIIa rather than GPIbα to be the major mechano-receptor that mediated platelet activation in temporal shear gradient which also required calcium influx (Goncalves et al., 2005). A stable intermediate affinity state of GPIIbIIIa was identified by our lab as a result of shear gradient-induced GPIbα mechano-signaling and it mediates the biomechanical thrombus growth (Y. Chen et al., 2019). The follow-up questions focus on the intracellular molecules participating in the crosstalk between GPIbα and GPIIbIIIa. In this chapter of the thesis, we will extend the stenosis microfluidics study to a few important mouse models to test their aggregation.

Talin's role in rapid biomechanical platelet aggregation was relatively unexplored, although its mechanical properties and interactions with vinculin had been well studied in the context of focal adhesions and cell migration (Elosegui-Artola et al., 2016; Jiang, Giannone, Critchley, Fukumoto, & Sheetz, 2003; Kumar et al., 2016; Margadant et al.,

2011; Yao et al., 2016). Even though integrin function in fibroblasts and white blood cells is distinct from that in platelets (Klapholz & Brown, 2017), talin is a well-conserved major mechanosensor that links the integrin to the cytoskeleton. Since talin is the last step of integrin inside-out activation, we postulate that talin is involved in GPIbα mechano-signaling, but whether both MDR and MPR interactions are involved is yet to be specified. The contribution of Rap1, immediately upstream of talin, particularly in platelet, is also likely significant. Phosphoinositide 3-kinase (PI3K) had been identified as essential for shear-dependent platelet firm adhesion and spreading on vWF (Yap et al., 2002). PI3K would be an early effector in GPIbα mechano-signaling, as it could directly interact with 14-3-3ζ which is an adaptor-signaling molecule for GPIbα (Y. Chen, Ruggeri, & Du, 2018). However, the study by Yap et al. in 2002 was not done in the discoid platelet aggregation in disturbed flow context. We explored calcium signal integrator for platelet activation (diacylglycerol, or DAG-regulated guanine nucleotide exchange factor: CalDAG-GEFI), which can activate Rap1 (Stefanini & Bergmeier, 2010), and intracellular calcium sensor stromal interaction molecule 1 (STIM1) that is more important for pro-coagulant than pro-adhesive activity (Ahmad et al., 2011; Lang, Munzer, Gawaz, & Borst, 2013).

4.2 Results

4.2.1 Optimization of a stenosis microfluidics technique to study murine platelet "biomechanical" aggregation that is mediated by GPIbα-vWF interaction

We first need to establish a method to evaluate the biomechanical aggregation of murine platelets. Unlike human platelets that can aggregate even without any prior coating (Brazilek et al., 2017; Nesbitt et al., 2009), murine platelets do not aggregate without prior coating nor with murine vWF, monomeric or dimeric A1 (data not shown). Thus, artificial

forcing of linkage between vWF and the GPIbα by botrocetin (Bc) was found to be necessary to initiate platelet deposition and aggregation, which was recently described (Selvadurai et al., 2019). We adapted this coating method and experimental protocol to establish consistent formation of platelet aggregates with WT mice in our 50 μm-high devices (as opposed to the 100 μm-high in the publication). Due to the fabrication limit of soft photolithography at the Georgia Tech nano-facility, and the observation that most aggregates form on the bottom (due to gravity) portion of the channel (Brazilek et al., 2017), we deem the 50 μm-high adaption appropriate. We empirically found the flow rate optimal for observing steady platelet aggregation to be 18 μL/min for the 80% and 13 μL/min for the 90% stenosis channel.

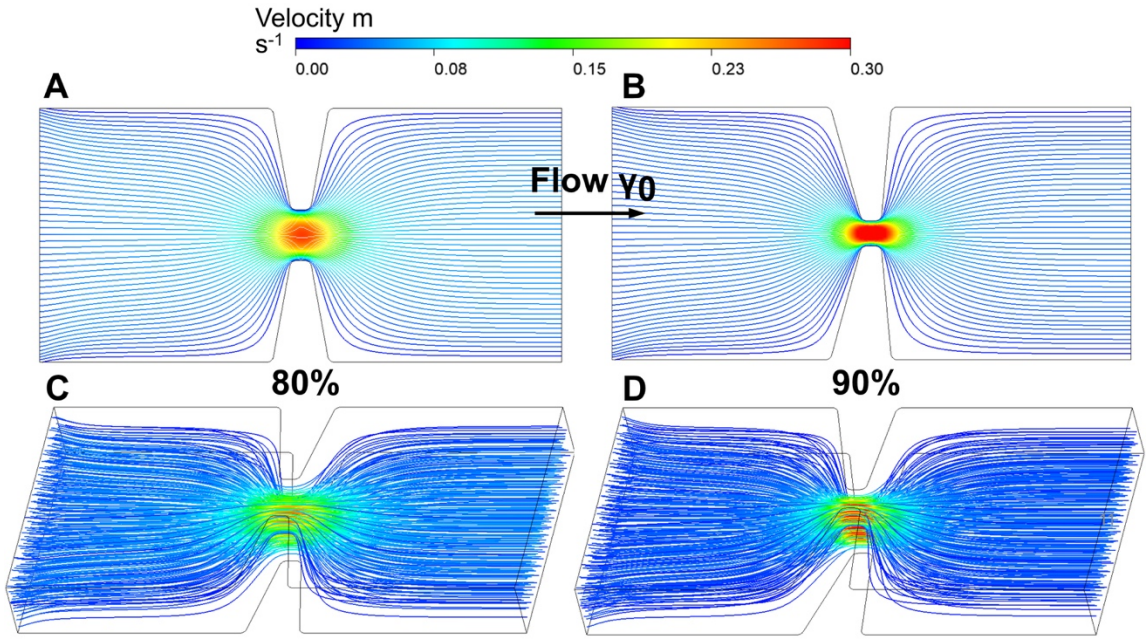

Figure 4.1. CFD simulation: 2D and 3D velocity gradient of the 80% and 90% stenosis channels. (A) 2D velocity streamlines for 80% stenosis channel, (B) 2D velocity streamlines for 90% stenosis channel, (C) 3D velocity streamlines for 80% stenosis channel, (D) 3D velocity streamlines for 90% stenosis channel. Simulations and graphs contributed by Yunduo "Charles" Zhao from the University of Sydney.

CFD simulation showed the velocity sharply increased right before the stenosis (acceleration or contraction zone) and quickly decreased immediately downstream of the stenosis (deceleration or expansion zone) for both the 80% and 90% stenosis channels, with the 90% having a steeper gradient (Figure 4.1). Platelets would accumulate in the expansion zone post-stenosis. CFD simulation found the bulk shear rate to be 3460 s^{-1} for the 80% stenosis and 2500 s^{-1} for the 90% stenosis channel (Figure 4.2). The 2D image (Figure 4.2 A and B) showed streamlines a plane at the mid-point of the z-direction. Peak strain rate (1 μm away from the tip of the pillar) was ~54,880 s^{-1} for the 80% stenosis and ~112,200 s^{-1} for the 90% stenosis channel. Shear rate near the pillar tip was mostly around 15k s^{-1} for the 80% and 30k s^{-1} for the 90% stenosis channel. In severe stenosis regions in the body, shear rate of up to 400,000 s^{-1} can be found (D. Kim, Bresette, Liu, & Ku, 2019).

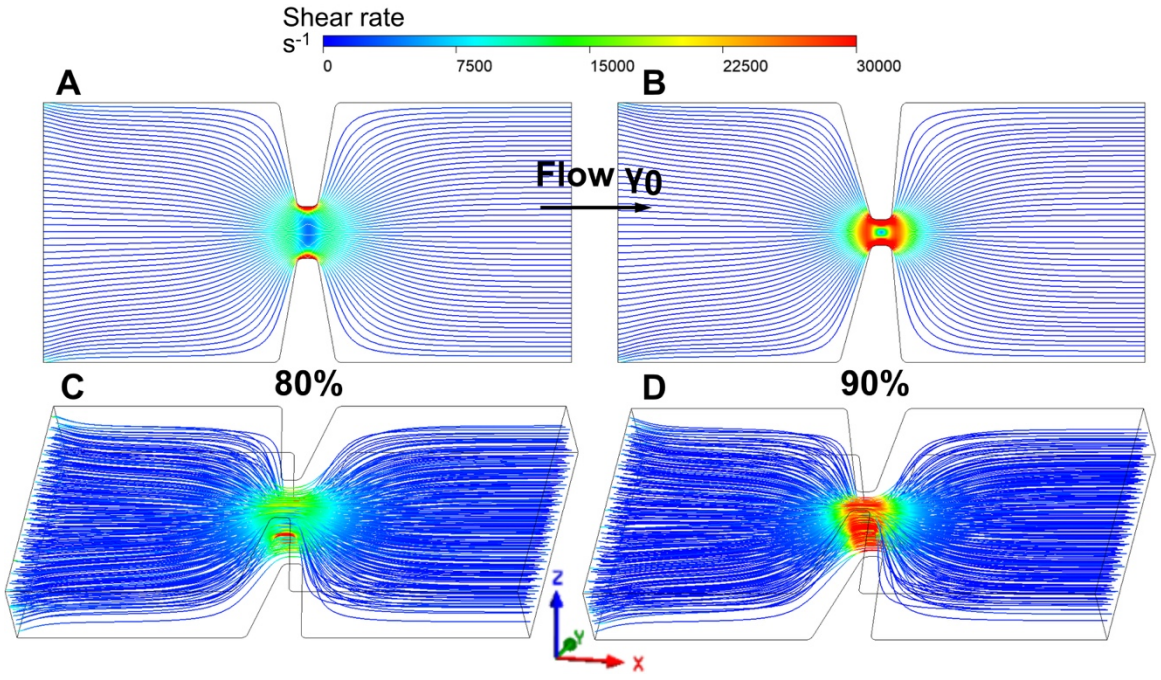

Figure 4.2. CFD simulation: 2D and 3D shear gradient of the 80% and 90% stenosis channels. (A) 2D shear rate streamlines for 80% stenosis channel, (B) 2D shear rate streamlines for 90% stenosis channel, (C) 3D shear rate streamlines for 80% stenosis channel, (D) 3D shear rate streamlines for 90% stenosis channel.

Simulations and graphs contributed by Yunduo "Charles" Zhao from the University of Sydney.

4.2.2 Rap1-talin axis is important for biomechanical aggregation of platelets while CalDAG-GEFI and STIM1 seem dispensable

Perfusion of ALB whole blood labelled with platelet receptor-specific fluorophore (GPIX antibody-conjugated) through the stenosis channel gives rise to platelet aggregation that can be quantified with thresholding (Figure 4.3). Platelets were mostly in discoid shape (videos not shown). We plotted the fluorescence area (μm^2) over time (s) (mean + SEM), shown in Figure 4.4, for both the 80% and 90% stenosis channels. Talin WA mutant, integrin β_3 LA mutant, talin F1 mutant all showed defective aggregation and generally less stable platelet aggregates during the ~5 min aggregation process compared to the WT controls. Surprisingly, talin LR mutant did not seem to show any defect (n=2), even though in collagen flow chamber, they had the most impaired phenotype similar to talin KO (Stefanini et al., 2014). In vivo data in (Stefanini et al., 2014) also showed full protection from thrombosis in LR mice. Unfortunately, the difficulty of LR mouse breeding left us no chance to repeat the experiment.

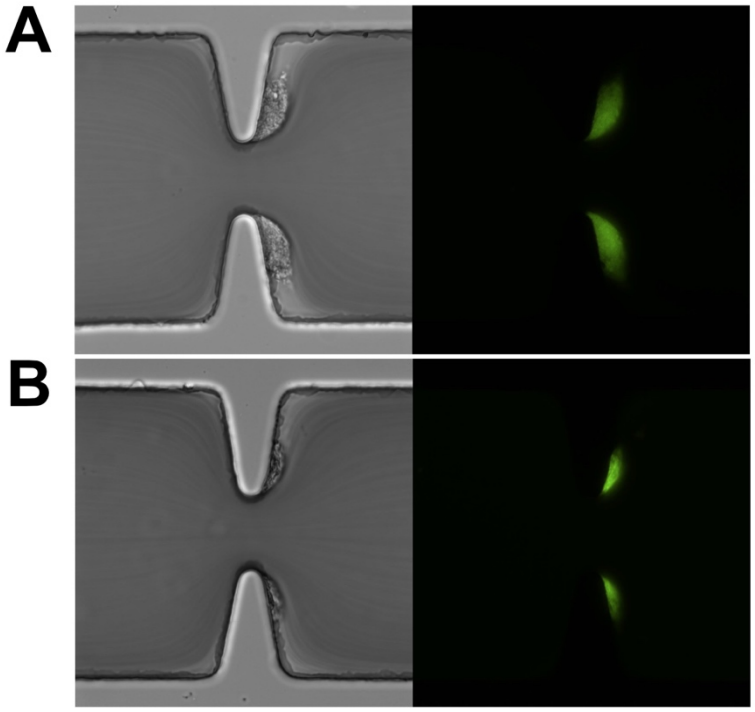

Figure 4.3. Representative images of the stenosis microfluidics experiment. (A) Snapshot of WT platelet aggregation in DIC and confocal fluorescent channel; (B) Snapshot at similar running time point of β_3 LA mutant platelet aggregation in DIC and confocal fluorescent channel.

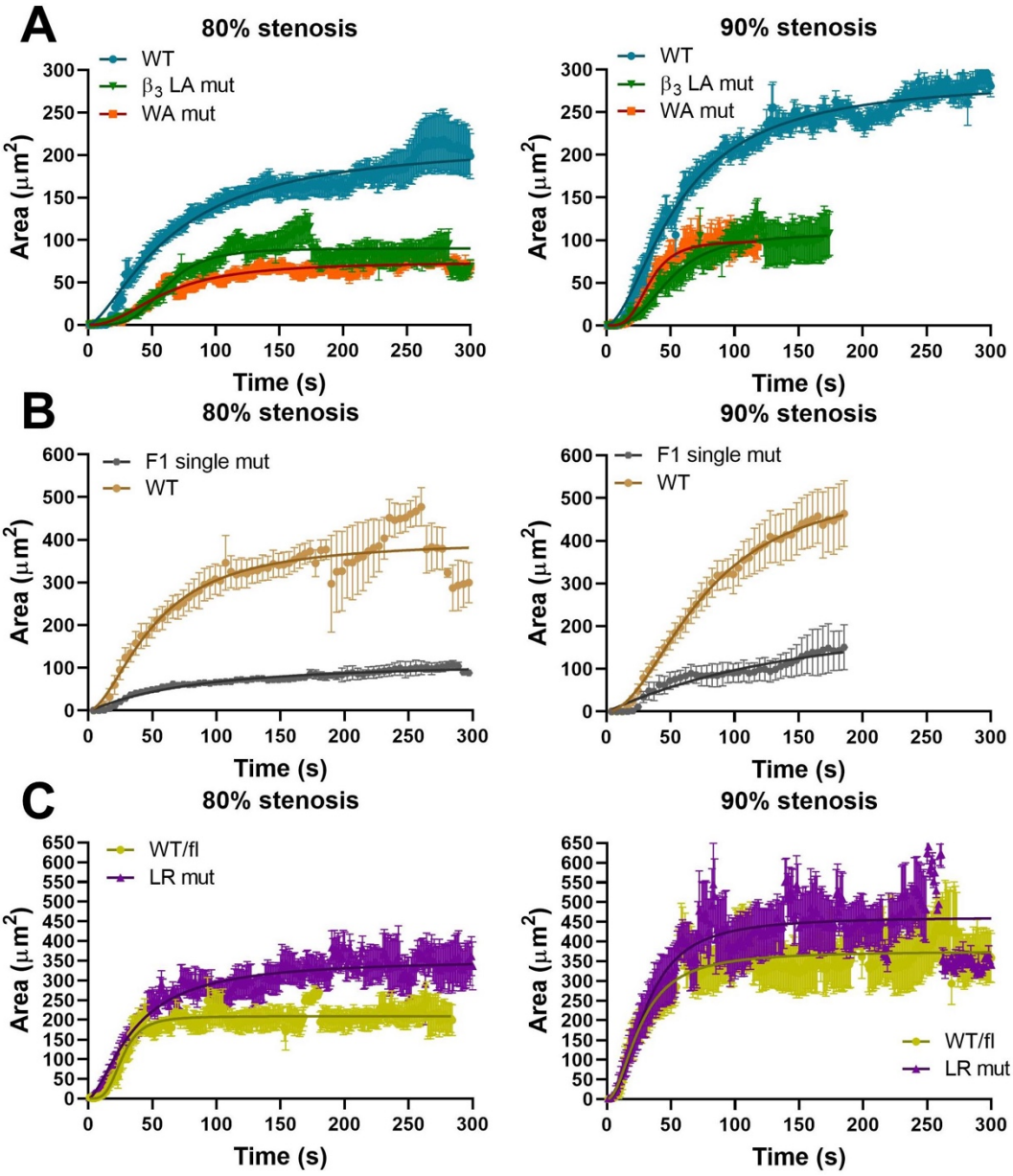

Figure 4.4. Fluorescence area of platelet aggregates in stenosis microfluidics reveals defects of talin and integrin β_3 mutants. All graphs show mean ± SEM over time with sigmoidal line fitting described in methods, and the left side presents results from 80% stenosis channels while the right side 90% stenosis channels. (A) WT control, talin WA mutant, and integrin β_3 LA mutant; (B) WT control and talin F1 single mutant; (C) WT/fl control and talin LR mutant. Each data trace represents ≥ 4 experiments (most far more than 4); 2 of each type of mouse were used.

To quantitatively compare the fluorescence traces of each experiment for the mouse models, we fitted the mean fluorescence areas (by mouse and channel type) with the Hill

equation as most of the traces appeared sigmoidal (lines in Figure 4.4, parameters in Figure 4.5). The fitted parameters were A, K, and N. A represents the saturation level of the curve, and we interpret that the larger the A, the bulkier platelet aggregate is. K reflects the rate of growth to reach the saturation, but since for each mouse type, the saturation levels largely differ, this parameter cannot truly be used to compare how fast the aggregate grows. A better way to compare growth rate is getting the instantaneous rate of change; we plotted the first derivative of the curves but found it's easier to just see from Figure 4.4 which mean traces have larger slopes. N represents how "sigmoidal", or how much lag time before the first platelet deposit; the smaller the N, the less lag there is, which would imply more pro-thrombotic.

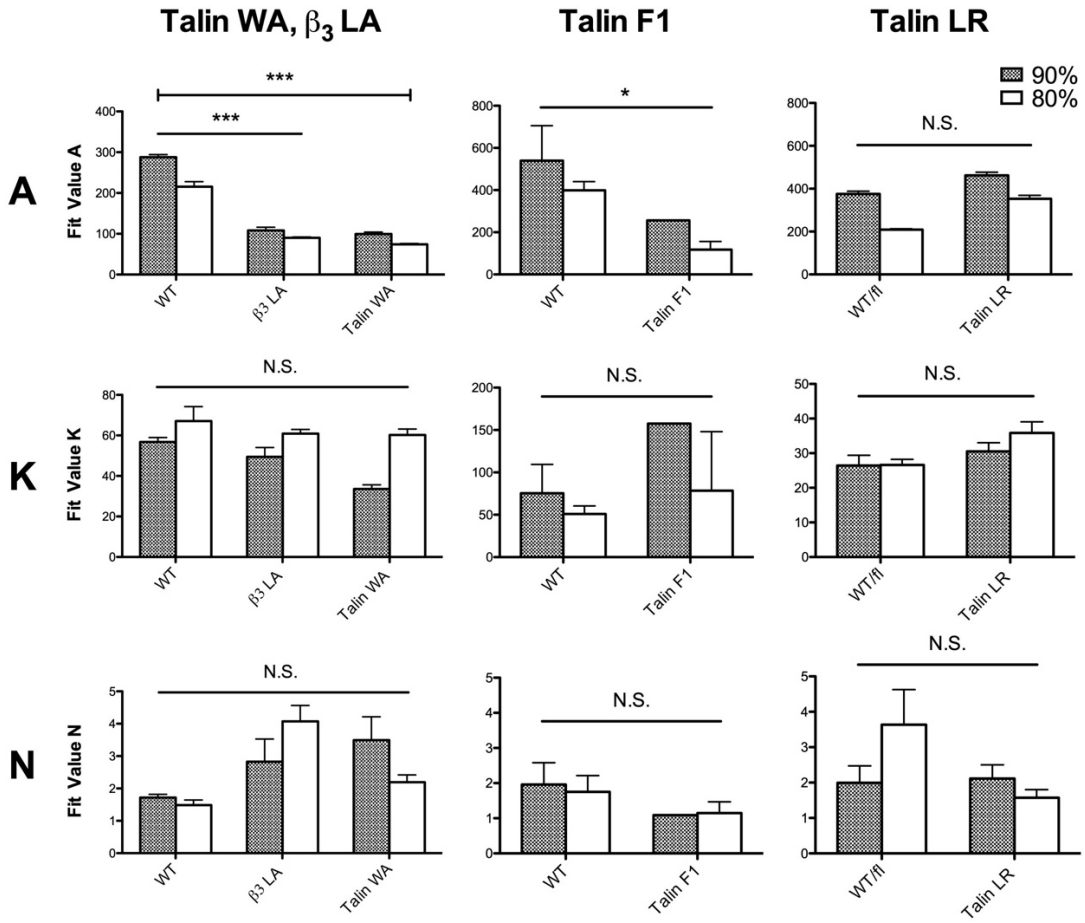

Figure 4.5. Fit values of the mean fluorescence area traces show difference of mutants in both rate and bulkiness of platelet aggregation. All data display mean values with 95% CI. Shown in the graphs are A, K, and N fit values for WT control, talin WA mutant, and integrin β_3 LA mutant, WT control and talin F1 single mutant, and WT/fl control and talin LR mutant. Statistics was performed using one-way ANOVA with Tukey's test.

The results show WA and LA had much less bulky platelet aggregates compared to the WT control, and talin F1 single mutant also barely aggregated at all so the fit with the Hill equation was worse. Even though no significant difference was found for N among WA, LA, and WT control, the trend was larger Ns for the mutants for both 80% and 90% channels compared to WT, which meant more lag time for the mutants. There was no difference between the WA and LA mutants. Since both mutations disrupt the same general binding site, while WA is on talin, and LA on β_3 integrins only, the results from both being similar suggests that β_3 integrins are the predominant mediator of the biomechanical platelet aggregation, and their linkage to the cytoskeleton by talin is critical to maintain the aggregate under pathologically high shear. To confirm that the aggregation was initiated by GPIbα-vWF binding, channel control experiments were performed using botrocetin-coating only (sans the human vWF) or with same coating but pre-incubating the blood with murine GPIbα inhibitor (Figure 4.7 B), and platelets hardly aggregated at all in those conditions. To be more confident about the phenotypical results due to disruption of talin-integrin or talin-Rap1 interactions, we measured the GPIbα expression level of the LA and WA mutants along with their controls on the same day and found no apparent difference (Table 4.1). Note that for the comparison purpose, the unit mean fluorescence intensity (MFI) was used instead of number of copies because the F/P ratio of the fluorescently-tagged antibody was not determined.

Table 4.1. FACS results show platelets from mutant mice have similar size and GPIbα expression level.

	WT	β_3 LA mut	WT/fl	Talin WA mut
GPIbα expression (MFI/μm^2)	1190	1188	1143	1380
Platelet size (FSC-A)	99,884	94,607	100,493	96,560

In search for other potential intracellular mediators, we travelled to University of North Carolina Chapel Hill to test other platelet mutants on the stenosis microfluidics. For this batch of mice with a different bleeding method (retro-orbital), the platelet aggregation generally saturated at a large size, and increased more linearly (Figure 4.6), thus the comparison was made with the linearly-fitted slopes of the mean traces. Interestingly, CalDAG-GEFI and STIM1 did not show a defect, while talin KO and Rap1 KO did (Figure 4.7 A). The results reinforced what was observed for the talin mutants, and suggest that the mechano-signalling pathway from GPIbα to GPIIbIIIa is a specific pathway that merges with other pathways at Rap1 and talin, the common last-step of all agonist-induced inside-out activation pathways of integrins (Shattil et al., 2010).

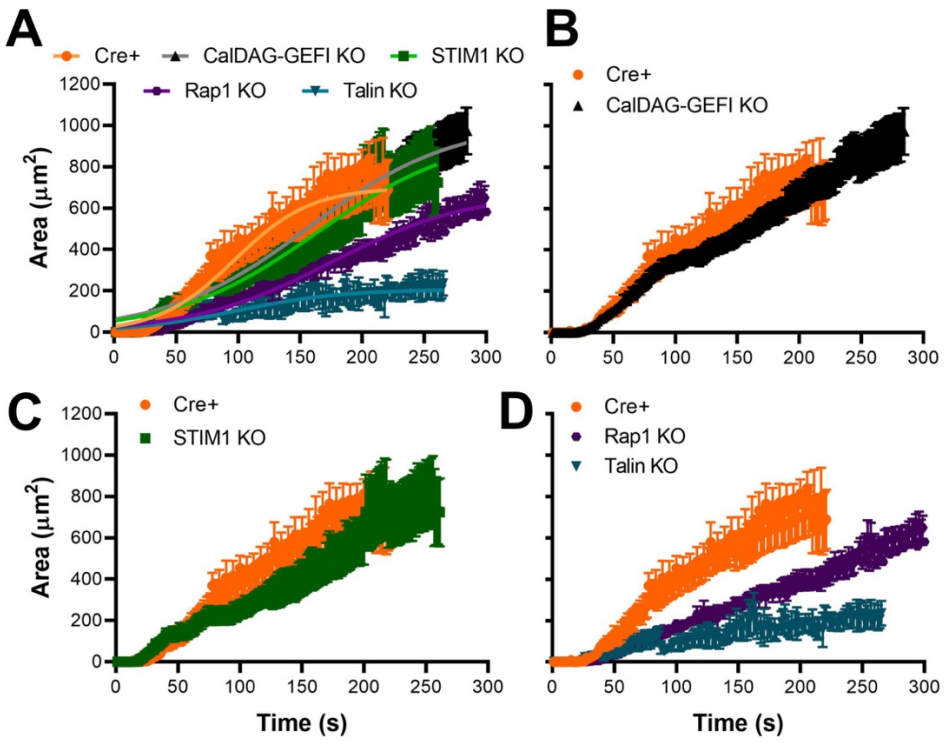

Figure 4.6. Fluorescence area of platelet aggregates in stenosis microfluidics reveals defects of Rap1 KO and talin KO, but not CalDAG-GEFI KO or STIM1 KO. All plots are mean ± SEM over time. (A) Traces altogether, (B) Overlay of CalDAG-GEFI KO and the Cre+ control, (C) Overlay of STIM1 KO and the Cre+ control, (D) Overlay of talin KO, Rap1 KO, and the Cre+ control. ≥ 2 of each type of mouse were used.

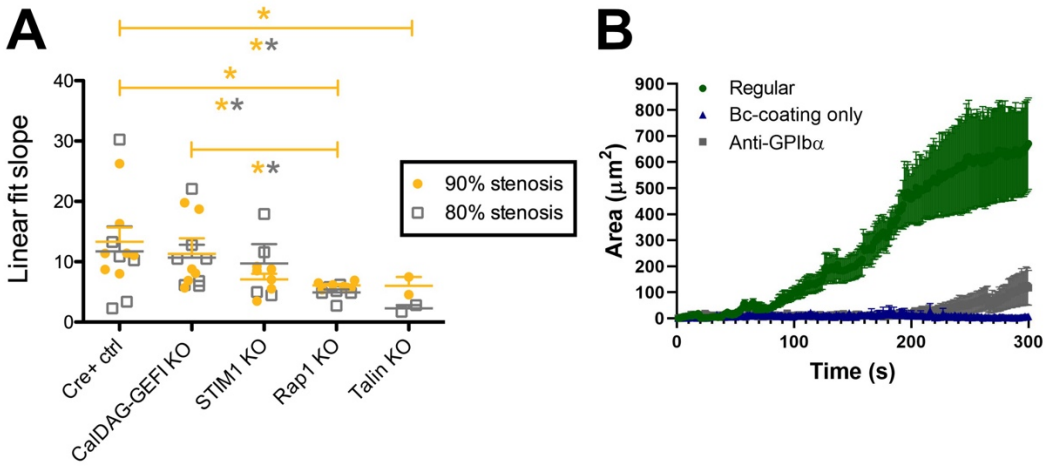

Figure 4.7. Fit values of fluorescence area traces show differences of knockouts in both rate and bulkiness of platelet aggregation. (A) Comparison of slopes of the

linear fits for each trace (yellow, 90% stenosis; gray, 80% stenosis) – two-tailed unpaired t-test with Welch's correction was used for the comparisons. Since the 80% and 90% stenosis aggregation dynamics looked similar, two stars (**) noted with both yellow and gray colors show the significance if considering 80% and 90% results together. Single star (*) indicated significance if just considering 90% stenosis results. (B) Control experiments with channel coated with only botrocetin without vWF (Bc-coating only) or with GPIbα inhibitor-incubated whole blood (Anti-GPIbα) show that in these conditions, aggregates barely formed compared to the experiments with normal coating and without GPIbα inhibitor (Regular).

4.2.3 Characterization of a rapid method to test if talin binding to integrin GPIIbIIIa is necessary in the crosstalk between GPIbα and the integrin independent of resisting shear forces

Talin has at least two roles when interacting with integrins – activating and linking integrin to the cytoskeleton. To elucidate talin's function in the mechano-signaling through GPIbα, we want to compare integrin's affinity state when it can normally bind talin versus when it cannot. The stenosis microfluidics is a useful tool for platelet functional studies, but not so useful to identify the affinity state of integrins because the assay is convoluted with the effect of cytoskeletal linkage. When a defect is observed for platelet aggregation for the talin mutant, it is unclear whether platelets not being able to withstand shear forces was due to weak cytoskeletal support or the integrin affinity state being lower. We needed a method to probe integrin and ended up choosing the cone/plate viscometer, or rheometer (Y. Chen et al., 2019; Deng et al., 2016). The instrument can uniformly shear platelet mixture or PRP, or even whole blood; after the shearing application, one can perform subsequent biochemical assays to study the effect of such shear forces using methods such as flow cytometry (Chow, Hellums, Moake, & Kroll, 1992; Deng et al., 2016; Quach et al., 2018) and Western blot (Moake, Turner, Stathopoulos, Nolasco, & Hellums, 1988; Razdan, Hellums, & Kroll, 1994). This method

is modular because one can define the shear rate/shear force, time, and temperature, and have the flexibility of performing a variety of concurrent or subsequent assays.

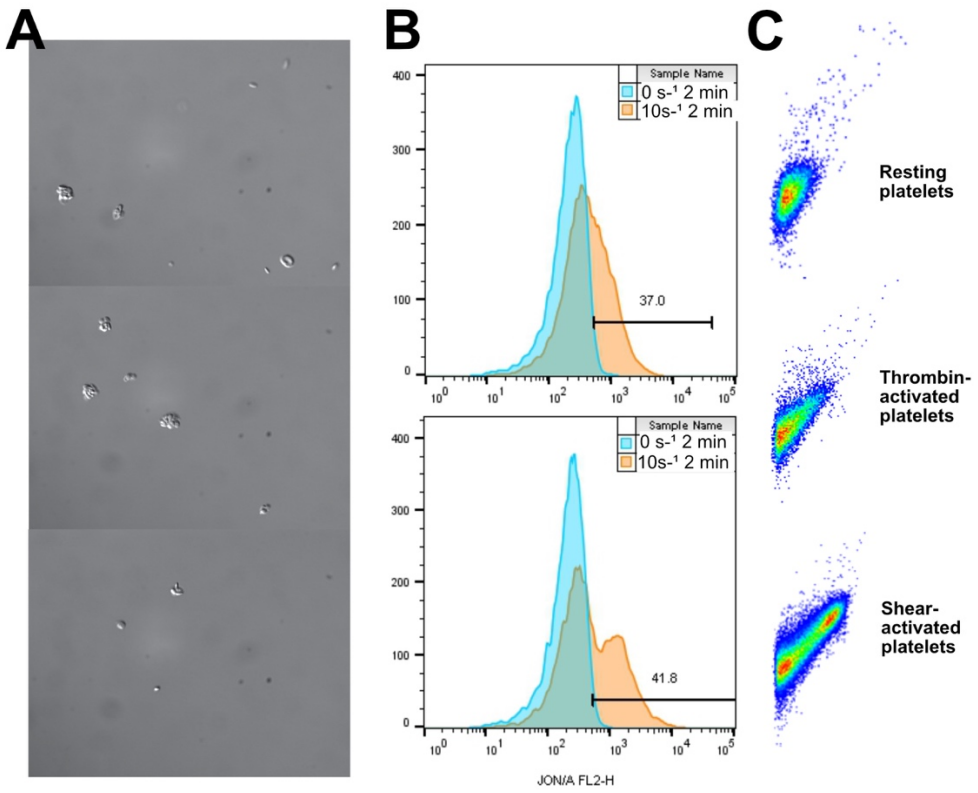

Figure 4.8. Cone/plate shearing experiments show distinct platelet aggregate/ agglutinate population. (A) Sample DIC images of platelets after shearing at 10k s^{-1}. (B) Sample FACS histograms of platelets stained with JON/A antibody: orange is after shearing at 10k s^{-1} for 2 minutes, and cyan is no shear but just placement on the viscometer for the same period of time. The number on the histogram shows percentage (%) platelets with positive JON/A staining, where threshold of resting platelets is ~2%. (C) Sample forward scatter (FSC, horizontal) and side scatter (SSC, vertical) profiles of platelets in resting condition, after thrombin activation for 5 min, and after shearing with botrocetin for 2 min.

When the murine platelets were sheared with botrocetin at high speed (up to 10k s^{-1}, where platelets in PRP at 37 °C would experience ~ 80–130 dyne/cm^2 shear stress if assuming PRP has 0.8-1.3 mPa·s viscosity) that corresponds to pathological shear condition (Y. Chen et al., 2019; Kesmarky, Kenyeres, Rabai, & Toth, 2008), they form

two distinct populations shown on the forward and side scatter (Figure 4.8). One population consisted of mostly single platelets, and the other aggregates of tens of platelets. From the DIC images, platelets even in aggregates/agglutinates were predominantly in discoid shape. The fluorescent channel is for binding of an antibody, JON/A-PE, that detects only activated murine integrins. This process is confirmed to be driven by GPIbα and vWF binding that is ensured by botrocetin, as for IL4Rα/GPIbα-tg (IL4) mice where the extracellular domain of GPIbα is replaced with that of human IL-4 receptor (Kanaji, Russell, & Ware, 2002), no aggregates nor positive JON/A signal were observed (Figure 4.9). The formation of "aggregates" was also mostly agglutination mediated only by GPIbα, as integrilin (namely Eptifibatide, a peptide drug that blocks GPIIbIIIa binding to ligands) did not diminish the aggregate population, but did abolish JON/A signal (because it competes with JON/A binding) (Bergmeier et al., 2002). Adding ALB did not change the shear-induced agglutination/aggregation outcome (APPENDIX B), which suggested the mechano-signaling was the primary pathway.

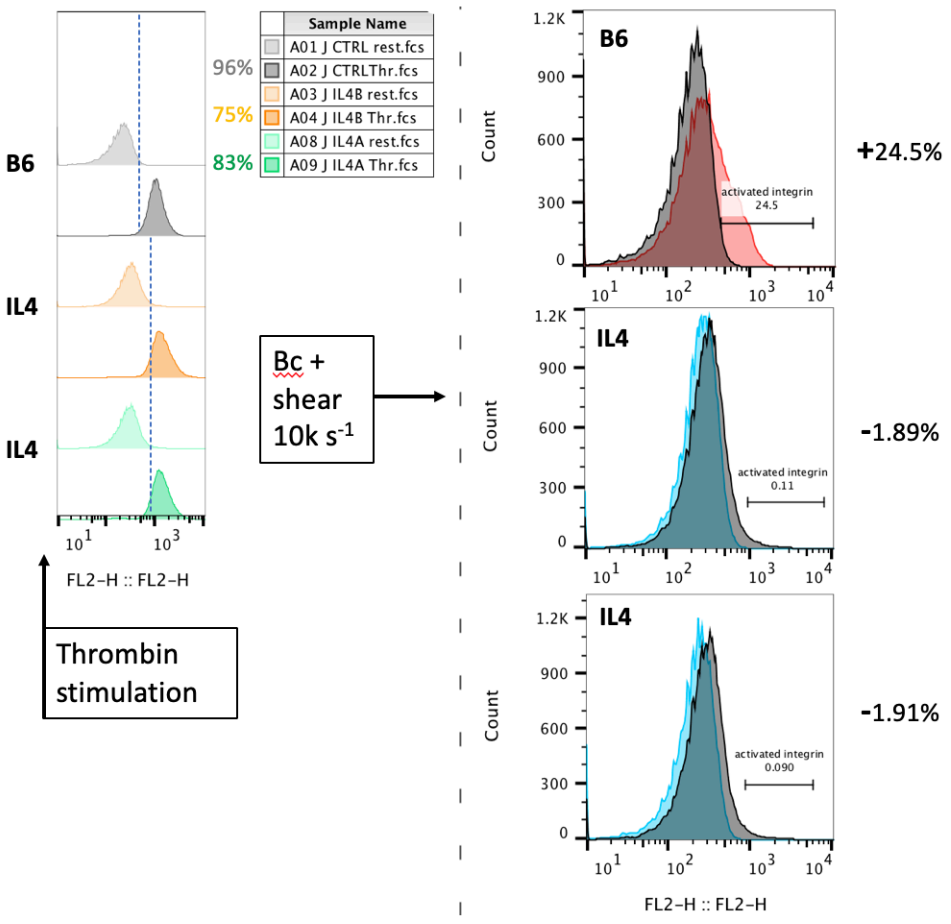

Figure 4.9. Platelets from IL4 mice show normal activation by agonist (thrombin) but completely abolished agglutination and aggregation. Data from two IL4 mice were compared with typical B6 response.

To establish the baseline and test the validity of this method, we applied a range of shear rate on the PRP. Remarkably, a shear dosage-increase leads to a dosage increase of JON/A positive signal (thresholding at ~2% baseline) (Figure 4.10 D). This directly corresponds to a dosage increase of the percentage of platelets in the aggregate population as well (Figure 4.10 Ai - Aviii). Shearing at 10k s^{-1} with JON/A but without Bc did not result in any aggregate population or JON/A signal increase (Figure 4.10 B), which aligned with previous finding that both Bc and shear were needed (Deng et al., 2016; Quach et al., 2018). Shearing with the presence of 0.5 μM GsMTx-4 (inhibitor of

cation-selective mechanosensitive channels) generated similar results (APPENDIX E), which suggested calcium influx through mechanosensitive channels had minimal contribution to this process. Since FACS counts events – be it single platelet or aggregates, larger aggregates would inevitably emit more fluorescence, masking the effect of true increase of JON/A signal. In other words, it is hard to decipher what percentage of integrins are shifted to higher affinity states that can be recognized by JON/A. Even though the cone/plate viscometer–FACS method has been used as a major tool in an important GPIbα-induced platelet clearance study (Deng et al., 2016), this issue was not properly discussed.

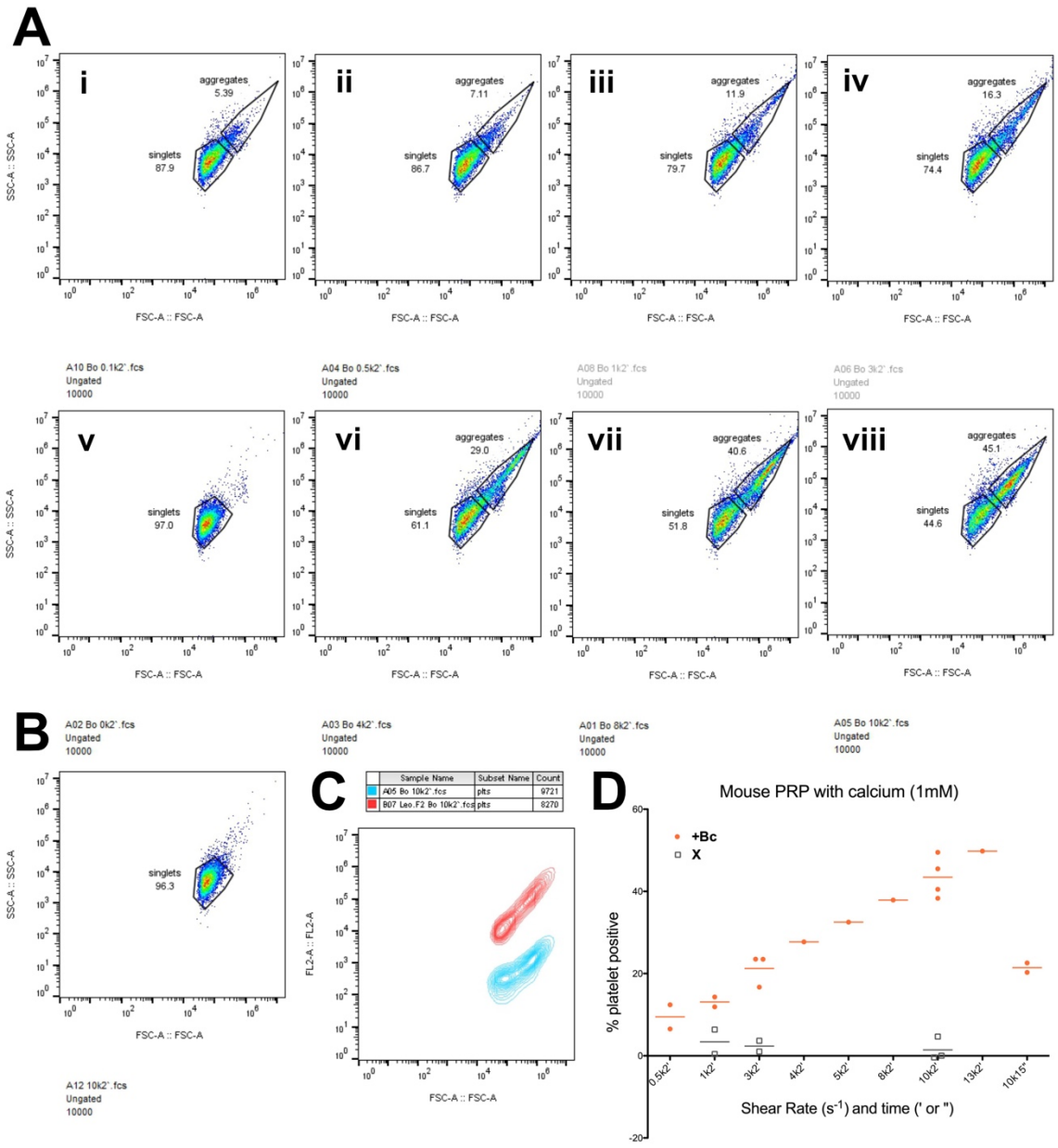

Figure 4.10. Mechanical dosage response of platelet agglutination/aggregation. (A) i through viii (except for v) are SSC vs FSC plots that show progressively more platelets getting into the aggregate population: 100, 500, 1000, 3000, 0 (non-sheared control sample), 4000, 8000, 10k s^{-1}. (B) SSC vs FSC profile of sample that was sheared at 10k s^{-1} for the same time duration (2 min) but without botrocetin. (C) FL2 (fluorescent channel) vs FSC that shows the difference of JON/A and Leo.F2 as FL2. (D) % platelet positively stained with JON/A as a function of shear rate. +Bc means botrocetin added, and X means no botrocetin added. Each dot is an experiment, and the line represent mean.

We needed to provide evidence that the fluorescent signal shift was not all due to the increase of event/particle size, but also because more integrins were indeed activated. We sheared platelets with a different antibody, Leo.F2 (emfret), that binds integrins of all conformations, not just the activated. As expected, the aggregate population also emerged along with increase of Leo.F2 signal. Plotting the FSC against the fluorescent channel did not provide sufficient information on how different the fluorescent channel and the FSC are (Figure 4.10 C), as there are two distinct populations. Another option is to compare the two histograms of size and of fluorescence intensity using a q-q- plot.

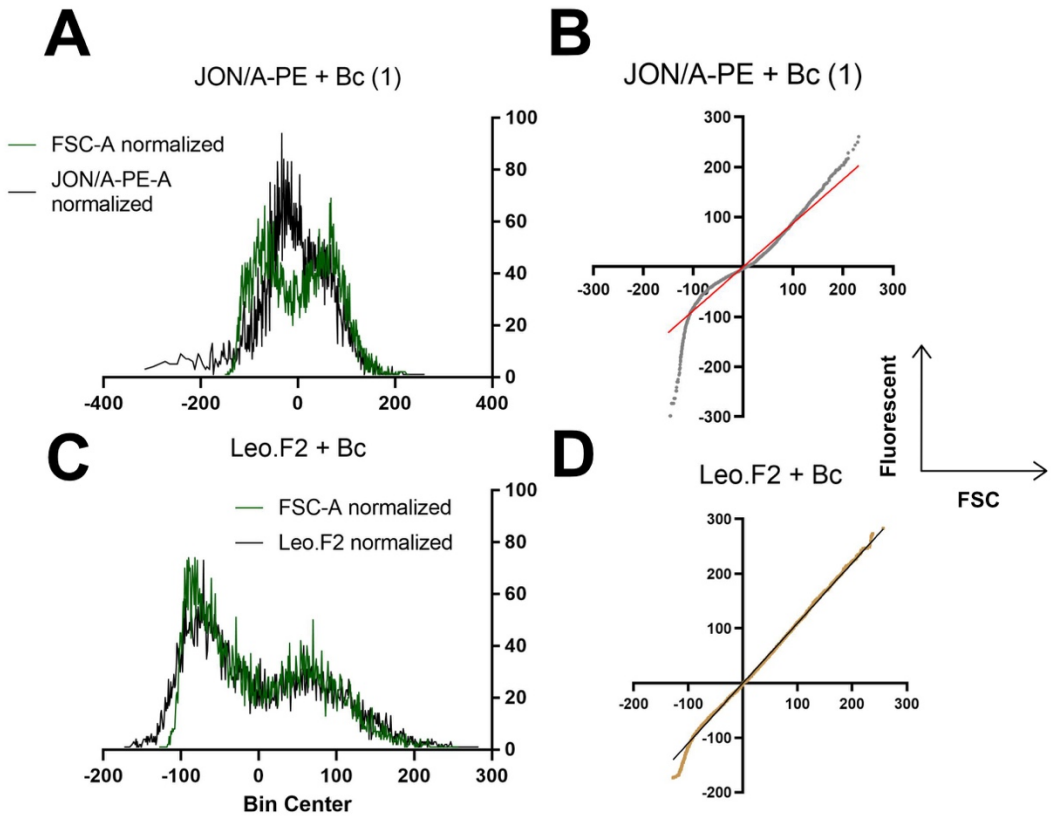

Figure 4.11. Histograms and q-q plots of fluorescent channels vs FSC show distinction between antibody that only recognizes activated integrins and antibody that recognizes integrins of all conformations. (A) Histograms JON/A-PE and FSC, (B) q-q plot of JON/A-PE and FSC: gray dots, and red linear line, (C) Histograms of Leo.F2-PE and FSC, (D) q-q plot of Leo.F2-PE and FSC: brown dots, and black linear line. Each event/particle is counted as a quantile.

An overlay plot of the histograms and a q-q plot (each particle/event as a quantile) show that the JON/A channel is indeed different than the FSC: the histograms are visually dissimilar (Figure 4.11 A), and the q-q plot does not fit well on the linear line (Figure 4.11 B) (the more similar two histograms are, the more linear the q-q plot would be (Gibbons & Chakraborti, 2014; WILK & GNANADESIKAN, 1968)).

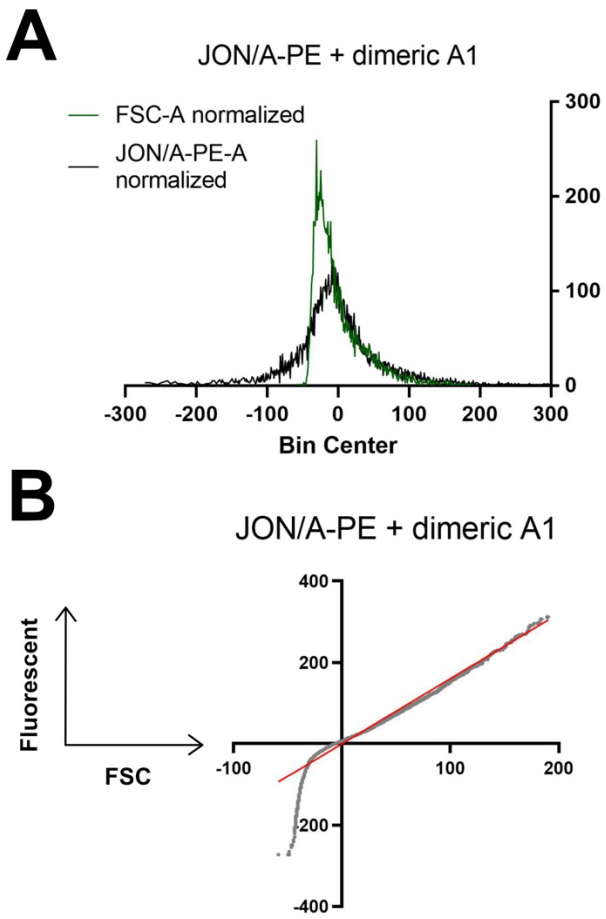

Figure 4.12. Histograms and q-q plots of fluorescent channels vs FSC show that in the presence dimeric A1 instead of botrocetin, the fluorescent channel and FSC are very similar. (A) Histograms JON/A-PE and FSC in the presence of dimeric A1 without botrocetin; (B) q-q plot of JON/A-PE and FSC in such condition: gray dots, and red linear line.

To note, we do not care much about the lower quantiles (left of the q-q plot and low-value population on the histogram) because these are the single-platelet population. The higher quantiles are the aggregates that formed upon shearing with vWF-GPIbα pulling, which are the focus of the study. In contrast, Leo.F2 and FSC histograms visually overlapped well, and the q-q plot fitted much better with a linear line (Figure 4.11 C, D). This analysis was done on > three independent experiments and all reached similar conclusions (APPENDIX C). The results suggest that the JON/A signal shift was only partially due to the increase of particle size, and thus the cone/plate-FACS method can still be promising for studying mechano-signaling, though in a semi-quantitative fashion. Additionally, shearing washed platelets with dimeric A1 (without botrocetin) generated JON/A histogram similar to that of FSC and a linear q-q plot (Figure 4.12), confirming that both botrocetin and shear are required for signaling and detectable integrin activation in this experimental condition.

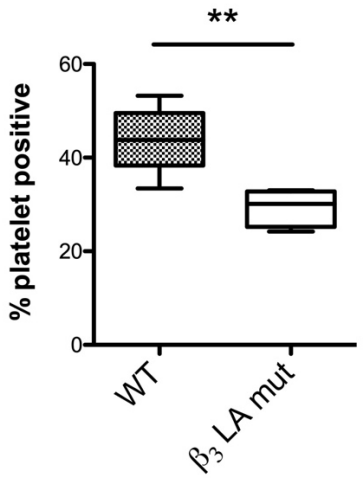

Figure 4.13. Percentage of platelet stained positive for JON/A are lower for the β_3 LA mutant than for the WT control. Data presents mean with whiskers marking min to max. Statistics was performed using two-tailed unpaired t-test (n > 4).

Using this method, we sheared PRP from both β_3 LA mutant and the WT ctrl mice and found the % platelet positive for JON/A signal was less for the LA mut (Figure 4.13). However, the result does not equate % less integrins were in active form for the LA mut, as the extend of agglutination (size) could also vary based on mouse condition – age, stress, and other factors. The result could be interpreted as such: if β_3 tail-talin linkage is impaired, less integrins may be activated through the pulling of GPIbα with vWF.

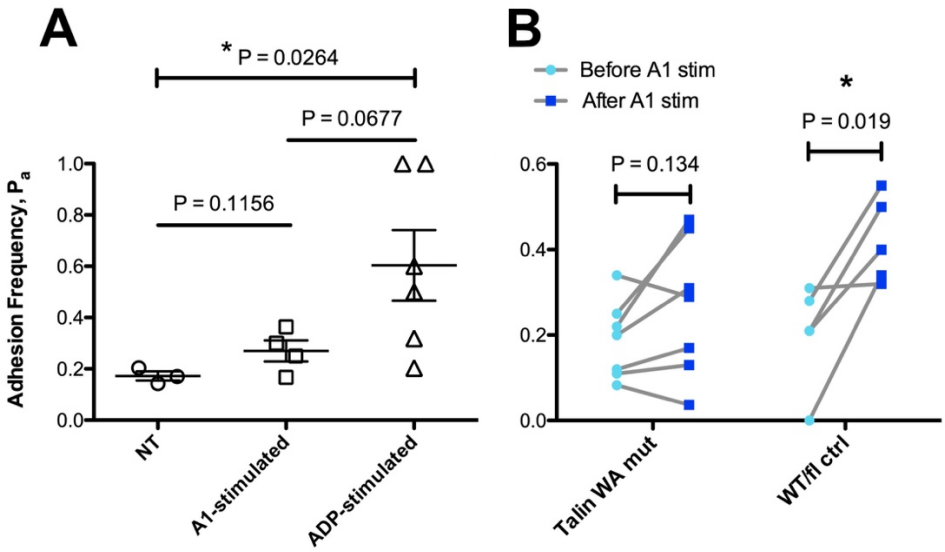

Figure 4.14. Dual BFP results suggest talin WA mutant has impaired integrin activation through GPIbα mechano-signaling. (A) Unpaired comparison (two-tailed, unpaired t-test with Welch's correction) of baseline binding of integrin with fibrinogen (NT), mouse A1-stimulated, and ADP-stimulated (individual points with mean ± SEM). (B) Paired comparison of each platelet: adhesion to fibrinogen before and after A1 stimulation (two-tailed, paired t-test). Each dot represents one platelet.

To test the validity of the interpretation, we used a previously established but low throughput method: the dual BFP (Y. Chen et al., 2019). First, we tried to test if the mouse platelet integrin, like the human counterpart, presents an intermediate affinity state that can be induced by A1 stimulation. Although not significant, the trend showed potentially graded integrin affinity state: low (NT), intermediate (A1-stimulated), and

high (ADP-stimulated) (Figure 4.14 A). The large variation of platelet adhesion in the stimulated conditions can attribute to the heterogeneity of platelets (existence of subtypes or different level of stimulation) due to age and other intrinsic factors (Blair, Michelson, & Frelinger, 2018; Donati, Gupta, & Reviakine, 2016; Jobe, 2017; Jongen, MacArthur, Englyst, & West, 2020). For this reason, we decided to use a paired dual-BFP test. Each platelet's baseline binding to fibrinogen was determined first (< 30 contacts to prevent activation); after > one-minute resting, the platelet was brought to interact with mouse monomeric A1; after a lifetime > 2s was established, the platelet was switched to interact with fibrinogen again to determine probability of adhesion. Using this test, WT/fl platelets showed a significant increase of adhesiveness to fibrinogen after the A1 stimulation ($P < 0.019$), while talin WA did not show the striking effect of A1 binding (Figure 4.14 B). The dual BFP and cone/plate results indicated the likely compromised integrin affinity maturation triggered by GPIbα-vWF forced binding due to impaired talin-integrin linkage.

4.3 Discussion

The expansion of platelet aggregation study beyond aggregometry using microfluidics as presented in this chapter can greatly advance the field as such methods, when paired with appropriate inhibitors, can single out the mechanical-geometrical effect. We first discovered that the talin mutation (W359A) that disrupts binding to the integrin tail, which was confirmed by disrupting this interaction with an integrin β_3 L746A mutant, reduced the extent of early-stage platelet aggregation without agonist amplification. The results suggest that talin is a crucial regulator of the biomechanical platelet aggregation that is driven by disturbed flow. Based on the prior studies on human platelets, the integrins

are mostly in the extended-close, intermediate affinity state (Y. Chen et al., 2019). It has been reported that talin without other stimuli can induce leukocyte integrin $\alpha_L\beta_2$ to an intermediate affinity state (Lefort et al., 2012; Y. F. Li, Tang, Puan, Law, & Tan, 2007). Considering these results together, talin likely mediates the intermediate state that was initiated by GPIbα signaling, and without further activation by agonists, the intermediate state is stable. Given talin's importance in integrin inside-out activation through all known agonists, its involvement in GPIbα mechano-signaling is not surprising and highlights the versatility and complexity of talin function.

The result from the LR mutant (albeit the need for repeats to confirm) was surprising as the platelet adhesion and aggregation on collagen was greatly reduced in both physiological and pathological shear rates (Stefanini et al., 2014). However, the same mutation for neutrophils had a different narrative: LR neutrophils presented normal P-selectin-induced slow rolling through LFA-1 (a β_2 integrin), in contrast to the WA neutrophils with defective slow rolling and chemokine-induced arrest (Yago et al., 2015). Functionally, the LR mutation offered protection from renal ischemia-reperfusion injury, an inflammatory disorder where neutrophils play a key role. Our results imply that cytoskeletal engagement of integrin through talin is sufficient to resist the extremely high shear forces, and it indirectly showed that the integrins were not in activated form that requires talin MPR interaction. Perhaps the LR mutation is only crucial for soluble agonist-induced integrin activation and not mechano-binding induced activation that happens at an even shorter time scale (sub-seconds). Taken together, we learn that 1) disruption of MPR or MDR interactions leads to distinct outcome in different cell systems and diseases (thrombosis vs. ischemia-reperfusion), and 2) for platelets, collagen flow chamber assay is

a better predictor for thrombosis and hemostasis phenotype of mice compared to our aggregation assay through vWF, although it does not offer as much mechanistic insight.

Non-impaired biomechanical aggregation of CalDAG-GEFI KO platelets was unexpected because CalDAG-GEFI was found to be crucial for platelet adhesion and aggregation (Stefanini & Bergmeier, 2010; Stefanini, Roden, & Bergmeier, 2009). More repeats are needed to confirm the finding, and the most proper control for CalDAG-GEFI KO was WT/wt, not Pf4-Cre+ (Cre+) mice. We didn't test the WT mice due to time and resource constraint, but generally Cre+ and WT mice do not show a difference in integrin activation (Stefanini et al., 2014). The result suggested diverging pathways of integrin activation initiated by soluble weak agonist vs GPIbα pulling, as CalDAG-GEFI KO and platelets expressing low levels of CalDAG-GEFI both showed diminished integrin activation with ADP stimulation (Piatt et al., 2016). As expected, STIM1 KO did not affect the platelet aggregation as STIM1 was previously identified to be dispensable for platelet aggregation in both aggregometer and collagen flow chamber assay (Ahmad et al., 2011).

The involvement of Rap1 is interesting as talin-Rap1 interaction was suggested to anchor talin to the plasma membrane so that talin can be well-oriented to activate integrins (Goult et al., 2010; Lagarrigue et al., 2020). Perhaps talin need to be recruited to the plasma membrane first to have a higher chance of interacting with integrins, or even if they are in proximity of the membrane, they need stabilization with both the membrane and actin filament to properly modulate integrin function. The cone/plate viscometer and dual BFP results implied that not only is cytoskeletal linkage important, GPIIbIIIa needs normal talin-integrin binding to mature to a higher affinity. We preliminarily propose the following mechanism that could fit the results: talin first needs to be recruited to the plasma

membrane by the lipids and Rap1 to be stabilized and properly oriented, and it needs to access the integrin tail to link to the cytoskeleton while maintaining the intermediate affinity of integrins. How talin and Rap1 were brought to interact in the first place could be a result of simultaneous inside-out signaling and mechanosensing. Talin itself is a mechanosensor and mechano-buffer that can unfold in response to mechanical pulling (Elosegui-Artola et al., 2016; Kumar et al., 2016; Yao et al., 2016). It is also a smart molecule that can filter out noise and responds to cyclic mechanical signals (Tapia-Rojo & Fernandez, 2020), and could experiences repeated stretching and relaxation by actin flow in cell spreading (Margadant et al., 2011). The biomechanical platelet aggregation is likely mediated by multiple mechanosensors including talin.

A puzzling question still remains: what are the intracellular players upstream of Rap1 and talin for mechano-activation of GPIIbIIIa by GPIbα? Protein kinase C (PKC) could be a candidate as agonist-activation studies suggested CalDAG-GEFI and PKC to represent separate but synergizing pathways for GPIIbIIIa activation (Cifuni, Wagner, & Bergmeier, 2008), and for gradient shear-driven platelet aggregation without blocking the agonist amplification loop, the P2Y12 ADP receptor, a co-signalling molecule for PKC, was the most important (out of P2Y1, and thromboxane A2) for clot accumulation (Brazilek et al., 2017), even though we did not observe a noticeable difference between perfusion with or without ALB for murine platelet aggregation.

Overall, the results suggest that GPIIbIIIa activation via GPIbα mechano-signaling seems to require both Rap1 activation (which recruits talin to the membrane) and talin binding to integrin, but not necessarily talin's activating effect by interactions at the membrane proximal region of β_3 tail.

CHAPTER 5. TALIN FINETUNES FORCE-MEDIATED DISCOID PLATELET ADHESION TO INTEGRIN LIGAND

Disclaimer: this chapter was made possible because of Dr. Brian Petrich's generous supply of the transgenic mice housed at the animal facility at Emory University.

5.1 Introduction

It's clear that talin plays a pivotal role in inside-out activation of integrins via biochemical stimulation of GPCRs and mechano-binding of GPIbα. Talin's function in integrin outside-in activation in early time stage is not clearly delineated. Particularly, whether talin plays a role in not pre-activated platelets binding to immobilized ligand had not been systematically studied. A seminal paper on bidirectional integrin signaling showed talin and $G\alpha_{13}$ competitively bind to the β_3 tail, while $G\alpha_{13}$ predominantly controls integrin outside-in signaling (Shen et al., 2013). The study mostly focused on outside-in signaling after inside-out stimulation. The adhesion assay that emphasized ligand-induced integrin activation was performed on a long timescale (one hour), but nevertheless revealed the necessity of talin's presence for this process. We then ask whether talin is involved at the very beginning – one single forced interaction of integrin and fibrinogen – and how talin's specific interactions with the integrin and Rap1 could mediate the binding on such a short timescale.

The GPIIbIIIa integrin cannot bind to soluble fibrinogen without activation by agonist, manganese ion, or activating antibody. But it knowingly can bind to immobilized fibrinogen, even when extension about the α_{IIb} genu or swing-out of the β_3 hybrid domain was locked with engineered disulfide bonds (Blue et al., 2010; Cheng, Li, Negri, & Coller,

2013), although preventing hybrid domain swing-out disabled outside-in signaling and cytoskeleton reorganization. To note, the integrin is always in some thermodynamic equilibrium with all of the conformational/affinity states (Sun, Costell, & Fassler, 2019). In majority of the time, integrins are in the bent-closed conformer, and they could engage ligand in the ephemeral time they spend in the extended-closed or extended-open conformer, although crystallography and EM images have shown bent integrins in complex with small RGD ligands as well (Adair et al., 2005; Xiong et al., 2002).

Since biomechanical platelet aggregation depends on the β_3 integrin's lasting engagement with talin (and cytoskeleton), we propose to interrogate talin's effect on force-mediated ligand binding of the integrin. Our preliminary study with flow chamber coated with fibrinogen showed promising results: merely increasing the shear rate from 100 to 400 s^{-1} greatly reduced stable adhesion of talin WA mutant platelets without agonists' presence, while for the WT/fl control, the number of stably adhered platelets were comparable for the two shear rates tested (Figure 5.1). The results implicated talin WA's higher sensitivity to increased flow or weakened ability to withstand forces. In this chapter, we present the findings on how integrin-fibrinogen 2D kinetics are altered with 1) absence of talin, 2) mutation that decelerates talin-integrin binding, 3) mutation that debilitates talin to activate integrins, and 4) mutations that disrupt binding of talin with Rap1.

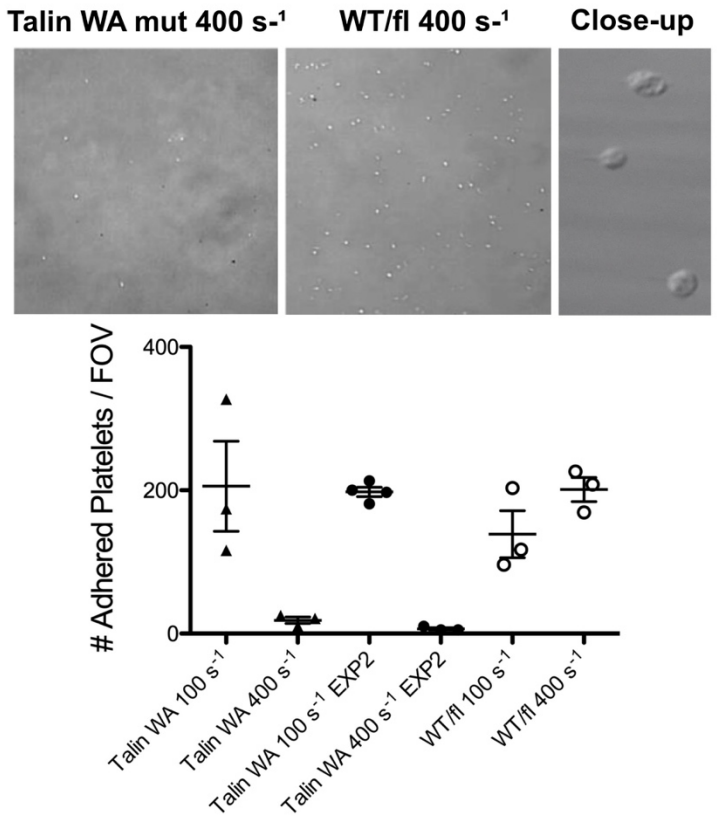

Figure 5.1. Talin WA mutant platelets cannot adhere as well on fibrinogen at higher shear rate. Each dot is field of view. Two independent experiments were done for talin WA mutant.

5.2 Results

5.2.1 Talin regulates the force-mediated off-rate but not 2D effective affinity of integrin-ligand binding kinetics

To study the mechanism of talin's regulation on forced integrin-binding, we deployed single-cell force spectroscopy (Figure 3.2). Cycles of impinging platelets (without prior activation) to fibrinogen-coated beads and clamping at preset distances that allowed integrin-fibrinogen bond formation and dissociation under force yielded lifetime-force curves that were binned by average force. Since GPIIbIIIa is the most abundant and

functionally important integrin on platelet surface with ~80,000 copies per platelet, we assume other fibrinogen-binding integrins, namely $\alpha_v\beta_3$ which has only several hundred copies per platelet (>>100 fold less than GPIIbIIIa), contribute a negligible amount of formed bonds (Bennett, Berger, & Billings, 2009). Moreover, we have previously found for human platelet, adhesion with fibrinogen-coated bead in the presence of the available $\alpha_v\beta_3$ or $\alpha_{IIb}\beta_3$ inhibitors yielded ~50 folds less average number of bonds formed with $\alpha_v\beta_3$ than that of $\alpha_{IIB}\beta_3$ (Y. Chen et al., 2019).

Negative control with just streptavidin (SA) coated beads exhibited < 3% non-specific binding. Adhesion frequency was controlled to be ~20% so that most bonds formed are single bond. GPIIbIIIa and fibrinogen forms catch bond (or catch-slip bond), signified by prolonged average lifetime as force increases in the lower force regime, and shortened average lifetime as force increases in the higher force regime (Figure 5.2 A). The WA mutation on talin abolished the catch bond; rather, the force-lifetime relationship became a slip bond where the average lifetime monotonically decreased with incrementing force (Figure 5.2 A). The LA mutation on the β_3 tail gave rise to lifetimes on similar magnitude except for perhaps the lowest force bin (Figure 5.2 B). However, statistics show that the LA mutant may not exhibit a catch bond with shorter lifetimes, as there did not appear to be a difference of lifetimes in the first three (lowest three) force bins. The result from talin KO was comparable to the LA (Figure 5.2 D). Talin LR also gave rise to substantially shorter lifetimes with the ligand (Figure 5.2 C), but the shape of the force-lifetime curve was different from that of talin WA (more details in 5.2.2). Mutations that disrupt talin-Rap1 interactions (F1 single, and F1/F0 double mutants) also generated shorter lifetimes (still no evident catch bonds) on similar scale as the talin-integrin mutants, although the WT/fl control had unusually shorter average lifetimes (Figure 5.5 D). Some inconsistency

could be attributed to that these mice were shipped from a different lab and the WT/fl control was not a black 6 background. Overall, talin KO and mutations that disrupt talin-integrin or talin-Rap1 binding or talin's ability to activate the integrin all shortened GPIIbIIIa-fibrinogen single-bond lifetimes, which corresponds to higher forced off-rate for the KO and mutants.

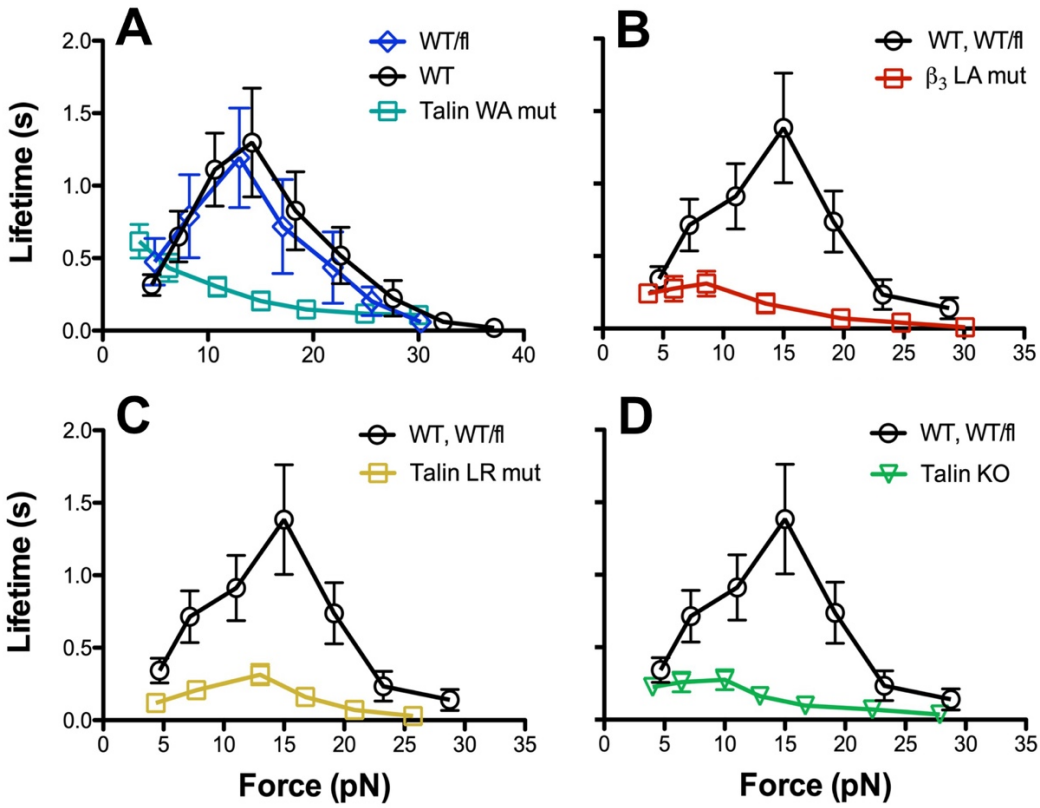

Figure 5.2. Lifetime vs force curves show weakened integrin-fibrinogen bonds with mutation on talin-integrin interactions. (A) Lifetime over force curve of WT, WT/fl, and talin WA mutant. (B) Lifetime over force curve of mixed WT and WT/fl and β_3 LA mutant. (C) Lifetime over force curve of mixed WT and WT/fl and talin LR mutant. (D) Lifetime over force curve of mixed WT and WT/fl and talin KO. The mixed WT, WT/fl curve is shown repeatedly in (B), (C), and (D). Each dot represents mean lifetime ± SEM of a force bin; each bin has > 50 events for forces below 25 pN.

To confirm that weakened bond strength was the main reason for the abolishment of the catch bond with the WA mutation, we also used the rupture force assay to record at which force level each bond would break by setting the retraction way beyond the force the interaction could bear (1000 pN). Histograms comparison showed that WT/fl bonds rupture at higher forces compared to the WA bonds that could not maintain the binding beyond 45 pN (Figure 5.3).

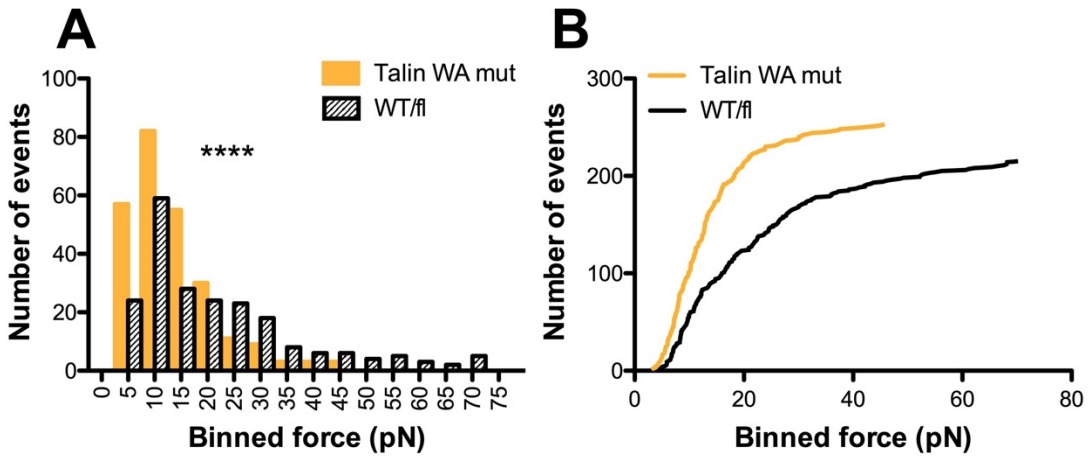

Figure 5.3. Integrin-ligand bonds of talin WA mutant rupture at lower forces compared to the WT control. (A) Histogram of binned rupture forces; Difference of the WA and WT/fl histograms is significant by both Mann-Whitney and Kolmogorov-Smirnov tests. (B) Accumulative histogram of WA and WT/fl rupture forces.

In contrast, the apparent 2D effective affinity A_cK_a (free of force loading) obtained from fitting the probability of adhesion curve (Figure 5.4 A) are all similar among the mutants and the WT/fl control except for talin KO (Figure 5.4 B). Talin KO has the lowest and the only different apparent 2D effective affinity. The fitted apparent off-rate k_{off} (also free of force loading) were not different among the mouse types. To clarify, the affinity and off-rate were "apparent" because for the cell expression level and bead coating density measurement, the true F/P ratios of the GPIIbIIIa and fibrinogen antibodies were unknown,

and thus the values were not the true affinity but were an accurate reflection of the relative 2D effective affinities for comparison purposes. The results show that integrins are just as likely to bind immobilized fibrinogen even when one (not all) talin head-integrin tail interaction site is disrupted. However, if talin is largely absent, the likelihood of bond formation is reduced.

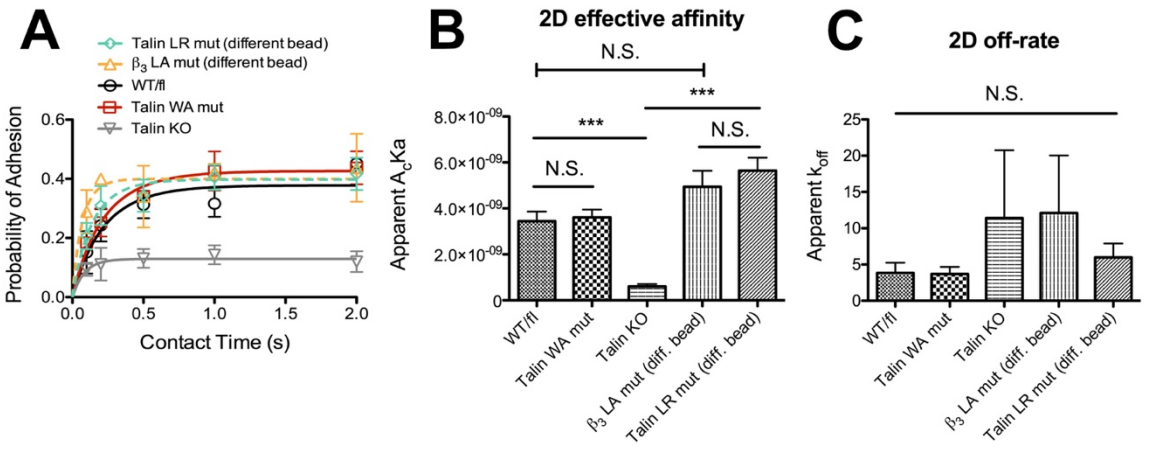

Figure 5.4. 2D effective affinities of talin and β3 mutants do not differ from WT control. (A) Adhesion frequency over contact time curve for WT/fl, talin WA, LR mutants, talin KO, and β3 LA mutant. The BFP beads for the LR and LA mutant experiments were from a different batch than the ones used for the rest. Each data point represents ≥ 4 pairs of cell-bead. (B) Apparent A_cKa (2D effective affinity) from fitting of the adhesion frequency curve. (C) Apparent k_{off} from fitting of the adhesion frequency curve. All data represent mean ± SEM. Statistics was performed using one-way ANOVA with Tukey's test.

5.2.2 Cytoskeletal support, stabilization of talin by Rap1, and integrin function all contribute to formation of normal GPIIbIIIa-fibrinogen catch bond

The talin WA and LR mutants exhibited different force-lifetime relationship as LR showed a clear catch bond albeit the shorter average lifetimes (Figure 5.5 C). Since L325 on talin only weakly interact with integrin tail and is not the major binding site to link the integrin to cytoskeleton, we then ask: how important is normal linkage of integrin to intact

cytoskeleton for integrin binding kinetics? We treated WT platelets with cytochalasin D (CytD) which inhibits actin polymerization and found the integrins were not able to form catch bond either (Figure 5.5 A). DMSO (which was used to dissolve CytD) -treated WT platelets average lifetimes essentially overlapped with those of WT platelets with no treatment. The CytD treated platelets appeared to have higher average lifetimes at the lower force regime (Figure 5.5 B).

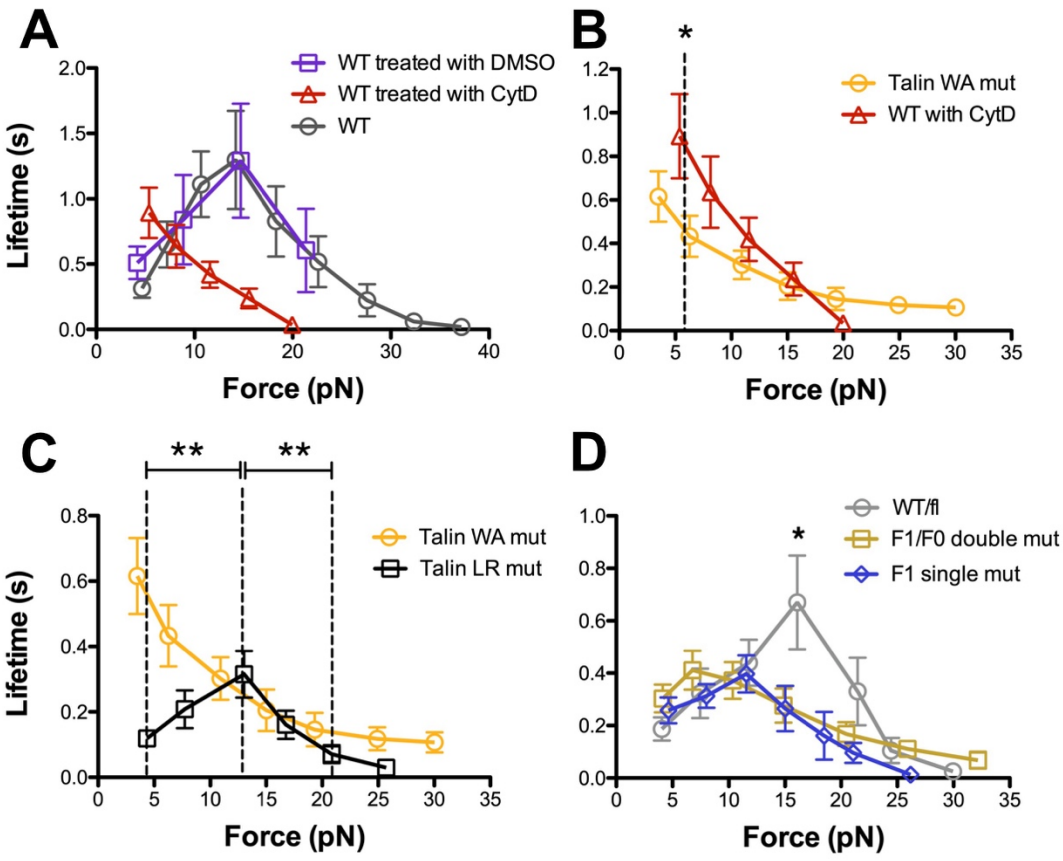

Figure 5.5. Lifetime vs force curves show weakened integrin-fibrinogen bonds with mutation on talin-integrin interactions. (A) Lifetime over force curve of WT treated with DMSO, WT treated with cytochalasin D that is dissolved in DMSO (CytD), and WT control. (B) Overlay of lifetime over force curve of talin WA mutant and WT treated with CytD for comparison. (C) Overlay of lifetime over force curve of talin WA mutant and talin LR mutant for comparison. (D) Lifetime over force curve of talin F1/F0 double mutant, talin F1 single mutant, and WT/fl control; the lifetimes of WT/fl in 15 – 20 pN force bin are higher than the F1 and F1/F0 mutants. Two-tailed unpaired t-test with Welch's correction was used for comparisons.

The results suggest that both normal cytoskeletal support and integrin activatability are important for the formation of GPIIbIIIa-fibrinogen catch bond, and the "feedback" of cytoskeleton seems instant: upon GPIIbIIIa-fibrinogen engagement, the absence or delay of cytoskeleton linkage can affect how long a bond could last. This is remarkable given that the platelets are largely quiescent and maintain their discoid shape, and the consensus is that talin is in its autoinhibitory form when there is no activation cue.

5.2.3 The short-, intermediate-, and long-lived bonds of integrins differ by force bin

To gain additional insight on how the GPIIbIIIa-Fg bonds differ when talin can regularly link integrin to the cytoskeleton versus when it cannot, the bond lifetime survival frequency of each force bin was plotted (Figure 5.6). For the WT control, the bin with the longest average lifetime is around 15 pN (catch regime), which is shown on the survival plot; conversely for the WA mutant, the survival frequencies monotonically shift left as force increases, signifying the slip bond. The survival frequency can be fitted with one, two, or three state exponential decay (Wei Chen et al., 2011), denoting one, two, or three species of bonds that can be ranked from slowest to fastest dissociation (off-rate). These bonds can also be called short-, intermediate-, and long-lived bonds if there are three states; for two-state, there would be relatively a fast and slow bond species. For the WA mutant and WT control, the most appropriate fitting was determined with the best fit, starting from the simplest (one-state). Figure 5.7 A and E showed representative survival curves (dots) of WA and control with 3-state fitting (line). Both k_{off} and fraction of each bond species per force bin can be obtained by the fitting (Figure 5.7 B, D, F, H). Figure 5.7 C and G showed log of off-rates so that k_{off} of each species can be fitted with a linear line (Bell model).

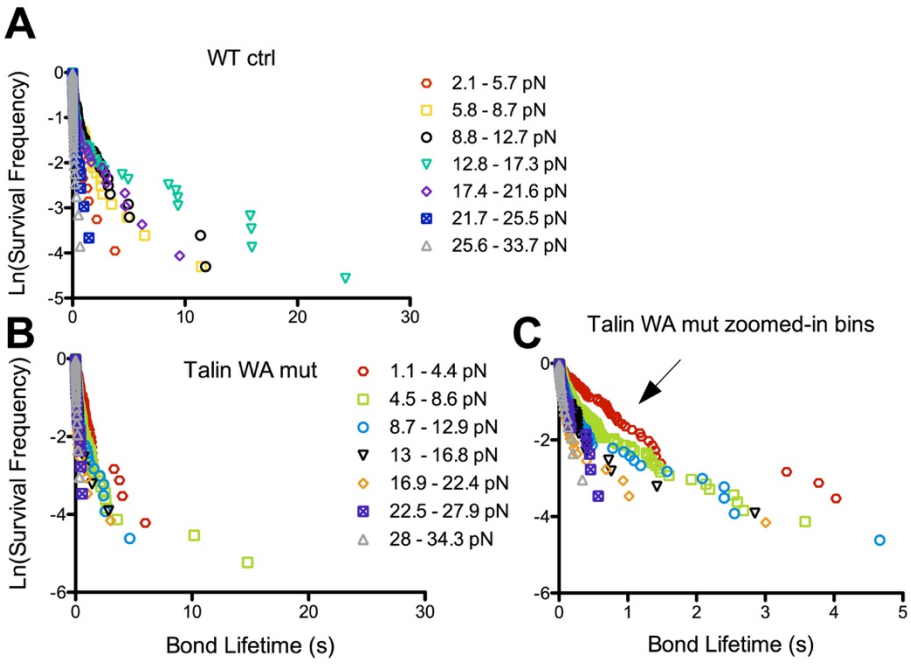

Figure 5.6. Bond lifetime distributions reinforce the difference shown by catch vs slip bond of WT control and talin WA mutant. (A) Survival frequency of bond lifetimes by force bins of WT control (mixed WT and WT/fl). (B) Survival frequency of bond lifetimes by force bins of talin WA mutant. (C) Survival frequency of bond lifetimes by force bins of talin WA mutant zoomed to lower lifetimes (5 s cutoff).

For talin WA, the fast-, intermediate-, and slow-dissociating bonds all fitted well with the Bell model, and the fraction of each species showed that short-lived bonds generally decreased, while intermediate- and long-lived bonds generally trended up with incrementing force. Moreover, the slowest-dissociating bonds did not appear in the lowest force bin and the fastest-dissociating bonds disappeared after 15 pN (three-state model cannot fit the data). For the WT control however, the off-rates of mostly three bond species could not fit well with the Bell model (Figure 5.7 G). By speculation, the WA may have more states than the WT, as there would be the integrin population unable to link to talin, and a small amount of leftover unmutated talin could still facilitate the binding.

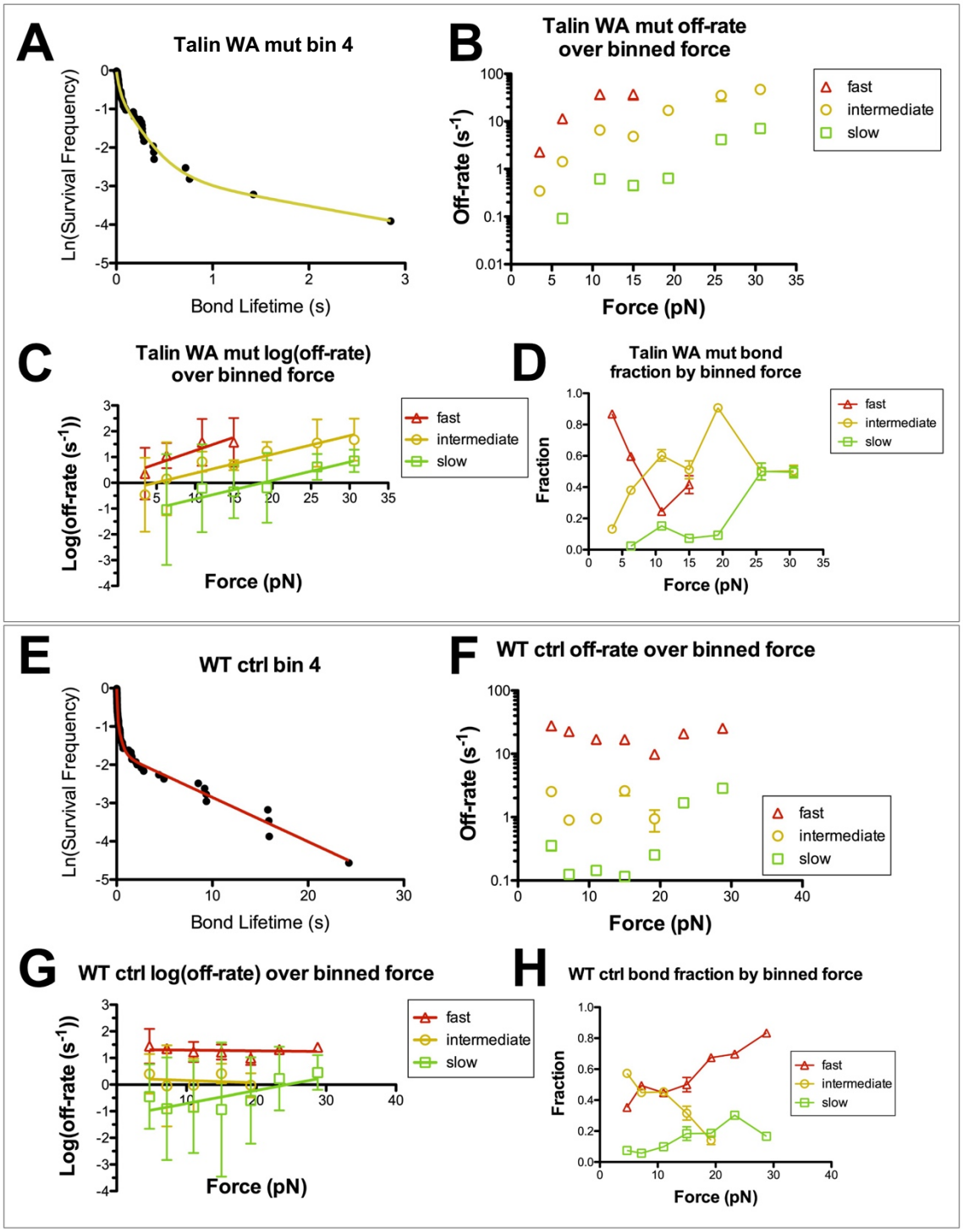

Figure 5.7. Fittings of the bond lifetime distributions imply bond species differ between talin WA mutant and WT control. (A – D) are for talin WA mutant. (A) Example fitting of bond lifetime survival frequency curve (the 4th force bin chosen, 3-state fitting). (B) Fitted forced off-rates of fast-, intermediate-, and slow-dissociation bonds. (C) Log of the off-rates in (B) to show linear fitting, which

corresponds to fitting with the Bell model. (D) Fitted fraction of fast-, intermediate-, and slow-dissociation bonds. (E – H) are the same as (A – D) but for the WT control (WT, WT/fl mixed). Data with error bars were shown mean ± SEM.

A two-state model may be the right model for the WT as described by previous publications, but for this data set it would be a forced fit for some bins and may require additional manipulation of binning and more experiments. Nevertheless, how many states GPIIbIIIa possesses is still debatable (Y. Chen et al., 2019; Litvinov et al., 2011; Litvinov, Bennett, Weisel, & Shuman, 2005; Litvinov, Shuman, Bennett, & Weisel, 2002).

5.2.4 On force history: memory effect seems to depend on talin, but not cyclic mechanical reinforcement

Force history – including past bond formation and force loading of the current adhesion event – impacts frequency and quality of bonds for receptors such as T cell receptors (TCR) and integrins (Yunfeng Chen et al., 2019; Kong et al., 2013; Zarnitsyna et al., 2007). Thus, we tested whether defects on talin-integrin linkage can alter the force history effects. First, we analysed running frequency of integrin adhesion – as integrins supposedly stochastically form bonds with the ligand, we did not see an upward trend in adhesion frequency (APPENDIX A), which suggests the platelets were not progressively getting activated as they repeatedly experienced bond association and dissociation. The Bernoulli sequence (independent and identically distributed) of adhesion events was challenged by our lab, where "memory effect" was discovered (Zarnitsyna et al., 2007). TCR and human platelet integrin GPIIbIIIa (data not shown) were found to exhibit positive memory, meaning a bond formed increases the probability of a subsequent bond formation. The memory index was used as a metric for the memory effect: if the index is positive, a bond forms would likely increase the probability a subsequent bond formation;

if the index is negative, a bond formed would likely inhibit the next bond formation; if the index is close to zero, a bond formed would have no impact on future bond formation. Remarkably, mouse GPIIbIIIa also exhibited positive memory to fibrinogen, but talin WA mutation greatly reduced it (Figure 5.8).

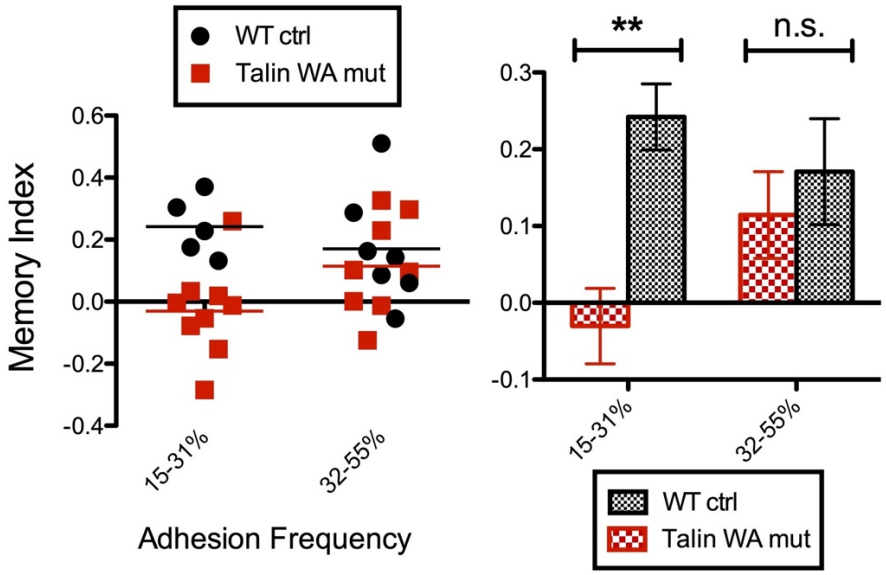

Figure 5.8. Memory index calculations suggest talin WA mutation abrogates the integrin-ligand binding memory effect in at least certain adhesion frequency ranges. (A) Memory index of talin WA mutant and WT control for 15-31% and 32-55% adhesion frequency ranges. Each point represents a platelet. (B) Mean ± SEM of the data points in (A); statistics was performed using two-way ANOVA with Bonferroni correction.

A more immediate force history impact comes from the force loading just preceding a bond lifetime. Our lab reported the phenomenon "cyclic mechanical reinforcement" (CMR) of lifetime lengthening of an integrin following repeated loading and unloading on the receptor (Kong et al., 2013) and described it with a kinetic model (Z. Li, Kong, & Zhu, 2016). Instead of a single distance (corresponding to force) clamp assay demonstrated in

Figure 3.3, multiple loading and unloading cycles can be applied to a formed bond, and the lifetime can be measured if a bond can survive the multiple loadings (Figure 5.9).

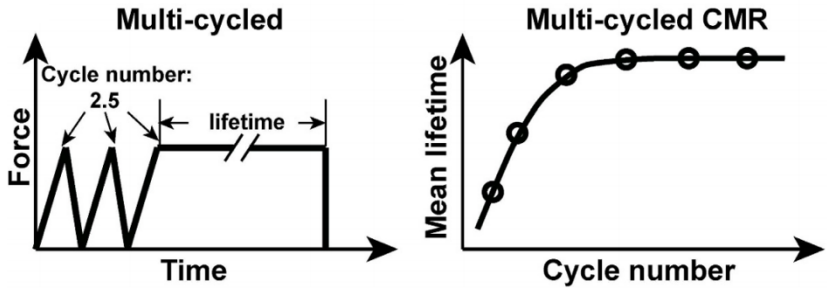

Figure 5.9. Illustration of cyclic mechanical reinforcement (CMR) assay. The left depicts a multiple-cycled BFP event; the right shows increase of cycle number pre-clamp generally raises the lifetime at the clamped force. Adapted from (Z. Li et al., 2016).

We chose 3.5 cycles of cyclical pulling to be applied to integrin-fibrinogen bond to amplify the effect of CMR. Mean lifetime was indeed increased for WT platelets particularly near the "catch" region ~15 pN (Figure 5.10 A). Comparing the lifetime distributions of CMR and non-CMR bonds, one can see that the longest lifetimes were comparable for both conditions (Figure 5.10 B-C). However, if comparing the first slopes of the distributions (the most vertical slope), the ones from CMR are larger (less negative), which indicates that the majority short to medium lifetimes (< 5s) are generally longer. The effect of CMR tended to eliminate very short lifetimes (<0.01 s) instead of rendering very long lifetimes, which generally aligned with our previous findings on $\alpha_5\beta_1$ (Kong et al., 2013). To exclude the possibility that the CMR effect was due to pre-selection of long-lived bonds because more short-lived bonds may not survive the repeated loading-unloading process, we quantified the fraction of lifetimes established out of all adhesion events for CMR and single force clamp and found no difference (APPENDIX G). For β_3 LA mutant, mean lifetimes, especially at higher force bins also increased with CMR

(Figure 5.10 D), albeit being still quite short compared to WT. Disruption of talin head binding to integrin did not have a clear impact on the CMR phenomenon.

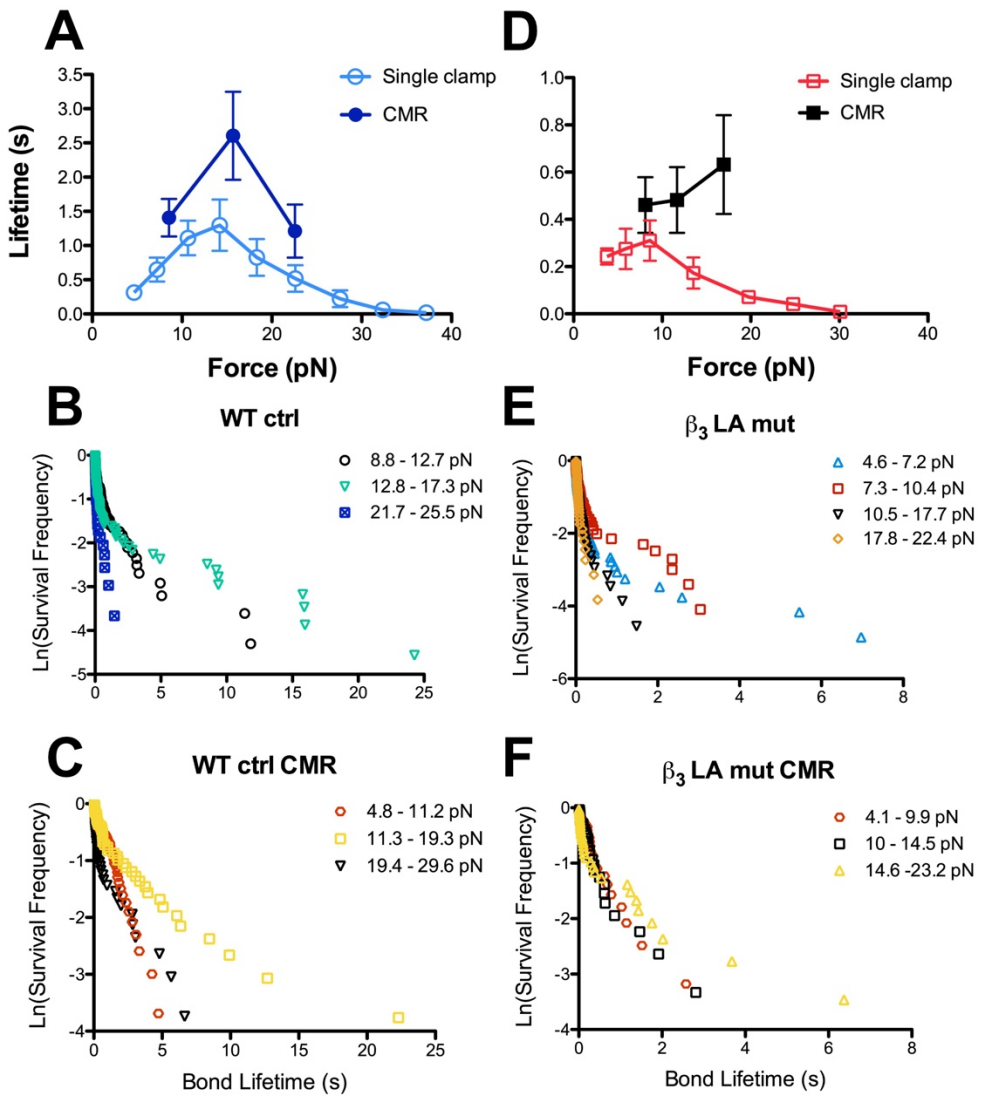

Figure 5.10. Cyclic mechanical reinforcement (CMR) appears to be a feature of integrin mechanobiology that may not involve talin. (A) Comparison of lifetime over force of WT with single force clamp or CMR. Lifetime distributions of equivalent force bins for single force clamp (B) and CMR (C) for WT. (D) Comparison of lifetime over force of β_3 LA mutant with single force clamp or CMR. Lifetime distributions of equivalent force bins for single force clamp (E) and CMR (F) for β_3 LA mutant.

5.2.5 *On ADP agonist and manganese ion stimulation: talin WA mutation impacts affinity more than force-mediated off-rate*

To provide a more complete view of the role of talin-integrin binding in integrin binding to immobilized ligand, we conducted the following activation studies with the WA and WT/fl platelets: 1) stimulating platelets with ADP agonist (high dose, 50 μM) for 5 minutes, and 2) activating integrins with the potent activator Mn^{2+} (by replacing the normal 1 mM Ca^{2+} with 0.5 mM Mn^{2+} in the chamber buffer) before measuring adhesion frequency and lifetimes with fibrinogen on the BFP.

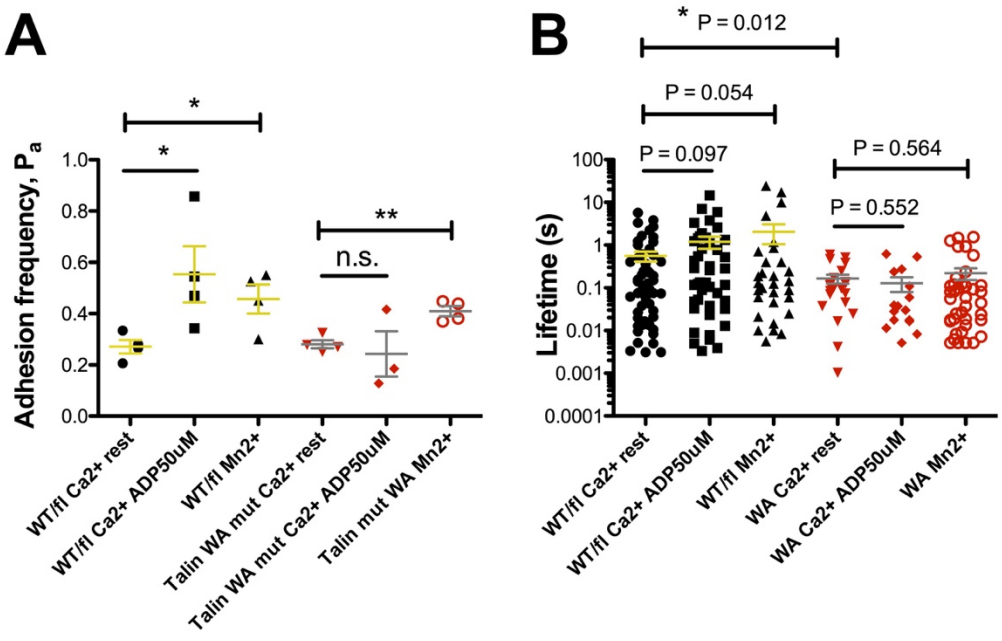

Figure 5.11. Activation of integrin by ADP and manganese ions show talin WA mutation impacts affinity more than force-mediated off rate. (A) Adhesion frequency (probability of adhesion, P_a) of WT/fl control and talin WA in resting condition (Ca^{2+} rest, with the regular condition 1 mM Ca^{2+}), 50 μM ADP, and 0.5 mM Mn^{2+}; each point represents a platelet. (B) Bond lifetimes of the same conditions as in (A); each point is a lifetime event. Statistics was performed using two-tailed, unpaired t-test, except for comparing the lifetimes of WT/fl and WA in Ca^{2+} rest condition where Welch's correction was applied.

Both ADP and Mn^{2+} stimulations increased the probability of adhesion (P_a) for the WT/fl platelets, which was expected (Figure 5.11 A, black). ADP did not increase the P_a for talin WA mut platelets, but Mn^{2+} did (Figure 5.11 A, red). This result was also expected because talin WA platelets had impaired spreading on fibrinogen with ADP and defective integrin activation even with more potent agonists (Stefanini et al., 2014), and our data with β_3 LA mutant platelets showed reduced integrin activation upon ADP stimulation (APPENDIX D). Mn^{2+} is an exogenous activator for integrins and had been shown to bypass talin for platelet adhesion and spreading on fibrinogen, which involves outside-in signaling (Shen et al., 2013). The data suggested that Mn^{2+} can further increase integrin affinity even for the WA mutant, corroborating that the 2D effective affinity is not affected by talin's ability to engage the integrin.

In contrast, lifetimes from WA platelets stimulated with ADP and Mn^{2+} both did not show an increase compared to the resting state. For WT/fl, no significance was found either, but the P values indicated show that there was a much higher probability that ADP and Mn^{2+} prolonged the integrin-fibrinogen lifetimes. To note, Mn^{2+} treatment increased the encounter of tethering when the platelets were impinged and retracted from the Fg bead, and those events were not counted due to inaccurate lifetime measurements. It needs to be noted that Mn^{2+} could potentially induce clustering of integrins (Cluzel et al., 2005), which made the lifetime measurement difficult as there could be multiple bond dissociations. Overall, the lifetime results implied that Mn^{2+} cannot rescue the bond lifetime defect of talin WA, which aligned with our understanding that the cytoplasmic support of talin and actin is crucial for the forced off-rate.

5.3 Discussion

It is to our surprise that all talin and β_3 mutants that disrupt the Rap1-talin-integrin axis reduced integrin-fibrinogen bond lifetimes of resting platelets. For each single bond event, the only "stimulation" the platelet received was the 15-25 pN impingement of the cell with the bead, and the loading of the bond (if one formed) at 500-800 pN/s loading rate prior to lifetime measured at the varied clamped forces. Most of the contacts were sub-seconds to less than two seconds, so talin would need to engage Rap1 and integrin in those short time frames. We cannot exclude the possibility that due to the method limitation, repeated integrin-ligand engagement resulted in overall longer lifetimes by the WT platelets; but this is unlikely as we did not observe progressively longer lifetimes or increased probability of adhesion for the WT. Integrin engagement with the ligand could have prompted talin to engage. However, adhesion frequency assay showed that talin KO still possessed lower 2D effective affinity compared to the WT and other mutants. Two possibilities could have precipitated the result: 1) there are still some baseline interactions of talin and integrin so that the integrin affinity is higher, and 2) the multiple impingement of the cell, loading, and rupture of integrin-Fg bonds primed talin to interact with integrins. It is unlikely that baseline affinity of the WT and mutant integrins are higher than those from talin KO because staining of integrins on resting platelets with JON/A (activation marker) or soluble fibrinogen were all comparable (Stefanini et al., 2014). The results point to a likely scenario that just a few impingements of the cell and pulling of the integrins could have increase the chance of talin-integrin interactions that could prime integrins to bind ligands.

Even though the average bond lifetimes of the LR mut are much shorter compared to the WT control, the integrin can still form catch bond with Fg (Figure 5.5 C). Relating back to the seemingly not defective biomechanical aggregation result, the force clamp result implicated how platelets maintain their bond strength through integrins. For the biomechanical platelet adhesion and aggregation, linkage to cytoskeleton seems much more important than the competence of integrin activation that's mostly observed in agonist stimulation. The catch-slip signature of bonds rather than the length of average lifetime had been reported to be the critical factor in receptor function (Wei Chen et al., 2011; Liu B, 2014; Bryan T Marshall et al., 2003). Receptors usually form slip bond with their monoclonal antibodies and have average lifetimes folds higher than those with their natural ligands, but the strong binding does not necessarily lead to signalling. Thus, each molecular pair has its "norm" of lifetime value, and the "catch" behaviour could evince more about the bond strengthening mechanism (Sokurenko, Vogel, & Thomas, 2008). Considering the published and our results, it seems that talin W359-β_3 L746 interaction is critical for integrin mechanobiology while L325-β_3 F727 and F730 interactions are more important for biochemical activation of integrins.

The bond lifetime data may reconcile a disagreement between purified system and cell system: our previous study using force probe on live platelets showed GPIIbIIIa and fibrinogen form catch bond (Y. Chen et al., 2019), but with all purified molecules, the Weisel group saw slip bond instead (Litvinov et al., 2011). GPIIbIIIa-fibrinogen catch bond formation requires cell environment where talin and Rap1 plays a pivotal role. Remarkably, even for a slip bond (talin WA) that would fit well with the Bell model, there still exists multiple species of bonds. The mechanism of talin's recruitment to the plasma membrane and integrin tail remains elusive. Rap1-interacting adaptor molecule (RIAM) was found

important for integrin activation in other focal adhesion-forming cells but not for platelets (Lee, Lim, Puzon-McLaughlin, Shattil, & Ginsberg, 2009; Stritt et al., 2015). A recent study demonstrated that talin was the major and perhaps only effector of Rap 1 for platelet integrin activation (Lagarrigue et al., 2020), which could explain the lack of RIAM function in platelets.

Our results largely agree with a previous report in which talin KO abrogated the biphasic adhesion behaviour between α5β1 and fibronectin in fibroblasts while kindlin KO did not but lowered the average rupture force, and that such adhesion requires F-actin coupling (Strohmeyer, Bharadwaj, Costell, Fässler, & Müller, 2017). Though in a different integrin and cell system, the machinery is likely preserved. The report however, used different retraction speeds to measure rupture forces; our experiments measured true lifetimes that least manipulated the receptor-ligand interactions (Yunfeng Chen et al., 2019). Actin retrograde flow is crucial for focal adhesions by aligning and orienting ligand-engaged integrins through talin (Swaminathan et al., 2017); we found here that even for early ligand engagement, actin polymerization plays a role in stabilizing the bond. Evidence show LFA-1 integrins on T cells need actin polymerization and myosin contraction to induce or stabilize the extended-open conformation for migration and immunological synapse formation (Comrie, Babich, & Burkhardt, 2015; Nordenfelt, Elliott, & Springer, 2016). In our study, the integrins should be predominantly in bent or extended-closed conformations due to the absence of agonist amplification, and intact actin flow could stabilize the bond.

The significance and mechanism of the memory effect have been relatively unexplored. Since signalling can be initiated by a single bond which has been demonstrated

in a few molecular systems (Ju, Chen, Xue, Du, & Zhu, 2016; Q. J. Li et al., 2004), GPIIbIIIa binding with fibrinogen could potentially trigger some level of signalling that contribute to the memory effect. Talin-integrin binding appeared important for positive feedback of mostly single integrin-ligand bonds (since the adhesion frequency is low). On the higher adhesion frequency window, the memory index difference between the talin WA mutant and control was diminished. Clustering of integrins may happen when adhesion frequency is higher as the bond dissociation is more likely not single, and it might mask the memory effect.

CMR could be an integrin-specific property that may involve other modulators but not talin and cytoskeleton linkage. It would be difficult to decouple the mechanosensory of talin and integrin as they work in tandem. We cannot exclude the possibility that the cyclic loading and unloading (which happened to be in the frequency range that talin was found to be responsive to via unfolding (Tapia-Rojo & Fernandez, 2020)) sensitized talin and accelerated its binding to integrin despite the mutation. The L746A point mutation only decelerates talin-integrin binding nonetheless. Recent study showed that just membrane deformation can activate integrins, which is independent of signalling including the talin (J. Kim et al., 2020). We argue that there exist multiple pathways to increase the adhesiveness of integrins, and the context for each pathway's contribution needs further exploration.

The Mn^{2+} activation experiments provided information relating TM domain and ectodomain of the integrin during activation. Mn^{2+} and activating mAb PT25-2 can activate integrins to bind soluble ligands even when α and β subunit TM domains were covalently clasped (Luo, Springer, & Takagi, 2004). Mn^{2+} has been reported to increase on-rate and

affinity (accessibility) between GPIIbIIIa and fibrinogen but not off-rate, and marginally decrease the force-dependent off-rate (Litvinov et al., 2012). Our adhesion and lifetime results supported these previous reports and add that if talin cannot normally associate with the integrin, it cannot facilitate and maintain the forced bond lifetimes with ECM.

Overall, given that talin binding to integrin either in the membrane proximal or distal region, talin binding to Rap1, and actin polymerization, all could shorten the bond lifetimes particularly under forces in the "catch" region, the current paradigm of Rap1-talin-integrin axis for integrin-ligand binding may be incomplete. In the sub-second timescale, would Rap1 need to be activated to become GTP-bound first, then recruit talin to the membrane to interact with integrins? Since there should be no other inside-out activation cues, the bond strengthening would be induced by ligand ligation: more of an outside-in fashion. A plausible interpretation is that the bond strengthening would require both intact actin dynamics and accessibility to Rap1 on the plasma membrane, which could also contribute to the bond stability.

CHAPTER 6. DIABETES IMPACTS BIOMECHANICAL PLATELET AGGREGATION

Disclaimer: this chapter was made possible with the help of Dr. Angela Lee to tirelessly obtain patient blood samples at her clinic in the Heart Research Institute and Dr. Arnold Ju's help with bleeding of the diabetic mice at the University of Sydney. The research nurses from Dr. Eric Felner's clinic at the Emory Children's Center offered their help to obtain pediatric samples and undergraduate researcher Jeffrey Butler (mentee) helped run the stenosis microfluidics experiments.

6.1 Introduction

Diabetes affects ~425 million people globally and the prevalence is growing (statista, 2019, Sep 12). Cardiovascular complications from atherothrombosis are the primary cause of diabetes-related deaths (Emerging Risk Factors et al., 2010; Leon & Maddox, 2015; Moreno & Fuster, 2004). Both type I and type II diabetes accelerate CVD development largely due to the exaggerated thrombotic response, although the cellular and molecular mechanisms remain unclear (Chawla, Chawla, & Jaggi, 2016; Fowler, 2008). Diabetic patients are typically less responsive to conventional anti-coagulant and anti-platelet therapies that target the biochemical pathways of thrombosis, which further increases the risk of morbidity and mortality (Ju et al., 2018). In contrast, GPIIbIIIa antagonists appear to work most effectively for diabetic patients with acute coronary syndromes, albeit possible bleeding complications, suggesting that dysregulation of GPIIbIIIa in diabetes underlies the inflated risk of thrombosis (Lincoff, 2003; Roffi et al., 2001).

Atherosclerotic processes may begin during childhood even though CVDs generally do not appear in children or adolescents. Subclinical CVD, namely an increase in blood vessel intima-media thickness and plaque buildup, is more commonly seen in type I diabetic (T1DM) children, adolescents, and adults compared to their age- and sex-matched healthy controls (de Ferranti et al., 2014). Some studies showed that T1DM had about a 10-fold age-adjusted increased risk of CVD, even higher than that observed in patients with the insulin resistant, type II diabetes (T2DM) (de Ferranti et al., 2014; Wisinski & Kimple, 2016). Interestingly, hyperglycemia (higher blood glucose level) only had a weak association with CVD occurrence, suggesting other factors such as inflammation and oxidative stress may greatly contribute to the escalated CVD risk in T1DM patients (Orchard, Costacou, Kretowski, & Nesto, 2006; Wisinski & Kimple, 2016). Clinical data suggests that the higher risk of CVD in T1DM patients is at least partially due to platelets, independent of endothelium damage, oxidative stress, and other abnormalities that arise with aging and obesity (Wisinski & Kimple, 2016). Thus, elucidating how platelets, the central effector of thrombosis, are dysregulated in diabetes is crucial for advancing our understanding of the pathology of diabetes-induced CVD.

A recent paradigm-shifting paper by our collaborator showed that diabetes did not affect platelet response to soluble agonists; only when shear forces in the flow condition and compressive collision of red blood cells were present was there a pronounced enhancement of adhesion of diabetic platelets compared to the control (Ju et al., 2018). The *in vivo* study in the paper showed needle-induced flow disturbances in mouse blood vessel resulted in larger thrombi in diabetic mice compared to the control, and integrin GPIIbIIIa was the major mediator. A possible link with the redox pathway within the platelet was identified and with the aid of Network Analysis, the authors narrowed down to a key player,

PI3K, which regulated the hyperreactivity of platelet integrin. To follow up on this work, we aim to use the stenosis microfluidics with conformation-specific antibodies to probe the affinity state of GPIIbIIIa and investigate the involvement of GPIbα in the hyperreactive platelet phenotype.

6.2 Results

6.2.1 Stenosis microfluidics as a method for assessing thrombotic risk of type 1 diabetic patients

We first sought to see if there was a difference in platelet aggregation in the stenosis microfluidics device between samples from diabetic patients and non-diabetic controls. We used the stenosis device that has a single pillar, and with 16 μL/min flow rate to reach a bulk shear rate of 1800 s^{-1}, the peak shear rate within 5 μm of the pillar apex could reach > 20k s^{-1}, which were well-characterized previously (Tovar-Lopez et al., 2013). T1DM patient and non-diabetic control (all adults) whole blood samples labeled with antibody SZ22 that stains GPIIbIIIa integrins of all conformations were individually perfused through the channels and the aggregation processes over ~7 min were recorded. With 4-6 donors and 10 experiments for the diabetic (DM) and control (ctrl), we demonstrated that the diabetic platelets aggregates grew faster and reached higher plateau (Figure 6.1). The data shown were selected data where some outliers were excluded as some samples did not aggregate much and some control samples had exaggerated aggregation possibly due to blood draw that lysed RBCs. Overall, the method was not ideal for screening due to the sensitivity to the sample preparation and the large variation even within the same sample. The recruited patients and volunteers also had a large variation in age, body mass index (BMI), cholesterol level and other metabolic indicators, which could complicate the result

interpretation. Interestingly, we did not find a correlation between blood glucose level or HbA1c level and the extent of aggregation (patients information kept at the Heart Research Institute, Sydney), despite not enough patient samples were obtained. The result showed that more diabetic samples tended to exhibit exaggerated aggregation compared to the non-diabetic control group.

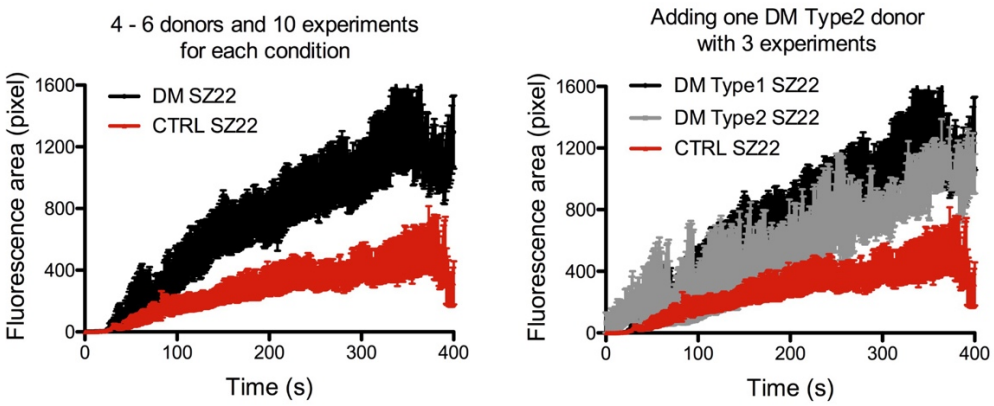

Figure 6.1. Platelets from adult diabetic patient samples accumulated at a higher rate and formed bulkier aggregates. Results were plotted as fluorescence area in pixel number (sufficed for comparison purpose) over time (s). The graphs shown are T1DM vs. control (left) and the same plot including a T2DM donor results (right). Data are shown mean ± SEM.

To examine more mechanistically, we stained the platelets (in the whole blood) with a combination of conformation-specific antibody and the SZ22. This would enable us to semi-quantify the fraction of integrins in different conformations, using SZ22 as the common denominator. The conformation-specific antibody was either MBC370.2 or AP5, which recognizes GPIIbIIIa extension or hybrid domain swing-out, respectively (Figure 6.2). The blood was labeled with either MBC370.2 + SZ22 or AP5 + SZ22 and each antibody was labeled with a different fluorophore. We did not use the gold-standard PAC-1 antibody, which recognizes GPIIbIIIa ligand binding site, because it is a large IgM

antibody that did not seem to penetrate the platelet aggregate well during our trial runs (completely negative signal).

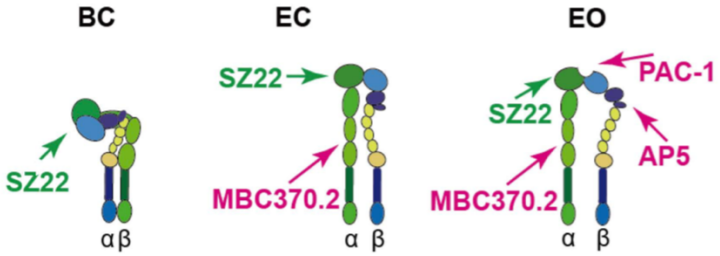

Figure 6.2. Schematic of conformation-specific antibodies for GPIIbIIIa. Bent-close (BC), extended-close (EC), and extended-open (EO) conformations are shown, where SZ22 stains all conformations, MBC370.2 stains the extended (closed and open), and AP5, similar to the gold-standard PAC-1 antibody, stains the extended open, fully activated integrin. Adapted from (Y. Chen et al., 2019).

We previously published that biomechanical aggregation was mediated by GPIIbIIIa in the EC conformer, which was largely MBC370.2-positive and AP5-negative (Y. Chen et al., 2019). We still see some AP5 staining but it was overall less than MBC370.2, and the ALB treatment did not seem to alter the aggregation dynamics. Fluorescence area at the saturation aggregation of each perfusion of MBC370.2 or AP5 normalized by SZ22 was plotted (Figure 6.3). Comparing the MBC370.2/SZ22 ratio of T1DM and control, the DM group displayed higher ratio regardless of the presence of ALB (Figure 6.3 B). In contrast, AP5/SZ22 ratio did not show any difference across the conditions, implying only the portion of EC integrins was higher for the DM group.

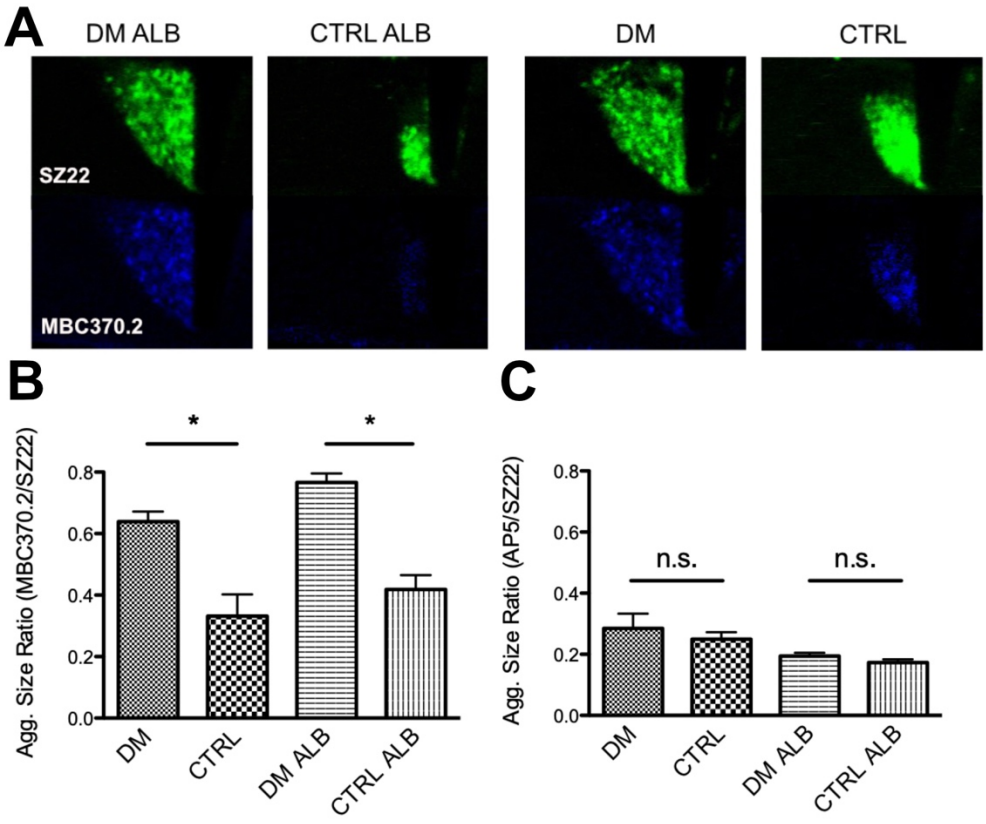

Figure 6.3. Fluorescence area ratio of conformation-specific antibody and SZ22 showed T1DM had more integrins in the extended-close conformation. (A) Representative images of the aggregates stained with SZ22 (green) and MBC370.2 (blue) from T1DM and ctrl samples with or without ALB. (B) Fluorescence area (aggregate size) ratio of MBC370.2 over SZ22, comparing the patient samples with and without ALB. (C) Fluorescence area (aggregate size) ratio of AP5 over SZ22, comparing the patient samples with and without ALB. For (B) and (C), each bar represents ≥ 3 ratios taken, and one-way ANOVA with Tukey's test was used.

Since the variation was large for adult patients, we decided to explore pediatric samples and to recruit patients of 8-17 years old. The 80% and 90% symmetrical stenosis devices were used to generate to the results (Figure 6.4). The data was segregated by racial heritage as each patient's "norm" of aggregation seemed distinct, and racial information was provided and could potentially be important. Figure 6.4 A shows all diabetic sample aggregation results (stained by SZ22) and B shows just the results of the Hispanic-native American and white patients since these two had very low level of aggregation. The patient

information is shown in Table 6.1. Two diabetic samples from black patients were obtained, and one sample each for the other racial heritages. Albeit the limited samples, no clear trend of aggregation result can be seen with sex, BMI, or HbA1c.

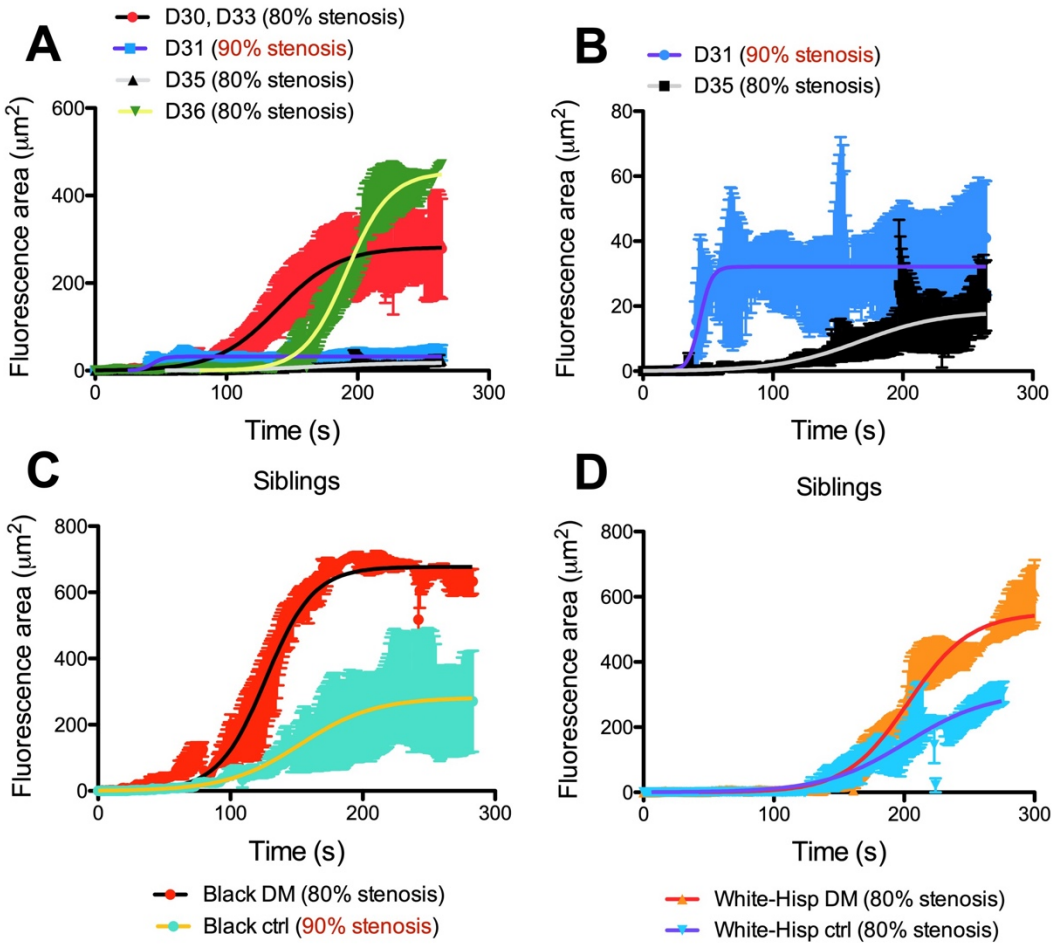

Figure 6.4. Platelet aggregation dynamics differ by patients. (A) T1DM patient results altogether, with the type of channel used noted, (B) same graph as (A) but only showing results from Hispanic-native American and white patients, (C) results from T1DM patient and a non-diabetic sibling in a black family, (D) results from T1DM patient and a non-diabetic sibling in a Hispanic-white family. Data are shown mean ± SEM with sigmoidal fitting; each data trace has n ≥ 2 experiments. All data that were collected were presented.

Since large differences can be seen from patient samples possibly due to their racial background among other reasons, we decided to test DM vs control samples from the same

household. On the days we could recruit a DM patient with his/her sibling with them, we would run both samples. We obtained such results from two different pairs of siblings (Figure 6.4 C-D). Albeit the limited samples, both pairs showed similar trends: DM sample aggregated faster to reach a higher saturation. To note, for the black family pair, the device used for the ctrl was 90% stenosis instead of 80% as for the DM; 90% stenosis channel has a steeper shear gradient that could be more activating to platelets (Figure 4.2). thus, the difference between the DM and ctrl for the black family pair could be even larger were they both run in the same type of channel. Information of the sibling pairs are shown in Table 6.1 (shaded rows). Neither BMI nor age had correlation with the extent of aggregation by inspection.

Table 6.1. Information of pediatric patients and sibling controls.

Patient ID	Sex	Race	Age	Diabetic	BMI	HbA1c (%)
D-30	F	Black	11	Yes	20.9	11.4
D-33	M	Black	10	Yes	34.2	12.9
C-18	F	Black	11	No	43.2	
D-36	M	White-Hispanic	13	Yes	16.8	8.1
C-19	M	White-Hispanic	10	No	17.2	
D-35	M	White-non-Hispanic	12	Yes	19.3	8.8
D-31	F	American Indian - Hispanic	15	Yes	26.5	11.3

6.2.2 *For diabetic platelets, GPIIbIIIa's response to force loading on itself or through GPIbα mechano-signalling seems not dysregulated*

From the stenosis microfluidics results, we were puzzled whether DM platelets inherently had more intermediate integrins or the GPIbα mechano-signaling pathway was dysregulated. To examine whether GPIIbIIIa affinity maturation through GPIbα signalling was altered in DM, we used the cone/plate-FACS method described in section 4.2.3 with samples from STZ-induced diabetic mice (mimicking chronic T1DM) and their age- and sex-matched littermate control. We added both botrocetin and murine dimeric A1 (though the dA1 was later found to not be necessary) to the platelet mix and sheared uniformly at 10k s^{-1} for 10 min. Shearing the sample generated the signature second population shown in Figure 4.8. Using 0 s^{-1} for 10 min as thresholding baseline, we obtained the % platelet positive and MFI stained by JON/A-PE but found no difference between the DM and ctrl, regardless of the presence of botrocetin. As a control experiment, shearing the sample with integrilin blockade did not prevent the agglutination (almost identical FSC and SSC) but abrogated JON/A-PE signal, as integrilin blocks JON/A access to GPIIbIIIa.

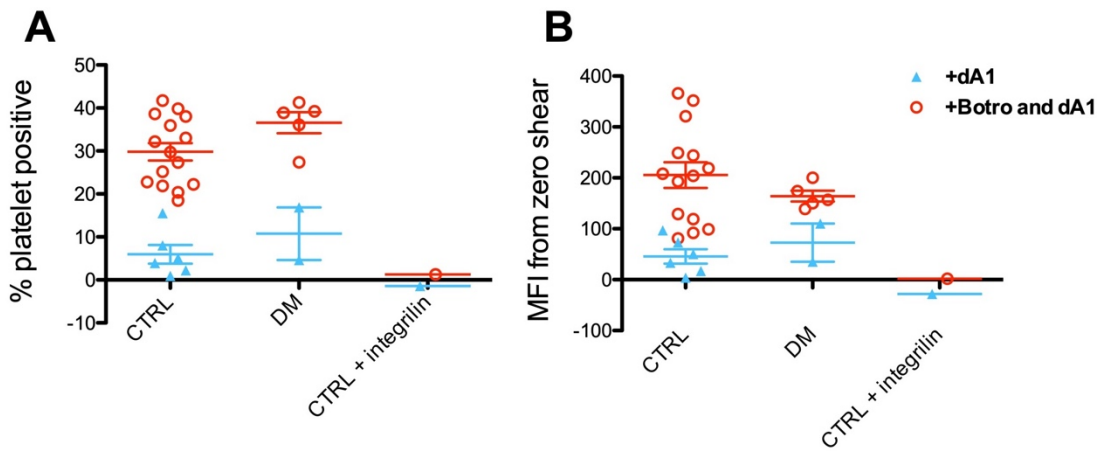

Figure 6.5. Cone/plate viscometer (rheometer) – FACS result showed no difference between diabetic and non-diabetic samples. (A) % platelet positive for JON/A-PE

signals. (B) Mean fluorescence intensity (MFI) of JON/A-PE. Each dot represents one experiment.

To further explore whether integrins on diabetic (STZ-induced) mouse platelets exhibit altered property that contributed to the hyperreactivity, we subjected them to varied force loading and measured succeeding bond lifetimes on the BFP. We chose this method to probe the integrins because we previously found that mouse GPIIbIIIa was exquisitely sensitive to force loading (Yunfeng Chen et al., 2019). The adhesion frequency was control to ~20% to measure mostly single bonds. However, we did not observe an impact of force loading rate on lifetimes in the diabetic platelets we tested (Figure 6.6). Even with rate 6x higher, the average lifetime or the range of lifetimes did not change. GPIIbIIIa on diabetic platelets did not show a response in bond strength to different loading rates; hence we did not pursue the same test on the non-diabetic controls.

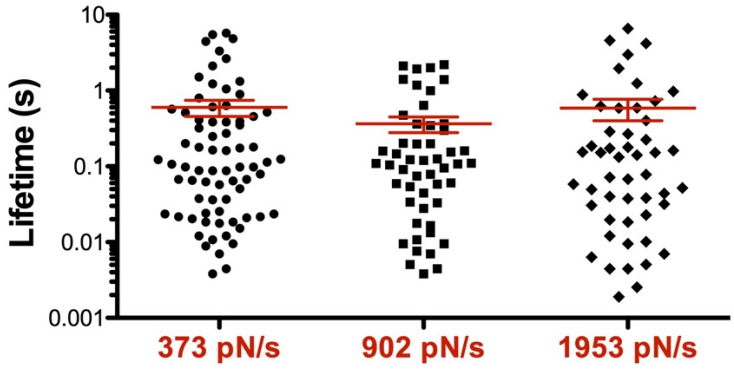

Figure 6.6. Lifetimes of integrin-fibrinogen bonds in varied force loadings showed no difference. Data was obtained from two STZ-induced diabetic mice; each point is one lifetime event; the bar shows mean ± SEM (red). X-axis shows binned force loading rates, with each rate being the average of that bin.

6.3 Discussion

Diabetes' impact on platelet in shear-induced activation and on the molecular level of detail was not examined until our collaborator's work which was recently published

(Ju et al., 2018). We followed up the study by comparing DM and ctrl gradient shear-induced platelet aggregation and found a trend of amplified aggregation of samples from the DM group for both adults (excluding some outliers) and adolescents. The adolescent (pediatric) samples may be better for this assay since there were less metabolic confounding factors. From the adult DM group, the extension-recognizing antibody showed more staining area normalized by the antibody recognizing all conformations of GPIIbIIIa, suggesting that the exaggerated aggregation may be due to more integrins in the intermediate affinity state. How the integrins got promoted to that affinity state was unclear – they could have been constitutively more activated, or the GPIbα mechano-signaling was dysregulated. However, using cone/plate viscometer–FACS did not show the more agglutination of DM platelets nor more activated GPIIbIIIa. The results suggested either our method was not sensitive enough or the difference between DM and ctrl was negligible. To note, these samples were sheared for 10 min, longer than the 2 min from Chapter 4, which could have masked any possible difference at an earlier time.

Using DM and non-DM siblings' samples on the same day demonstrated its potential of generating more consistent results, but the rarity of coming across such samples makes it difficult to obtain enough power. The success rate of the stenosis microfluidics experiments was not high due to the sensitivity of platelets to blood draw (how quiescent do they remain prior to the experiment), the channel imperfections, and particulates (from the PDMS, air, or blood tube) that occasionally come across the channel. Nevertheless, the results revealed a trend that corroborated our knowledge of increased CVD risk for diabetic patients and demand higher-throughput devices to be designed for the rare patient samples. Specifically, platelets' response to gradient-shear was enhanced in DM compared to the control group, which largely agreed with the

findings from mouse injury models (Ju et al., 2018). The force loading result was to our surprise given the sensitivity of integrin fine-tuning its kinetics in response to force history as we previously reported. Maybe we could have seen a difference in probability of adhesion in the varied loading rates, but given the response of bond lifetimes, a difference in this assay alone would be hard to interpret. Ju et al. found no difference in integrin-fibrinogen bond lifetimes between the DM and ctrl group (data not published), which suggested that the platelet integrin itself may not have significantly altered in diabetes, but the mechano-signalling pathways were altered as shown by integrin's outside-in signalling and the PI3K's involvement. Factors such as oxidative stress, compressive force sensing, and the likelihood of tether formation (Ju et al., 2018; Maxwell et al., 2007; Nesbitt et al., 2009) may be crucial for hyperactivity of DM platelets. For future therapies, targeting the intracellular enzymes (PI3K, Rap1) and adaptors (talin) involved in the mechano-signaling may lead to better clinical outcomes for DM patients.

CHAPTER 7. CONCLUSIONS AND FUTURE DIRECTIONS

7.1 Conclusions

We presented in this thesis the study of talin's regulation on platelet integrin mechanobiology on the single-cell, single-molecule level and population (aggregate) level. Mechanistically, we showed how talin, through interactions with other molecules namely Rap1 and actin filament, regulates force-mediated integrin binding of discoid platelets. Discoid platelets are in a low-activation state; despite their importance in gradient shear-induced platelet aggregation, their function was not well-examined as most studies in the field focused on mapping agonist-induced platelet activation pathways. With detailed conclusions discussed in each chapter, here we summarize the highlighted findings below:

1. On shear-induced discoid platelet aggregation:
    - Talin-integrin and talin-Rap1 binding are crucial for gradient shear-driven platelet aggregation.
    - Talin interacting with the integrin MPR seems more crucial for soluble agonist-induced and not mechano-binding induced integrin activation that happens at a shorter time scale
    - CalDAG-GEFI and STIM1 seemed dispensable for gradient shear-driven platelet aggregation.
    - Uniform shear-induced platelet agglutination and GPIIbIIIa affinity upregulation was mediated by GPIbα-vWF pulling.
    - Talin-integrin binding was needed for GPIIbIIIa maturation to a higher affinity via GPIbα mechano-signaling.

2. On force-mediated single-platelet adhesion to fibrinogen:
    - Disruption of talin-integrin binding or talin-Rap1 binding abolished the catch bond between GPIIbIIIa and fibrinogen.
    - Disruption of talin-integrin binding reduced integrin engagement to the cytoskeleton and resulted in lower bond strength.
    - Disruption of talin-integrin binding or the ability of talin to activate the integrin did not alter the affinity of GPIIbIIIa to immobilized fibrinogen.
    - Talin-integrin binding appeared important for the memory (encouragement of future bond formation by past bonds) of single integrin adhesion to fibrinogen
3. On the impact of diabetes on biomechanical platelet aggregation:
    - Diabetes seemed to amplify biomechanical platelet aggregation by promoting more GPIIbIIIa integrins to the intermediate conformational/ affinity state.
    - The difference between the DM and control group on the single molecular level (GPIIbIIIa) may be insignificant
    - Comparing the clotting response of DM and non-DM siblings may be more effective than comparing patients across demographics

We then updated the model of GPIbα mechano-signaling by adding talin, Rap1, and actin as important players: GPIbα signaling prompts actin-bound talin to release from its autoinhibited form and be recruited to the membrane by Rap1; once activated, talin engages integrins, linking to them actin retrograde flow.

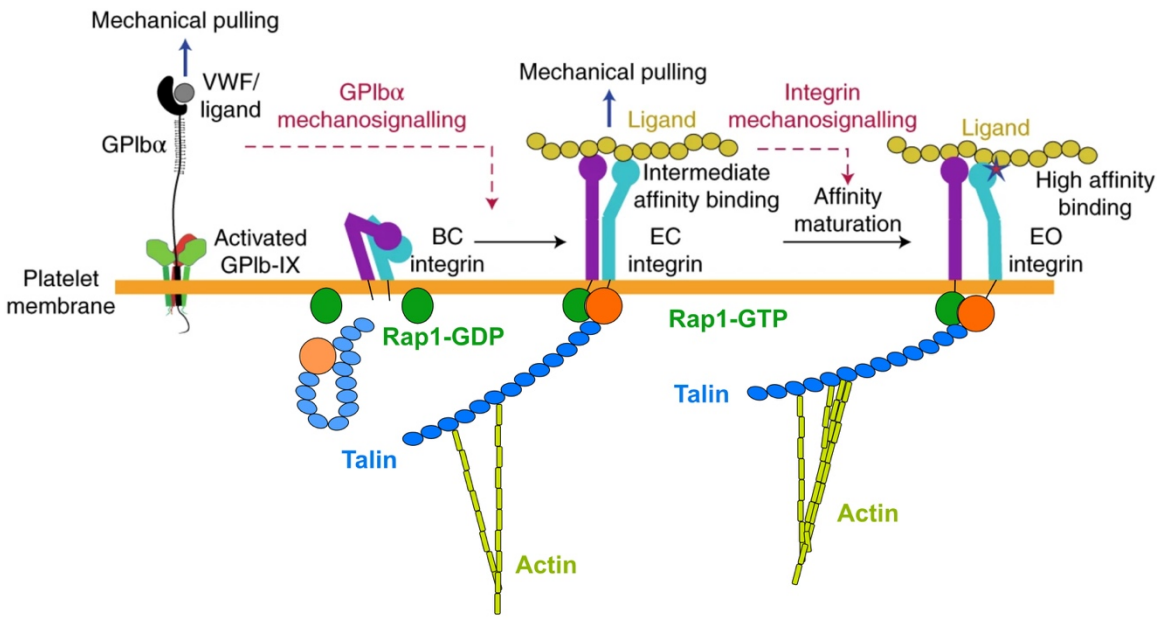

Figure 7.1. Updated model of crosstalk between GPIbα and GPIIbIIIa involving talin and actin. Adapted and modified from (X. F. Zhang & Cheng, 2019).

7.2 Future directions

The findings from this thesis raised more questions and many questions still were left unanswered. For the immediate follow-ups: the memory assay and cone/plate – FACS or the dual BFP assay could be performed with talin LR mutant platelets to complete delineating the roles of specific talin-integrin interactions. The thermal fluctuation assay that more accurately measures 2D on-rate and off-rate at zero force (W. Chen, Evans, McEver, & Zhu, 2008) could be used to help answer the questions about whether talin KO and mutants could affect force-free off-rate, and whether impingement alone could have primed talin to bind integrins. Adhesion frequency assay could be completed with the talin F1 and F1/F0 mutants to obtain a full picture of how Rap1-talin binding affects integrin 2D kinetics. The memory effect assay could be performed with cytochalasin D-treated WT platelets to examine whether intact actin retrograde flow is needed for adhesion memory. To fully examine cytoskeletal support, other treatments such as myosin inhibitor

blebbistatin and ROCK inhibitor Y-27632 should be used to understand the roles of other cytoskeleton components on the forced binding of integrins. For the CMR analysis, varying the number of loading-unloading cycles could create a curve that could potentially reveal some difference between the WT and the talin mutant.

To expand the study herein, talin's role in outside-in signalling of integrins under flow condition could be investigated. For example, flowing talin KO, mutant, or WT platelets over vWF- or fibrinogen-coated chamber and examine calcium flux of arrested platelets over time. Cone/plate viscometer combined with Western could be a powerful tool to investigate further the cytoplasmic players between GPIbα and GPIIbIIIa crosstalk. Potentially, and based on our preliminary data (not shown), one could measure integrin β_3 tail phosphorylation, total Akt and Akt serine 437 and threonine 308 phosphorylation (specific phosphorylation sites may matter), total Src and phosphorylated Src, and total PKC and phosphorylated PKC, using FAK and phosphorylated FAK as a control (since it is more important for outside-in signalling).

For the diabetic platelet aggregation study, more patients, especially sibling pairs could be recruited which would eliminate many confounding factors, so that a more definitive conclusion that diabetes exacerbates biomechanical thrombosis independent of agonist amplification could be reached. The conclusion was drawn from mouse platelet adhesion *in vitro* and aggregation *in vivo* but needs to be clearly demonstrated for human samples. Other aspects such as talin concentration and the occurrence of tethering in DM platelets compared to the control could be examined to help answering the question of why DM platelets seemed to have more integrins in the intermediate state. The stenosis device also needs innovation and improvement to increase the throughput and ease of use by

designing better particulate traps, multi-channel for a single run, and automatic pumping via, for example, a pneumatic mechanism (Szydzik et al., 2019). By presenting a striking difference between the DM and ctrl group, we would be better positioned to convince the community to focus on the biomechanical aspect of platelet activation to address the CVD susceptibility of the diabetic population.

APPENDIX A. RUNNING FREQUENCY OF PLATELET ADHESION TO FIBRINOGEN

Methods: Running frequency was obtained by using the repeated BFP force clamp assay (platelet interacting with fibrinogen-coated bead) and continuously sliding a window of ten contacts to obtain adhesion frequency over contacts.

Results: Running frequency of **WT/fl** platelets: each line represents one platelet. Overall, no clear upward or downward trend was observed, which suggested that platelet integrins were not getting activated over time. However, cycles of increase and decrease of adhesion frequency were observed, which prompted the study of memory.

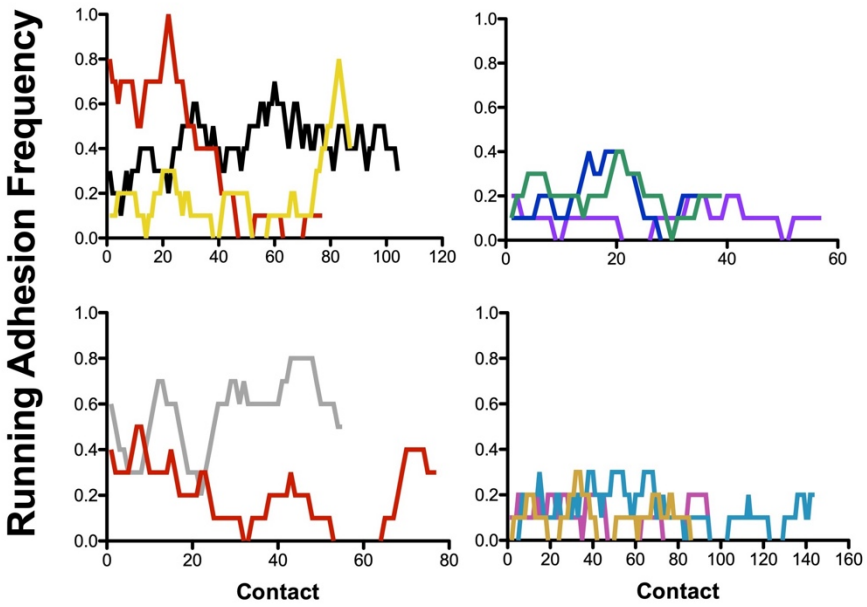

Results: Running frequency of **talin WA** platelets: each line represents one platelet.

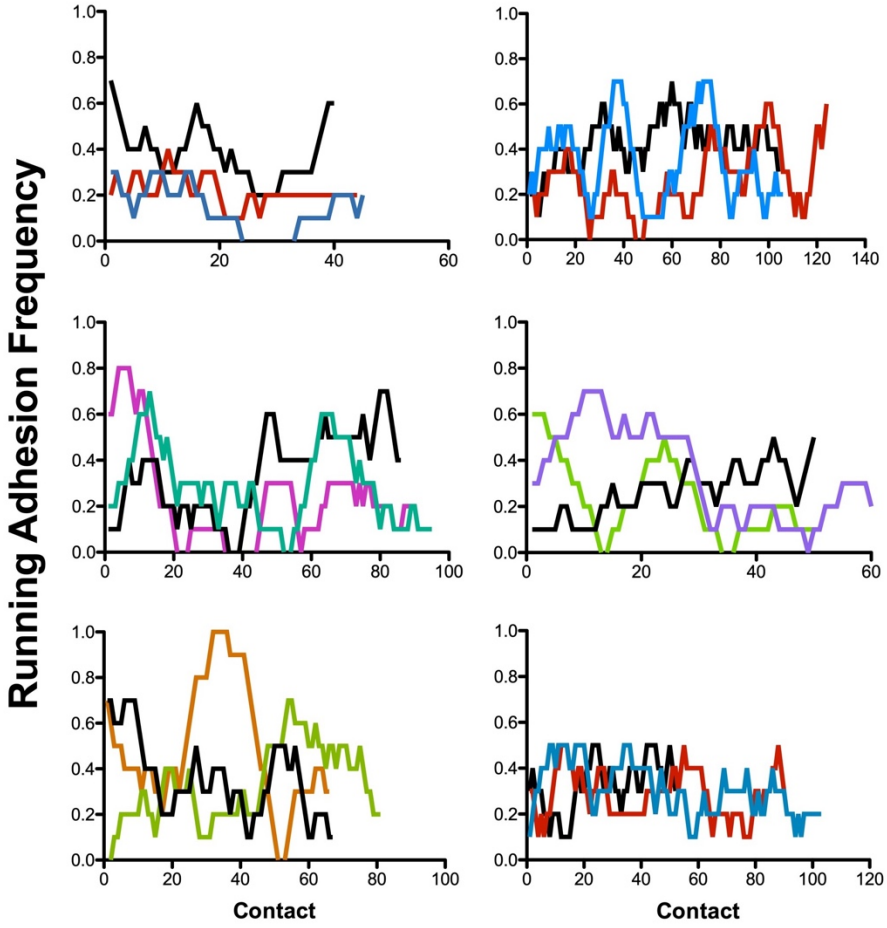

APPENDIX B. CONE/PLATE VISCOMETER–FACS REPRESENTATIVE RESULT FROM PLATELETS INCUBATED WITH ALB

Methods: Washed platelets were incubated with ALB, dimeric A1, botrocetin, and JON/A-PE, and sheared on the rheometer for 15 min at 10k s^{-1}. Afterwards, JON/A-PE staining was read on FACS. Activated integrin number means % shift of JON/A-PE with resting baseline of 2%.

Results: Left represents a typical result in the range of experiments without ALB; right represents an outlier where platelets did not agglutinate well.

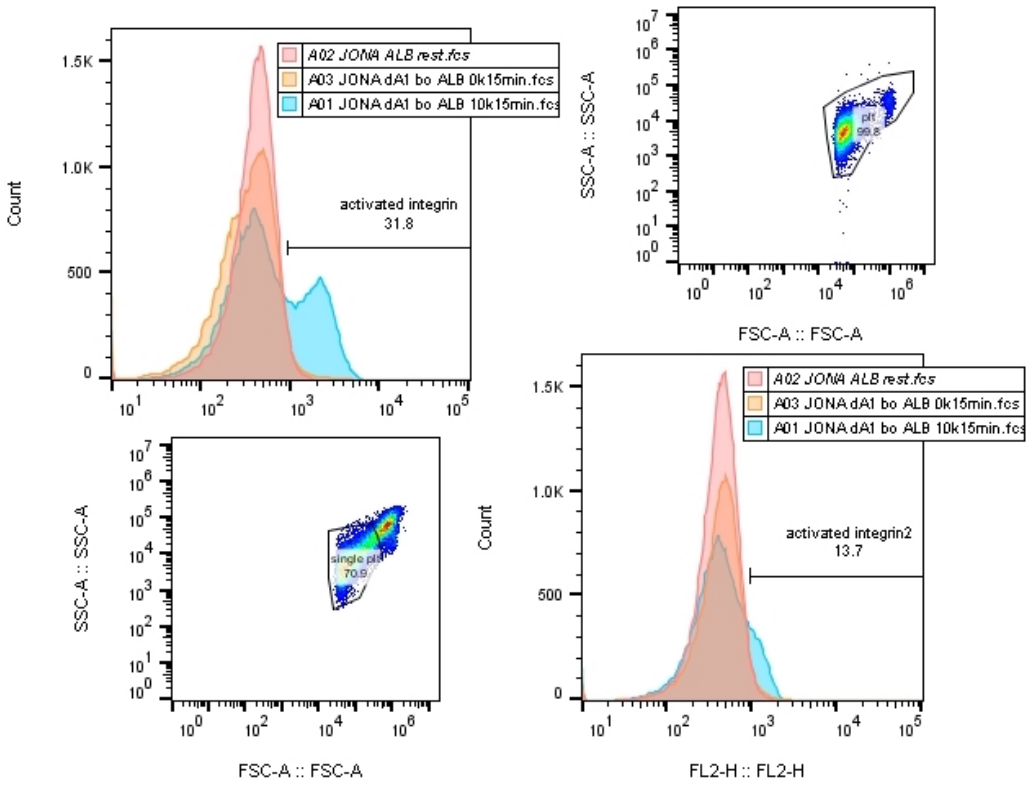

APPENDIX C. REPEATS OF Q-Q PLOT OF JON/A-PE VS. FSC WITH OR WITHOUT ALB

Methods: Platelet rich plasma was incubated with botrocetin (Bc) and JON/A-PE (with or without ALB) and sheared on the cone/plate viscometer for 2 min at 10k s^{-1}. Afterwards, JON/A-PE staining was read on FACS. Data from FSC and JON/A-PE fluorescent channel were obtained and displayed in overlay histograms and quantile-quantile (q-q) plots.

Results: All experiments regardless of ALB's presence exhibited nonlinear q-q plots particularly on the higher quantile region, which suggested that JON/A-PE signal increase was not merely due to the size of particle increase.

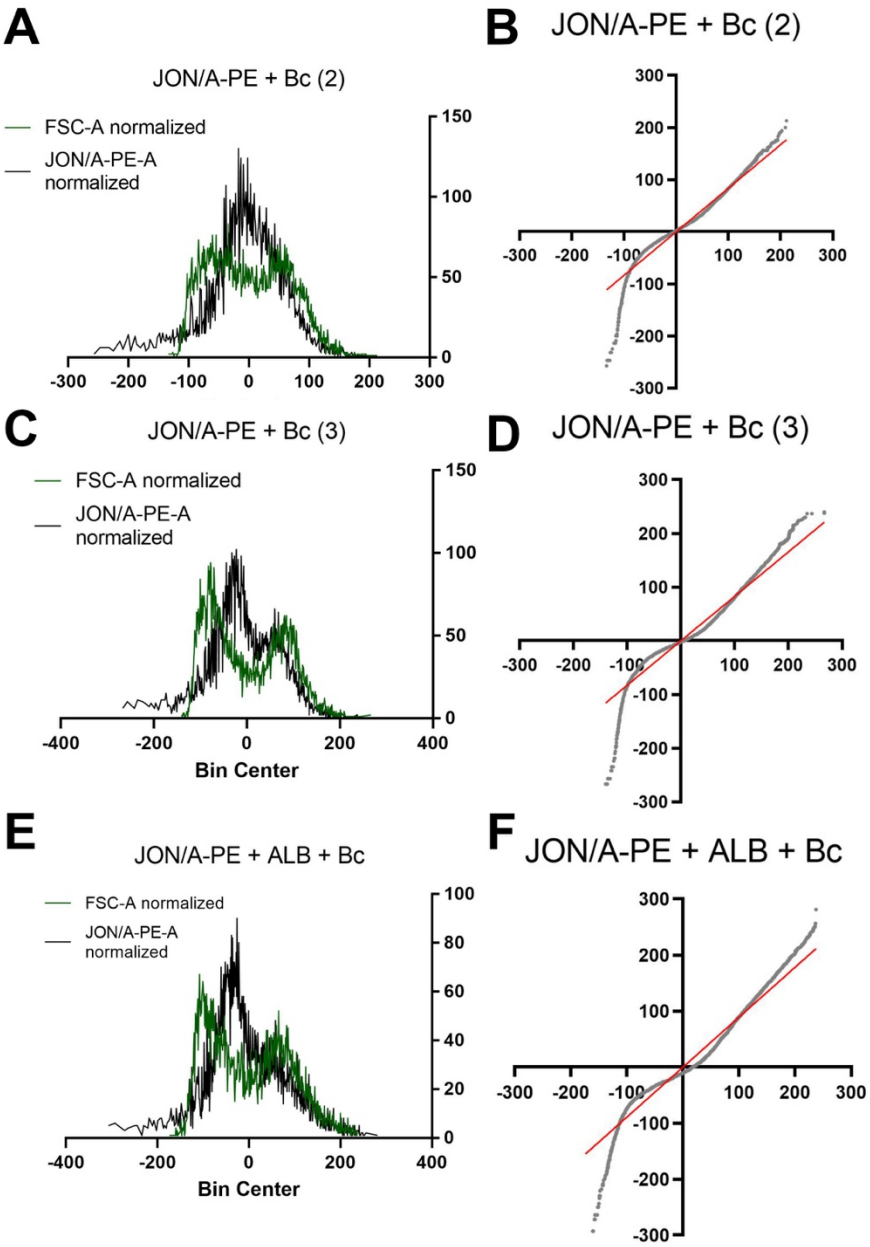
A
JON/A-PE + Bc (2)
FSC-A normalized
JON/A-PE-A normalized
B
JON/A-PE + Bc (2)
C
JON/A-PE + Bc (3)
FSC-A normalized
JON/A-PE-A normalized
Bin Center
D
JON/A-PE + Bc (3)
E
JON/A-PE + ALB + Bc
FSC-A normalized
JON/A-PE-A normalized
Bin Center
F
JON/A-PE + ALB + Bc

APPENDIX D. COMPARISON OF B_3 LA MUTANT AND WT CONTROL IN AGONIST ACTIVATION

Methods: Washed platelets were incubated with JON/A-PE and 10 μM ADP or 1 U thrombin for 5 min, then fixed with 2% PFA and read on FACS.

Results: Gray – resting state, orange – ADP, and green – thrombin stimulated. The number of activated integrin indicates the % JON/A-PE shift for the thrombin condition, using ~2% threshold for the resting state. Comparing the WT control (top) and β_3 LA mut (bottom), β_3 LA mut exhibited impaired integrin activation for both ADP and thrombin conditions.

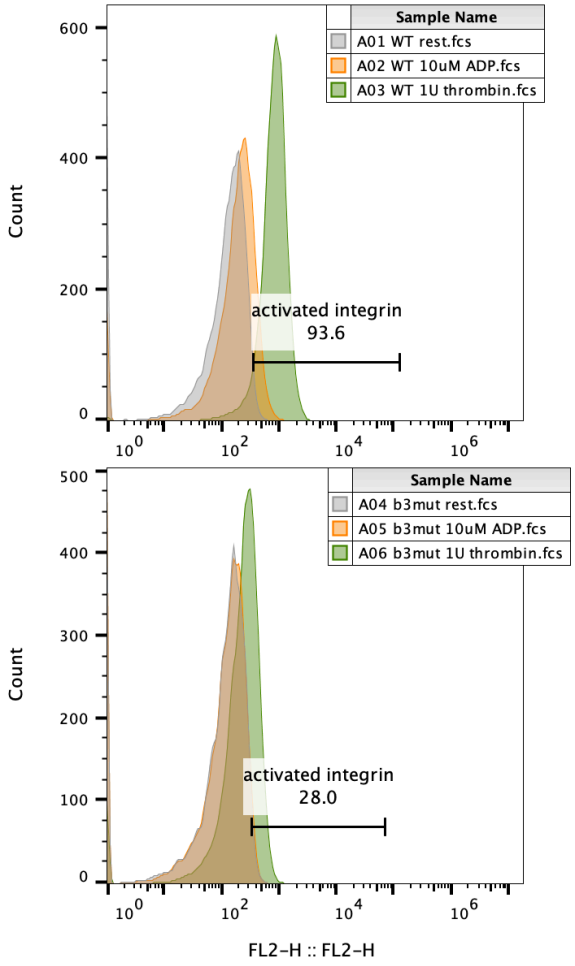

APPENDIX E. ADDITIONAL INFORMATION FROM THE CONE/PLATE UNIFORM SHEAR EXPERIMENTS

Methods: PRP incubated with Bc and JON/A-PE in ACD buffer (chelating most but not all Ca^{2+}) with (A) typical 1 mM Ca^{2+}, (B) without extra Ca^{2+} added, (C) Mg^{2+}/EGTA, and (D) 1 mM Ca^{2+} and GsMTx4 mechanosensitive cation channel inhibitor, were uniformly sheared on the cone/plate viscometer for 2 min at 10k s^{-1} and read on FACS afterwards.

Results: Platelets in saturated or reduced Ca^{2+} showed similar results, which suggested that not much extracellular Ca^{2+} was required for the agglutination, aggregation, and integrin activation. Platelets in Mg^{2+}/EGTA showed normal agglutination (C) but defective JON/A-PE staining, while GsMTx4-blocked showed normal agglutination and JON/A-PE staining (D). The result suggested either JON/A cannot bind GPIIbIIIa with Mg^{2+} and almost all Ca^{2+} chelated by EGTA, or that extracellular calcium is needed for this process, and they can center through other non-mechanosensitive channels. A shift in JON/A-PE binding can still be seen in Mg^{2+}/EGTA condition, although the staining from the aggregate population was even lower compared to the singlet population.

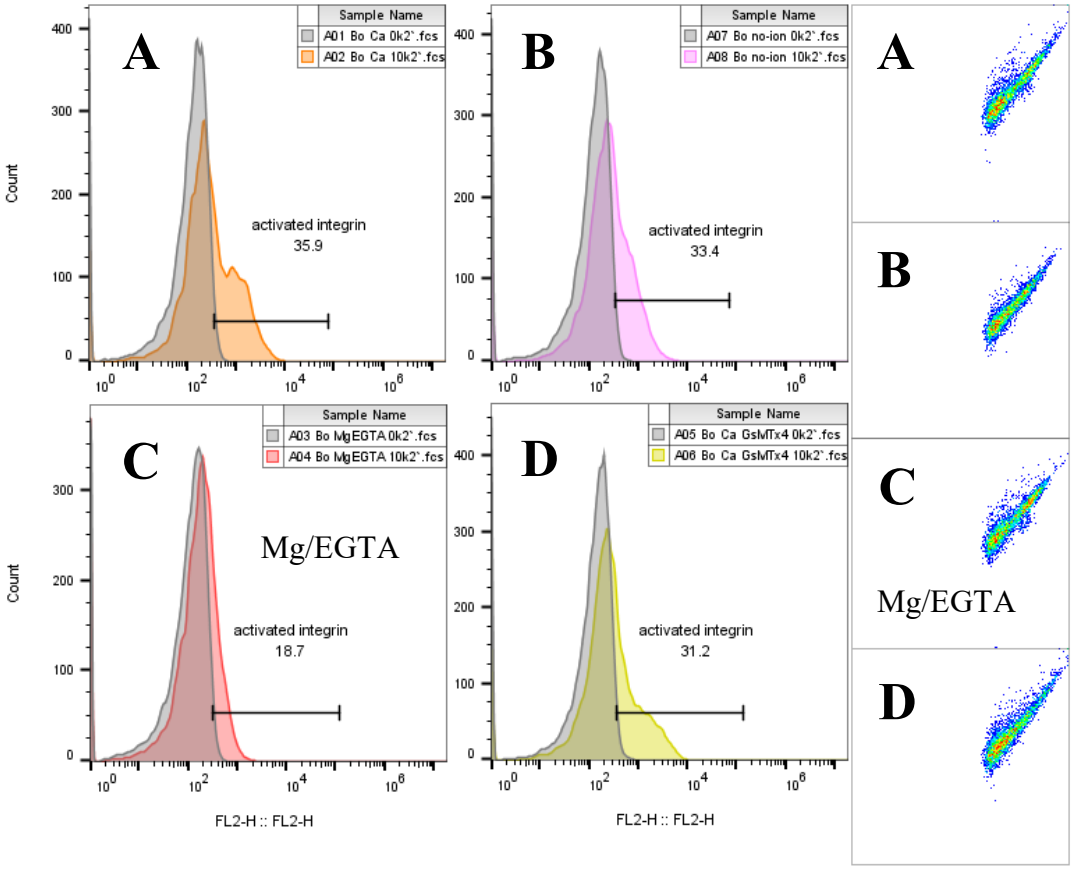
A
Sample Name
A01 Bo Ca 0k2`.fcs
A02 Bo Ca 10k2`.fcs
activated integrin
35.9
B
Sample Name
A07 Bo no-ion 0k2`.fcs
A08 Bo no-ion 10k2`.fcs
activated integrin
33.4
C
Sample Name
A03 Bo MgEGTA 0k2`.fcs
A04 Bo MgEGTA 10k2`.fcs
Mg/EGTA
activated integrin
18.7
D
Sample Name
A05 Bo Ca GsMTx4 0k2`.fcs
A06 Bo Ca GsMTx4 10k2`.fcs
activated integrin
31.2
Count
FL2-H :: FL2-H
A
B
C
Mg/EGTA
D

APPENDIX F. INTEGRIN GPIIBIIIA MOLECULAR STIFFNESS

Methods: Details of molecular stiffness analysis can be found in Y. Chen et al., 2019. Briefly, from BFP force clamp experiment, we can obtain molecular stiffness (regarding the receptor-ligand pair as spring-like materials and assuming the ligand fibrinogen does not change its conformations like integrins do).

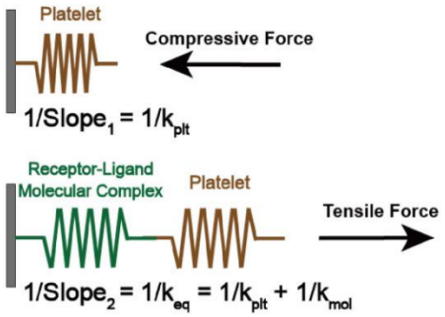

Results: (A) Overlay histograms of GPIIbIIIa molecular stiffness (pN/nm) of talin WA and WT/fl. (B) Overlay of histograms of GPIIbIIIa molecular stiffness of WT treated with cytochalasin D (in DMSO) and WT treated with equivalent volume DMSO. (C) Comparison of the mean stiffness ± SEM of the four conditions. It was implied that this assay could only measure the stiffness of the molecule pair itself as association of talin or intact cytoskeleton did not alter the result.

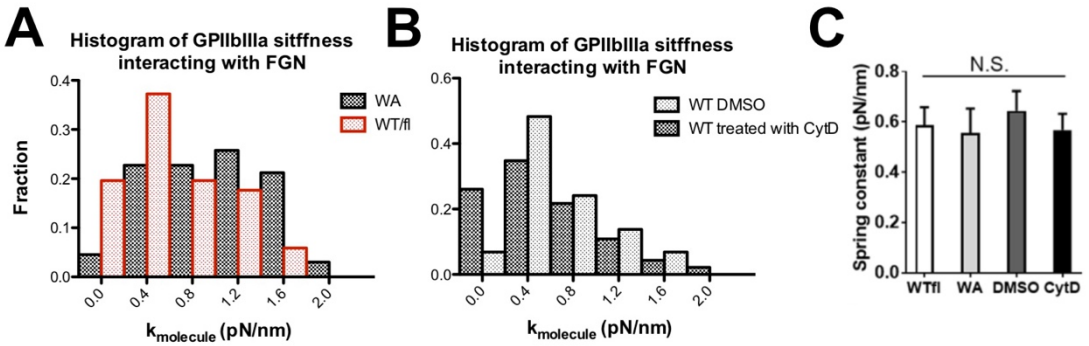

APPENDIX G. FRACTION OF LIFETIME EVENT FOR THE CMR AND NON-CMR ASSAYS

Methods: On the same day with platelets from the same WT mouse, the force clamp lifetime assay was conducted applying cyclic mechanical reinforcement (CMR) or just single force clamp. The fraction of lifetime event was calculated by the number of established lifetimesout divided by the number of all adhesion events for each platelet.

Results: No difference between CMR and non-CMR measurements was observed for the fraction of survived lifetimes, which suggested that CMR effect was not due to pre-selection of long-lived bonds.

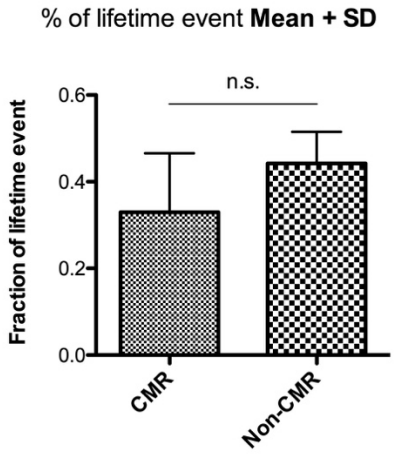

REFERENCES

Adair, B. D., Xiong, J. P., Maddock, C., Goodman, S. L., Arnaout, M. A., & Yeager, M. (2005). Three-dimensional EM structure of the ectodomain of integrin {alpha}V{beta}3 in a complex with fibronectin. *J Cell Biol, 168*(7), 1109-1118. doi:10.1083/jcb.200410068

Ahmad, F., Boulaftali, Y., Greene, T. K., Ouellette, T. D., Poncz, M., Feske, S., & Bergmeier, W. (2011). Relative contributions of stromal interaction molecule 1 and CalDAG-GEFI to calcium-dependent platelet activation and thrombosis. *J Thromb Haemost, 9*(10), 2077-2086. doi:10.1111/j.1538-7836.2011.04474.x

Ajzenberg, N., Aubry, P., Huisse, M. G., Cachier, A., El Amara, W., Feldman, L. J., . . . Steg, P. G. (2005). Enhanced shear-induced platelet aggregation in patients who experience subacute stent thrombosis: a case-control study. *J Am Coll Cardiol, 45*(11), 1753-1756. doi:10.1016/j.jacc.2004.10.079

Austen, K., Ringer, P., Mehlich, A., Chrostek-Grashoff, A., Kluger, C., Klingner, C., . . . Grashoff, C. (2015). Extracellular rigidity sensing by talin isoform-specific mechanical linkages. *Nat Cell Biol, 17*(12), 1597-1606. doi:10.1038/ncb3268

Bell, G. I. (1978). Models for the specific adhesion of cells to cells. *Science, 200*(4342), 618-627. doi:10.1126/science.347575

Bennett, J. S. (1996). Structural biology of glycoprotein IIb-IIIa. *Trends Cardiovasc Med, 6*(1), 31-36. doi:10.1016/1050-1738(95)00126-3

Bennett, J. S., Berger, B. W., & Billings, P. C. (2009). The structure and function of platelet integrins. *J Thromb Haemost, 7 Suppl 1*, 200-205. doi:10.1111/j.1538-7836.2009.03378.x

Bergmeier, W., Schulte, V., Brockhoff, G., Bier, U., Zirngibl, H., & Nieswandt, B. (2002). Flow cytometric detection of activated mouse integrin alphaIIbbeta3 with a novel monoclonal antibody. *Cytometry, 48*(2), 80-86. doi:10.1002/cyto.10114

Bevers, E. M., Comfurius, P., & Zwaal, R. F. (1983). Changes in membrane phospholipid distribution during platelet activation. *Biochim Biophys Acta, 736*(1), 57-66. doi:10.1016/0005-2736(83)90169-4

Blair, T. A., Michelson, A. D., & Frelinger, A. L., 3rd. (2018). Mass Cytometry Reveals Distinct Platelet Subtypes in Healthy Subjects and Novel Alterations in Surface Glycoproteins in Glanzmann Thrombasthenia. *Sci Rep, 8*(1), 10300. doi:10.1038/s41598-018-28211-5

Blue, R., Li, J., Steinberger, J., Murcia, M., Filizola, M., & Coller, B. S. (2010). Effects of limiting extension at the alphaIIb genu on ligand binding to integrin alphaIIbbeta3. *J Biol Chem, 285*(23), 17604-17613. doi:10.1074/jbc.M110.107763

Brazilek, R. J., Tovar-Lopez, F. J., Wong, A. K. T., Tran, H., Davis, A. S., McFadyen, J. D., . . . Nesbitt, W. S. (2017). Application of a strain rate gradient microfluidic device to von Willebrand's disease screening. *Lab Chip, 17*(15), 2595-2608. doi:10.1039/c7lc00498b

Bromberger, T., Zhu, L., Klapproth, S., Qin, J., & Moser, M. (2019). Rap1 and membrane lipids cooperatively recruit talin to trigger integrin activation. *J Cell Sci, 132*(21). doi:10.1242/jcs.235531

Calverley, D. C., Kavanagh, T. J., & Roth, G. J. (1998). Human signaling protein 14-3-3zeta interacts with platelet glycoprotein Ib subunits Ibalpha and Ibbeta. *Blood, 91*(4), 1295-1303. Retrieved from https://www.ncbi.nlm.nih.gov/pubmed/9454760

Chawla, A., Chawla, R., & Jaggi, S. (2016). Microvasular and macrovascular complications in diabetes mellitus: Distinct or continuum? *Indian J Endocrinol Metab, 20*(4), 546-551. doi:10.4103/2230-8210.183480

Chen, W., Evans, E. A., McEver, R. P., & Zhu, C. (2008). Monitoring receptor-ligand interactions between surfaces by thermal fluctuations. *Biophys J, 94*(2), 694-701. doi:10.1529/biophysj.107.117895

Chen, W., Lou, J., & Zhu, C. (2011). Forcing switch from short-to intermediate-and long-lived states of the αA domain generates LFA-1/ICAM-1 catch bonds. *The Journal of Biological Chemistry, 286*(20), 18344.

Chen, Y., Ju, L. A., Zhou, F., Liao, J., Xue, L., Su, Q. P., . . . Zhu, C. (2019). An integrin alphaIIbbeta3 intermediate affinity state mediates biomechanical platelet aggregation. *Nat Mater, 18*(7), 760-769. doi:10.1038/s41563-019-0323-6

Chen, Y., Liao, J., Yuan, Z., Li, K., Liu, B., Ju, L. A., & Zhu, C. (2019). Fast Force Loading Disrupts Molecular Binding Stability in Human and Mouse Cell Adhesions. *Molecular \& Cellular Biomechanics, 16*(3). doi:10.32604/mcb.2019.07267

Chen, Y., Liu, B., Ju, L., Hong, J., Ji, Q., Chen, W., & Zhu, C. (2015). Fluorescence biomembrane force probe: concurrent quantitation of receptor-ligand kinetics and binding-induced intracellular signaling on a single cell. *JoVE (Journal of Visualized Experiments)*(102), e52975-e52975.

Chen, Y., Ruggeri, Z. M., & Du, X. (2018). 14-3-3 proteins in platelet biology and glycoprotein Ib-IX signaling. *Blood, 131*(22), 2436-2448. doi:10.1182/blood-2017-09-742650

Cheng, M., Li, J., Negri, A., & Coller, B. S. (2013). Swing-Out of the β3 Hybrid Domain Is Required for αIIbβ3 Priming and Normal Cytoskeletal Reorganization, but Not Adhesion to Immobilized Fibrinogen. *PLoS One, 8*(12), e81609. doi:10.1371/journal.pone.0081609

Chesla, S. E., Selvaraj, P., & Zhu, C. (1998). Measuring two-dimensional receptor-ligand binding kinetics by micropipette. *Biophys J, 75*(3), 1553-1572. doi:10.1016/S0006-3495(98)74074-3

Chow, T. W., Hellums, J. D., Moake, J. L., & Kroll, M. H. (1992). Shear stress-induced von Willebrand factor binding to platelet glycoprotein Ib initiates calcium influx associated with aggregation. *Blood, 80*(1), 113-120. Retrieved from https://www.ncbi.nlm.nih.gov/pubmed/1611079

Cifuni, S. M., Wagner, D. D., & Bergmeier, W. (2008). CalDAG-GEFI and protein kinase C represent alternative pathways leading to activation of integrin alphaIIbbeta3 in platelets. *Blood, 112*(5), 1696-1703. doi:10.1182/blood-2008-02-139733

Cluzel, C., Saltel, F., Lussi, J., Paulhe, F., Imhof, B. A., & Wehrle-Haller, B. (2005). The mechanisms and dynamics of (alpha)v(beta)3 integrin clustering in living cells. *J Cell Biol, 171*(2), 383-392. doi:10.1083/jcb.200503017

Comrie, W. A., Babich, A., & Burkhardt, J. K. (2015). F-actin flow drives affinity maturation and spatial organization of LFA-1 at the immunological synapse. *J Cell Biol, 208*(4), 475-491. doi:10.1083/jcb.201406121

Cosemans, J. M., Iserbyt, B. F., Deckmyn, H., & Heemskerk, J. W. (2008). Multiple ways to switch platelet integrins on and off. *J Thromb Haemost, 6*(8), 1253-1261. doi:10.1111/j.1538-7836.2008.03041.x

Crittenden, J. R., Bergmeier, W., Zhang, Y., Piffath, C. L., Liang, Y., Wagner, D. D., . . . Graybiel, A. M. (2004). CalDAG-GEFI integrates signaling for platelet aggregation and thrombus formation. *Nat Med, 10*(9), 982-986. doi:http://www.nature.com/nm/journal/v10/n9/suppinfo/nm1098_S1.html

D'Souza, S. E., Ginsberg, M. H., Burke, T. A., & Plow, E. F. (1990). The ligand binding site of the platelet integrin receptor GPIIb-IIIa is proximal to the second calcium binding domain of its alpha subunit. *J Biol Chem, 265*(6), 3440-3446. Retrieved from https://www.ncbi.nlm.nih.gov/pubmed/2303453

de Ferranti, S. D., de Boer, I. H., Fonseca, V., Fox, C. S., Golden, S. H., Lavie, C. J., . . . Eckel, R. H. (2014). Type 1 diabetes mellitus and cardiovascular disease: a scientific statement from the American Heart Association and American Diabetes Association. *Diabetes Care, 37*(10), 2843-2863. doi:10.2337/dc14-1720

Deng, W., Xu, Y., Chen, W., Paul, D. S., Syed, A. K., Dragovich, M. A., . . . Li, R. (2016). Platelet clearance via shear-induced unfolding of a membrane mechanoreceptor. *Nat Commun, 7*, 12863. doi:10.1038/ncomms12863

Donati, A., Gupta, S., & Reviakine, I. (2016). Subpopulations in purified platelets adhering on glass. *Biointerphases, 11*(2). doi:Artn 029811

10.1116/1.4953866

Dumas, J. J., Kumar, R., McDonagh, T., Sullivan, F., Stahl, M. L., Somers, W. S., & Mosyak, L. (2004). Crystal structure of the wild-type von Willebrand factor A1-glycoprotein Ibalpha complex reveals conformation differences with a complex bearing von Willebrand disease mutations. *J Biol Chem, 279*(22), 23327-23334. doi:10.1074/jbc.M401659200

Elosegui-Artola, A., Oria, R., Chen, Y., Kosmalska, A., Perez-Gonzalez, C., Castro, N., . . . Roca-Cusachs, P. (2016). Mechanical regulation of a molecular clutch defines force transmission and transduction in response to matrix rigidity. *Nat Cell Biol, 18*(5), 540-548. doi:10.1038/ncb3336

Emerging Risk Factors, C., Sarwar, N., Gao, P., Seshasai, S. R., Gobin, R., Kaptoge, S., . . . Danesh, J. (2010). Diabetes mellitus, fasting blood glucose concentration, and risk of vascular disease: a collaborative meta-analysis of 102 prospective studies. *Lancet, 375*(9733), 2215-2222. doi:10.1016/S0140-6736(10)60484-9

Fan, Z., McArdle, S., Marki, A., Mikulski, Z., Gutierrez, E., Engelhardt, B., . . . Ley, K. (2016). Neutrophil recruitment limited by high-affinity bent beta2 integrin binding ligand in cis. *Nat Commun, 7*, 12658. doi:10.1038/ncomms12658

Fowler, M. J. (2008). Microvascular and Macrovascular Complications of Diabetes. *Clinical Diabetes, 26*(2), 77. doi:10.2337/diaclin.26.2.77

Fukuda, K., Doggett, T., Laurenzi, I. J., Liddington, R. C., & Diacovo, T. G. (2005). The snake venom protein botrocetin acts as a biological brace to promote dysfunctional platelet aggregation. *Nat Struct Mol Biol, 12*(2), 152-159. doi:10.1038/nsmb892

Garcia-Alvarez, B., de Pereda, J. M., Calderwood, D. A., Ulmer, T. S., Critchley, D., Campbell, I. D., . . . Liddington, R. C. (2003). Structural determinants of integrin recognition by talin. *Mol Cell, 11*(1), 49-58. doi:10.1016/s1097-2765(02)00823-7

Gibbons, J. D., & Chakraborti, S. (2014). *Nonparametric Statistical Inference, Fourth Edition: Revised and Expanded*: Taylor & Francis.

Gingras, A. R., Lagarrigue, F., Cuevas, M. N., Valadez, A. J., Zorovich, M., McLaughlin, W., . . . Ginsberg, M. H. (2019). Rap1 binding and a lipid-dependent helix in talin F1 domain promote integrin activation in tandem. *J Cell Biol, 218*(6), 1799-1809. doi:10.1083/jcb.201810061

Gingras, A. R., Vogel, K. P., Steinhoff, H. J., Ziegler, W. H., Patel, B., Emsley, J., . . . Barsukov, I. L. (2006). Structural and dynamic characterization of a vinculin binding site in the talin rod. *Biochemistry, 45*(6), 1805-1817. doi:10.1021/bi052136l

Goncalves, I., Nesbitt, W. S., Yuan, Y., & Jackson, S. P. (2005). Importance of temporal flow gradients and integrin alphaIIbbeta3 mechanotransduction for shear activation of platelets. *J Biol Chem, 280*(15), 15430-15437. doi:10.1074/jbc.M410235200

Goult, B. T., Bouaouina, M., Elliott, P. R., Bate, N., Patel, B., Gingras, A. R., . . . Barsukov, I. L. (2010). Structure of a double ubiquitin-like domain in the talin head: a role in integrin activation. *EMBO J, 29*(6), 1069-1080. doi:10.1038/emboj.2010.4

Haling, J. R., Monkley, S. J., Critchley, D. R., & Petrich, B. G. (2011). Talin-dependent integrin activation is required for fibrin clot retraction by platelets. *Blood, 117*(5), 1719-1722. doi:10.1182/blood-2010-09-305433

Hemmings, L., Rees, D. J., Ohanian, V., Bolton, S. J., Gilmore, A. P., Patel, B., . . . Critchley, D. R. (1996). Talin contains three actin-binding sites each of which is adjacent to a vinculin-binding site. *J Cell Sci, 109 (Pt 11)*, 2715-2726. Retrieved from https://www.ncbi.nlm.nih.gov/pubmed/8937989

Hynes, R. O. (2002). Integrins: bidirectional, allosteric signaling machines. *Cell, 110*(6), 673-687. doi:10.1016/s0092-8674(02)00971-6

Jackson, S. P., Nesbitt, W. S., & Westein, E. (2009). Dynamics of platelet thrombus formation. *J Thromb Haemost, 7 Suppl 1*, 17-20. doi:10.1111/j.1538-7836.2009.03401.x

Jiang, G. Y., Giannone, G., Critchley, D. R., Fukumoto, E., & Sheetz, M. P. (2003). Two-piconewton slip bond between fibronectin and the cytoskeleton depends on talin. *Nature, 424*(6946), 334-337. doi:10.1038/nature01805

Jobe, S. (2017). Platelet Heterogeneity. In P. Gresele, N. S. Kleiman, J. A. Lopez, & C. P. Page (Eds.), *Platelets in Thrombotic and Non-Thrombotic Disorders: Pathophysiology, Pharmacology and Therapeutics: an Update* (pp. 55-67). Cham: Springer International Publishing.

Jongen, M. S. A., MacArthur, B. D., Englyst, N. A., & West, J. (2020). Single platelet variability governs population sensitivity and initiates intrinsic heterotypic responses. *Communications Biology, 3*(1), 281. doi:10.1038/s42003-020-1002-5

Ju, L., Chen, Y., Li, K., Yuan, Z., Liu, B., Jackson, S. P., & Zhu, C. (2017). Dual Biomembrane Force Probe enables single-cell mechanical analysis of signal crosstalk between multiple molecular species. *Sci Rep, 7*(1), 14185. doi:10.1038/s41598-017-13793-3

Ju, L., Chen, Y., Xue, L., Du, X., & Zhu, C. (2016). Cooperative unfolding of distinctive mechanoreceptor domains transduces force into signals. *eLife, 5*. doi:10.7554/eLife.15447

Ju, L., Dong, J. F., Cruz, M. A., & Zhu, C. (2013). The N-terminal flanking region of the A1 domain regulates the force-dependent binding of von Willebrand factor to platelet glycoprotein Ibalpha. *J Biol Chem, 288*(45), 32289-32301. doi:10.1074/jbc.M113.504001

Ju, L., McFadyen, J. D., Al-Daher, S., Alwis, I., Chen, Y., Tonnesen, L. L., . . . Jackson, S. P. (2018). Compression force sensing regulates integrin alphaIIbbeta3 adhesive

function on diabetic platelets. *Nat Commun, 9*(1), 1087. doi:10.1038/s41467-018-03430-6

Kanaji, T., Russell, S., & Ware, J. (2002). Amelioration of the macrothrombocytopenia associated with the murine Bernard-Soulier syndrome. *Blood, 100*(6), 2102-2107. doi:10.1182/blood-2002-03-0997

Kaplan, Z. S., & Jackson, S. P. (2011). The role of platelets in atherothrombosis. *Hematology Am Soc Hematol Educ Program, 2011*, 51-61. doi:10.1182/asheducation-2011.1.51

Kesmarky, G., Kenyeres, P., Rabai, M., & Toth, K. (2008). Plasma viscosity: a forgotten variable. *Clin Hemorheol Microcirc, 39*(1-4), 243-246. Retrieved from https://www.ncbi.nlm.nih.gov/pubmed/18503132

Khan, R. B., & Goult, B. T. (2019). Adhesions Assemble!—Autoinhibition as a Major Regulatory Mechanism of Integrin-Mediated Adhesion. *Frontiers in Molecular Biosciences, 6*(144). doi:10.3389/fmolb.2019.00144

Kim, D., Bresette, C., Liu, Z., & Ku, D. N. (2019). Occlusive thrombosis in arteries. *APL Bioeng, 3*(4), 041502. doi:10.1063/1.5115554

Kim, J., Lee, J., Jang, J., Ye, F., Hong, S. J., Petrich, B. G., . . . Kim, C. (2020). Topological Adaptation of Transmembrane Domains to the Force-Modulated Lipid Bilayer Is a Basis of Sensing Mechanical Force. *Current Biology, 30*(9), 1614-+. doi:10.1016/j.cub.2020.02.028

Klapholz, B., & Brown, N. H. (2017). Talin - the master of integrin adhesions. *J Cell Sci, 130*(15), 2435-2446. doi:10.1242/jcs.190991

Kong, F., Li, Z., Parks, W. M., Dumbauld, D. W., Garcia, A. J., Mould, A. P., . . . Zhu, C. (2013). Cyclic mechanical reinforcement of integrin-ligand interactions. *Mol Cell, 49*(6), 1060-1068. doi:10.1016/j.molcel.2013.01.015

Kumar, A., Ouyang, M. X., Van den Dries, K., McGhee, E. J., Tanaka, K., Anderson, M. D., . . . Schwartz, M. A. (2016). Talin tension sensor reveals novel features of focal adhesion force transmission and mechanosensitivity (vol 213, pg 371, 2016). *Journal of Cell Biology, 214*(2), 231-231. doi:10.1083/jcb.20151001207062016c

Lagarrigue, F., Paul, D. S., Gingras, A. R., Valadez, A. J., Sun, H., Lin, J., . . . Ginsberg, M. H. (2020). Talin1 is the Principal Platelet Rap1 Effector of Integrin Activation. *Blood*. doi:10.1182/blood.2020005348

Lang, F., Munzer, P., Gawaz, M., & Borst, O. (2013). Regulation of STIM1/Orai1-dependent Ca2+ signalling in platelets. *Thrombosis and Haemostasis, 110*(5), 925-930. doi:10.1160/Th13-02-0176

Lee, H. S., Lim, C. J., Puzon-McLaughlin, W., Shattil, S. J., & Ginsberg, M. H. (2009). RIAM activates integrins by linking talin to ras GTPase membrane-targeting sequences. *J Biol Chem, 284*(8), 5119-5127. doi:10.1074/jbc.M807117200

Lefort, C. T., Rossaint, J., Moser, M., Petrich, B. G., Zarbock, A., Monkley, S. J., . . . Ley, K. (2012). Distinct roles for talin-1 and kindlin-3 in LFA-1 extension and affinity regulation. *Blood, 119*(18), 4275-4282. doi:10.1182/blood-2011-08-373118

Leon, B. M., & Maddox, T. M. (2015). Diabetes and cardiovascular disease: Epidemiology, biological mechanisms, treatment recommendations and future research. *World J Diabetes, 6*(13), 1246-1258. doi:10.4239/wjd.v6.i13.1246

Li, Q. J., Dinner, A. R., Qi, S. Y., Irvine, D. J., Huppa, J. B., Davis, M. M., & Chakraborty, A. K. (2004). CD4 enhances T cell sensitivity to antigen by coordinating Lck accumulation at the immunological synapse. *Nature Immunology, 5*(8), 791-799. doi:10.1038/ni1095

Li, Y. F., Tang, R. H., Puan, K. J., Law, S. K., & Tan, S. M. (2007). The cytosolic protein talin induces an intermediate affinity integrin alphaLbeta2. *J Biol Chem, 282*(33), 24310-24319. doi:10.1074/jbc.M701860200

Li, Z., Kong, F., & Zhu, C. (2016). A model for cyclic mechanical reinforcement. *Sci Rep, 6*, 35954. doi:10.1038/srep35954

Lincoff, A. M. (2003). Important triad in cardiovascular medicine: diabetes, coronary intervention, and platelet glycoprotein IIb/IIIa receptor blockade. *Circulation, 107*(11), 1556-1559. doi:10.1161/01.cir.0000055653.52489.e9

Litvinov, R. I., Barsegov, V., Schissler, A. J., Fisher, A. R., Bennett, J. S., Weisel, J. W., & Shuman, H. (2011). Dissociation of bimolecular alphaIIbbeta3-fibrinogen complex under a constant tensile force. *Biophys J, 100*(1), 165-173. doi:10.1016/j.bpj.2010.11.019

Litvinov, R. I., Bennett, J. S., Weisel, J. W., & Shuman, H. (2005). Multi-step fibrinogen binding to the integrin (alpha)IIb(beta)3 detected using force spectroscopy. *Biophys J, 89*(4), 2824-2834. doi:10.1529/biophysj.105.061887

Litvinov, R. I., Mekler, A., Shuman, H., Bennett, J. S., Barsegov, V., & Weisel, J. W. (2012). Resolving two-dimensional kinetics of the integrin alphaIIbbeta3-fibrinogen interactions using binding-unbinding correlation spectroscopy. *J Biol Chem, 287*(42), 35275-35285. doi:10.1074/jbc.M112.404848

Litvinov, R. I., Shuman, H., Bennett, J. S., & Weisel, J. W. (2002). Binding strength and activation state of single fibrinogen-integrin pairs on living cells. *Proc Natl Acad Sci U S A, 99*(11), 7426-7431. doi:10.1073/pnas.112194999

Liu B, C. W., Evavold B. D., Zhu C. (2014). Accumulation of Dynamic Catch Bonds between TCR and Agonist Peptide-MHC Triggers T Cell Signaling. *Cell, 157*(2).

Luo, B. H., Carman, C. V., & Springer, T. A. (2007). Structural basis of integrin regulation and signaling. *Annu Rev Immunol, 25*, 619-647. doi:10.1146/annurev.immunol.25.022106.141618

Luo, B. H., Springer, T. A., & Takagi, J. (2004). A specific interface between integrin transmembrane helices and affinity for ligand. *Plos Biology, 2*(6), 776-786. doi:ARTN e153

10.1371/journal.pbio.0020153

Margadant, F., Chew, L. L., Hu, X., Yu, H., Bate, N., Zhang, X., & Sheetz, M. (2011). Mechanotransduction in vivo by repeated talin stretch-relaxation events depends upon vinculin. *PLoS Biol, 9*(12), e1001223. doi:10.1371/journal.pbio.1001223

Marshall, B. T., Long, M., Piper, J. W., Yago, T., McEver, R. P., & Zhu, C. (2003). Direct observation of catch bonds involving cell-adhesion molecules. *Nature, 423*(6936), 190-193.

Marshall, B. T., Long, M., Piper, J. W., Yago, T., McEver, R. P., & Zhu, C. (2003). Direct observation of catch bonds involving cell-adhesion molecules. *Nature, 423*(6936), 190-193. doi:10.1038/nature01605

Maxwell, M. J., Westein, E., Nesbitt, W. S., Giuliano, S., Dopheide, S. M., & Jackson, S. P. (2007). Identification of a 2-stage platelet aggregation process mediating shear-dependent thrombus formation. *Blood, 109*(2), 566-576. doi:10.1182/blood-2006-07-028282

McEwan, P. A., Yang, W., Carr, K. H., Mo, X., Zheng, X., Li, R., & Emsley, J. (2011). Quaternary organization of GPIb-IX complex and insights into Bernard-Soulier syndrome revealed by the structures of GPIbbeta and a GPIbbeta/GPIX chimera. *Blood, 118*(19), 5292-5301. doi:10.1182/blood-2011-05-356253

Moake, J. L., Turner, N. A., Stathopoulos, N. A., Nolasco, L., & Hellums, J. D. (1988). Shear-induced platelet aggregation can be mediated by vWF released from platelets, as well as by exogenous large or unusually large vWF multimers, requires adenosine diphosphate, and is resistant to aspirin. *Blood, 71*(5), 1366-1374. doi:10.1182/blood.V71.5.1366.bloodjournal7151366

Moreno, P. R., & Fuster, V. (2004). New aspects in the pathogenesis of diabetic atherothrombosis. *J Am Coll Cardiol, 44*(12), 2293-2300. doi:10.1016/j.jacc.2004.07.060

Moser, M., Legate, K. R., Zent, R., & Fassler, R. (2009). The tail of integrins, talin, and kindlins. *Science, 324*(5929), 895-899. doi:10.1126/science.1163865

Nakazawa, T., Tadokoro, S., Kamae, T., Kiyomizu, K., Kashiwagi, H., Honda, S., . . . Tomiyama, Y. (2013). Agonist stimulation, talin-1, and kindlin-3 are crucial for alpha(IIb)beta(3) activation in a human megakaryoblastic cell line, CMK. *Exp Hematol, 41*(1), 79-90 e71. doi:10.1016/j.exphem.2012.09.011

Nesbitt, W. S., Kulkarni, S., Giuliano, S., Goncalves, I., Dopheide, S. M., Yap, C. L., . . . Jackson, S. P. (2002). Distinct glycoprotein Ib/V/IX and integrin alpha IIbbeta 3-dependent calcium signals cooperatively regulate platelet adhesion under flow. *J Biol Chem, 277*(4), 2965-2972. doi:10.1074/jbc.M110070200

Nesbitt, W. S., Westein, E., Tovar-Lopez, F. J., Tolouei, E., Mitchell, A., Fu, J., . . . Jackson, S. P. (2009). A shear gradient-dependent platelet aggregation mechanism drives thrombus formation. *Nat Med, 15*(6), 665-673. doi:10.1038/nm.1955

Nieswandt, B., Moser, M., Pleines, I., Varga-Szabo, D., Monkley, S., Critchley, D., & Fassler, R. (2007). Loss of talin1 in platelets abrogates integrin activation, platelet aggregation, and thrombus formation in vitro and in vivo. *J Exp Med, 204*(13), 3113-3118. doi:10.1084/jem.20071827

Nordenfelt, P., Elliott, H. L., & Springer, T. A. (2016). Coordinated integrin activation by actin-dependent force during T-cell migration. *Nat Commun, 7*, 13119. doi:10.1038/ncomms13119

Nuyttens, B. P., Thijs, T., Deckmyn, H., & Broos, K. (2011). Platelet adhesion to collagen. *Thromb Res, 127 Suppl 2*, S26-29. doi:10.1016/S0049-3848(10)70151-1

Orchard, T. J., Costacou, T., Kretowski, A., & Nesto, R. W. (2006). Type 1 diabetes and coronary artery disease. *Diabetes Care, 29*(11), 2528-2538. doi:10.2337/dc06-1161

Orlowski, A., Kukkurainen, S., Poyry, A., Rissanen, S., Vattulainen, I., Hytonen, V. P., & Rog, T. (2015). PIP2 and Talin Join Forces to Activate Integrin. *J Phys Chem B, 119*(38), 12381-12389. doi:10.1021/acs.jpcb.5b06457

Petrich, B. G., Fogelstrand, P., Partridge, A. W., Yousefi, N., Ablooglu, A. J., Shattil, S. J., & Ginsberg, M. H. (2007). The antithrombotic potential of selective blockade of talin-dependent integrin alpha IIb beta 3 (platelet GPIIb-IIIa) activation. *J Clin Invest, 117*(8), 2250-2259. doi:10.1172/JCI31024

Petrich, B. G., Marchese, P., Ruggeri, Z. M., Spiess, S., Weichert, R. A., Ye, F., . . . Ginsberg, M. H. (2007). Talin is required for integrin-mediated platelet function in hemostasis and thrombosis. *J Exp Med, 204*(13), 3103-3111. doi:10.1084/jem.20071800

Piatt, R., Paul, D. S., Lee, R. H., McKenzie, S. E., Parise, L. V., Cowley, D. O., . . . Bergmeier, W. (2016). Mice Expressing Low Levels of CalDAG-GEFI Exhibit Markedly Impaired Platelet Activation With Minor Impact on Hemostasis. *Arterioscler Thromb Vasc Biol, 36*(9), 1838-1846. doi:10.1161/ATVBAHA.116.307874

Quach, M. E., Dragovich, M. A., Chen, W. C., Syed, A. K., Cao, W. P., Liang, X., . . . Li, R. H. (2018). Fc-independent immune thrombocytopenia via mechanomolecular signaling in platelets. *Blood, 131*(7), 787-796. doi:10.1182/blood-2017-05-784975

Rana, A., Westein, E., Niego, B., & Hagemeyer, C. E. (2019). Shear-Dependent Platelet Aggregation: Mechanisms and Therapeutic Opportunities. *Front Cardiovasc Med, 6*, 141. doi:10.3389/fcvm.2019.00141

Razdan, K., Hellums, J. D., & Kroll, M. H. (1994). Shear-Stress-Induced Von-Willebrand-Factor Binding to Platelets Causes the Activation of Tyrosine Kinase(S). *Biochemical Journal, 302*, 681-686. doi:DOI 10.1042/bj3020681

Roberts, G. C., & Critchley, D. R. (2009). Structural and biophysical properties of the integrin-associated cytoskeletal protein talin. *Biophys Rev, 1*(2), 61-69. doi:10.1007/s12551-009-0009-4

Roffi, M., Chew, D. P., Mukherjee, D., Bhatt, D. L., White, J. A., Heeschen, C., . . . Topol, E. J. (2001). Platelet glycoprotein IIb/IIIa inhibitors reduce mortality in diabetic patients with non-ST-segment-elevation acute coronary syndromes. *Circulation, 104*(23), 2767-2771. doi:10.1161/hc4801.100029

Rosing, J., van Rijn, J. L., Bevers, E. M., van Dieijen, G., Comfurius, P., & Zwaal, R. F. (1985). The role of activated human platelets in prothrombin and factor X activation. *Blood, 65*(2), 319-332. Retrieved from https://www.ncbi.nlm.nih.gov/pubmed/3967085

Saltel, F., Mortier, E., Hytonen, V. P., Jacquier, M. C., Zimmermann, P., Vogel, V., . . . Wehrle-Haller, B. (2009). New PI(4,5)P2- and membrane proximal integrin-binding motifs in the talin head control beta3-integrin clustering. *J Cell Biol, 187*(5), 715-731. doi:10.1083/jcb.200908134

Savage, B., Saldivar, E., & Ruggeri, Z. M. (1996). Initiation of platelet adhesion by arrest onto fibrinogen or translocation on von Willebrand factor. *Cell, 84*(2), 289-297. doi:10.1016/s0092-8674(00)80983-6

Schneider, S. W., Nuschele, S., Wixforth, A., Gorzelanny, C., Alexander-Katz, A., Netz, R. R., & Schneider, M. F. (2007). Shear-induced unfolding triggers adhesion of von Willebrand factor fibers. *Proc Natl Acad Sci U S A, 104*(19), 7899-7903. doi:10.1073/pnas.0608422104

Sebe-Pedros, A., Roger, A. J., Lang, F. B., King, N., & Ruiz-Trillo, I. (2010). Ancient origin of the integrin-mediated adhesion and signaling machinery. *Proc Natl Acad Sci U S A, 107*(22), 10142-10147. doi:10.1073/pnas.1002257107

Selvadurai, M. V., Brazilek, R. J., Moon, M. J., Rinckel, J. Y., Eckly, A., Gachet, C., . . . Hamilton, J. R. (2019). The PI 3-kinase PI3KC2alpha regulates mouse platelet membrane structure and function independently of membrane lipid composition. *FEBS Lett, 593*(1), 88-96. doi:10.1002/1873-3468.13295

Shattil, S. J., Kim, C., & Ginsberg, M. H. (2010). The final steps of integrin activation: the end game. *Nat Rev Mol Cell Biol, 11*(4), 288-300. doi:10.1038/nrm2871

Shen, B., Delaney, M. K., & Du, X. (2012). Inside-out, outside-in, and inside-outside-in: G protein signaling in integrin-mediated cell adhesion, spreading, and retraction. *Curr Opin Cell Biol, 24*(5), 600-606. doi:10.1016/j.ceb.2012.08.011

Shen, B., Zhao, X., O'Brien, K. A., Stojanovic-Terpo, A., Delaney, M. K., Kim, K., . . . Du, X. (2013). A directional switch of integrin signalling and a new anti-thrombotic strategy. *Nature, 503*(7474), 131-135. doi:10.1038/nature12613

Sokurenko, E. V., Vogel, V., & Thomas, W. E. (2008). Catch-bond mechanism of force-enhanced adhesion: counterintuitive, elusive, but ... widespread? *Cell Host Microbe, 4*(4), 314-323. doi:10.1016/j.chom.2008.09.005

Song, X., Yang, J., Hirbawi, J., Ye, S., Perera, H. D., Goksoy, E., . . . Qin, J. (2012). A novel membrane-dependent on/off switch mechanism of talin FERM domain at sites of cell adhesion. *Cell Res, 22*(11), 1533-1545. doi:10.1038/cr.2012.97

Stalker, T. J., Traxler, E. A., Wu, J., Wannemacher, K. M., Cermignano, S. L., Voronov, R., . . . Brass, L. F. (2013). Hierarchical organization in the hemostatic response and its relationship to the platelet-signaling network. *Blood, 121*(10), 1875-1885. doi:10.1182/blood-2012-09-457739

statista. (2019, Sep 12). Diabetes - Statistics & Facts. Retrieved from https://www.statista.com/topics/1723/diabetes/#:~:text=According%20to%20the%20World%20Health,some%20629%20million%20diabetics%20globally.

Stefanini, L., & Bergmeier, W. (2010). CalDAG-GEFI and platelet activation. *Platelets, 21*(4), 239-243. doi:10.3109/09537101003639931

Stefanini, L., Lee, R. H., Paul, D. S., O'Shaughnessy, E. C., Ghalloussi, D., Jones, C. I., . . . Bergmeier, W. (2018). Functional redundancy between RAP1 isoforms in murine platelet production and function. *Blood, 132*(18), 1951-1962. doi:10.1182/blood-2018-03-838714

Stefanini, L., Roden, R. C., & Bergmeier, W. (2009). CalDAG-GEFI is at the nexus of calcium-dependent platelet activation. *Blood, 114*(12), 2506-2514. doi:10.1182/blood-2009-04-218768

Stefanini, L., Ye, F., Snider, A. K., Sarabakhsh, K., Piatt, R., Paul, D. S., . . . Petrich, B. G. (2014). A talin mutant that impairs talin-integrin binding in platelets decelerates alphaIIbbeta3 activation without pathological bleeding. *Blood, 123*(17), 2722-2731. doi:10.1182/blood-2013-12-543363

Stritt, S., Wolf, K., Lorenz, V., Vogtle, T., Gupta, S., Bosl, M. R., & Nieswandt, B. (2015). Rap1-GTP-interacting adaptor molecule (RIAM) is dispensable for platelet integrin activation and function in mice. *Blood, 125*(2), 219-222. doi:10.1182/blood-2014-08-597542

Strohmeyer, N., Bharadwaj, M., Costell, M., Fässler, R., & Müller, D. J. (2017). Fibronectin-bound α5β1 integrins sense load and signal to reinforce adhesion in less than a second. *Nature Materials, 16*(12), 1262-1270. doi:10.1038/nmat5023

Sun, Z., Costell, M., & Fassler, R. (2019). Integrin activation by talin, kindlin and mechanical forces. *Nat Cell Biol, 21*(1), 25-31. doi:10.1038/s41556-018-0234-9

Swaminathan, V., Kalappurakkal, J. M., Mehta, S. B., Nordenfelt, P., Moore, T. I., Koga, N., . . . Waterman, C. M. (2017). Actin retrograde flow actively aligns and orients ligand-engaged integrins in focal adhesions. *Proc Natl Acad Sci U S A, 114*(40), 10648-10653. doi:10.1073/pnas.1701136114

Szydzik, C., Brazilek, R. J., Akbaridoust, F., de Silva, C., Moon, M., Marusic, I., . . . Nesbitt, W. S. (2019). Active Micropump-Mixer for Rapid Antiplatelet Drug Screening in Whole Blood. *Anal Chem, 91*(16), 10830-10839. doi:10.1021/acs.analchem.9b02486

Tadokoro, S., Shattil, S. J., Eto, K., Tai, V., Liddington, R. C., de Pereda, J. M., . . . Calderwood, D. A. (2003). Talin binding to integrin beta tails: a final common step in integrin activation. *Science, 302*(5642), 103-106. doi:10.1126/science.1086652

Tapia-Rojo, R., & Fernandez, J. M. (2020). doi:10.1101/2020.01.10.901991

Tovar-Lopez, F. J., Rosengarten, G., Nasabi, M., Sivan, V., Khoshmanesh, K., Jackson, S. P., . . . Nesbitt, W. S. (2013). An investigation on platelet transport during thrombus formation at micro-scale stenosis. *PLoS One, 8*(10), e74123. doi:10.1371/journal.pone.0074123

Tovar-Lopez, F. J., Rosengarten, G., Westein, E., Khoshmanesh, K., Jackson, S. P., Mitchell, A., & Nesbitt, W. S. (2010). A microfluidics device to monitor platelet aggregation dynamics in response to strain rate micro-gradients in flowing blood. *Lab Chip, 10*(3), 291-302. doi:10.1039/b916757a

Varga-Szabo, D., Braun, A., & Nieswandt, B. (2009). Calcium signaling in platelets. *J Thromb Haemost, 7*(7), 1057-1066. doi:10.1111/j.1538-7836.2009.03455.x

Varga-Szabo, D., Pleines, I., & Nieswandt, B. (2008). Cell adhesion mechanisms in platelets. *Arterioscler Thromb Vasc Biol, 28*(3), 403-412. doi:10.1161/ATVBAHA.107.150474

Watanabe, N., Bodin, L., Pandey, M., Krause, M., Coughlin, S., Boussiotis, V. A., . . . Shattil, S. J. (2008). Mechanisms and consequences of agonist-induced talin recruitment to platelet integrin alphaIIbbeta3. *J Cell Biol, 181*(7), 1211-1222. doi:10.1083/jcb.200803094

Wegener, K. L., Partridge, A. W., Han, J., Pickford, A. R., Liddington, R. C., Ginsberg, M. H., & Campbell, I. D. (2007). Structural basis of integrin activation by talin. *Cell, 128*(1), 171-182. doi:10.1016/j.cell.2006.10.048

WILK, M. B., & GNANADESIKAN, R. (1968). Probability plotting methods for the analysis for the analysis of data. *Biometrika, 55*(1), 1-17. doi:10.1093/biomet/55.1.1

Wisinski, J. A., & Kimple, M. E. (2016). Platelet Dysfunction in Type 1 Diabetes: Stressing the Thromboxanes. *Diabetes, 65*(2), 349-351. doi:10.2337/dbi15-0032

World Health Organization. (2017, May 17). Cardiovascular diseases (CVDs). Retrieved from https://www.who.int/news-room/fact-sheets/detail/cardiovascular-diseases-(cvds)

Xiong, J. P., Stehle, T., Zhang, R., Joachimiak, A., Frech, M., Goodman, S. L., & Arnaout, M. A. (2002). Crystal structure of the extracellular segment of integrin alpha Vbeta3 in complex with an Arg-Gly-Asp ligand. *Science, 296*(5565), 151-155. doi:10.1126/science.1069040

Yago, T., Lou, J., Wu, T., Yang, J., Miner, J. J., Coburn, L., . . . Zhu, C. (2008). Platelet glycoprotein Ibalpha forms catch bonds with human WT vWF but not with type 2B von Willebrand disease vWF. *J Clin Invest, 118*(9), 3195-3207. doi:10.1172/JCI35754

Yago, T., Petrich, B. G., Zhang, N., Liu, Z., Shao, B., Ginsberg, M. H., & McEver, R. P. (2015). Blocking neutrophil integrin activation prevents ischemia-reperfusion injury. *J Exp Med, 212*(8), 1267-1281. doi:10.1084/jem.20142358

Yao, M., Goult, B. T., Klapholz, B., Hu, X., Toseland, C. P., Guo, Y., . . . Yan, J. (2016). The mechanical response of talin. *Nat Commun, 7*, 11966. doi:10.1038/ncomms11966

Yap, C. L., Anderson, K. E., Hughan, S. C., Dopheide, S. M., Salem, H. H., & Jackson, S. P. (2002). Essential role for phosphoinositide 3-kinase in shear-dependent signaling between platelet glycoprotein Ib/V/IX and integrin alpha(IIb)beta(3). *Blood, 99*(1), 151-158. doi:10.1182/blood.v99.1.151

Yong, A. S., Pennings, G. J., Chang, M., Hamzah, A., Chung, T., Qi, M., . . . Kritharides, L. (2011). Intracoronary shear-related up-regulation of platelet P-selectin and platelet-monocyte aggregation despite the use of aspirin and clopidogrel. *Blood, 117*(1), 11-20. doi:10.1182/blood-2010-04-278812

Zarnitsyna, V. I., Huang, J., Zhang, F., Chien, Y. H., Leckband, D., & Zhu, C. (2007). Memory in receptor-ligand-mediated cell adhesion. *Proc Natl Acad Sci U S A, 104*(46), 18037-18042. doi:10.1073/pnas.0704811104

Zhang, K., & Chen, J. (2012). The regulation of integrin function by divalent cations. *Cell Adh Migr, 6*(1), 20-29. doi:10.4161/cam.18702

Zhang, W., Deng, W., Zhou, L., Xu, Y., Yang, W., Liang, X., . . . Li, R. (2015). Identification of a juxtamembrane mechanosensitive domain in the platelet

mechanosensor glycoprotein Ib-IX complex. *Blood, 125*(3), 562-569. doi:10.1182/blood-2014-07-589507

Zhang, X. F., & Cheng, X. (2019). Platelet mechanosensing axis revealed. *Nature Materials, 18*(7), 661-662. doi:10.1038/s41563-019-0393-5